

AD-A043 027

AIR FORCE GEOPHYSICS LAB HANSCOM AFB MASS  
ANALYSIS OF SWEEP FREQUENCY OBLIQUE POLAR REGION HIGH FREQUENCY--ETC(U)  
APR 77 A E REILLY  
AFGL-TR-77-0102

F/G 20/14

UNCLASSIFIED

10F 2  
AD  
A043027

NL



AD A 043027

AFGL-TR-77-0102  
ENVIRONMENTAL RESEARCH PAPERS, NO. 596



12  
B.S.

# Analysis of Sweep Frequency Oblique Polar Region High Frequency Radio Propagation Measurements

ALFRED E. REILLY

27 April 1977

Approved for public release; distribution unlimited.

SPACE PHYSICS DIVISION PROJECT 7663

**AIR FORCE GEOPHYSICS LABORATORY**

HANSCOM AFB, MASSACHUSETTS 01731

DDC  
RECEIVED  
AUG 19 1977  
B

**AIR FORCE SYSTEMS COMMAND, USAF**

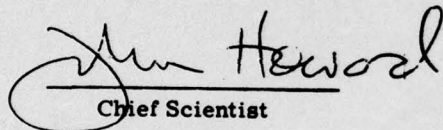


DDC FILE COPY

This report has been reviewed by the ESD Information Office (OI) and is releasable to the National Technical Information Service (NTIS).

This technical report has been reviewed and is approved for publication.

FOR THE COMMANDER

  
Chief Scientist

Qualified requestors may obtain additional copies from the Defense Documentation Center. All others should apply to the National Technical Information Service.

Analysis of Sweep Frequency Oblique Polar Region  
High Frequency Radio Propagation Measurements

ALFRED E. REILLY

27 April 1977

ERRATA

The organization referred to in the Preface is now World Data Center A,  
NOAA, Boulder, Col.

Page 47. The first  $R_1$  Index of Experiment 60 is "29" rather than "9".

Page 50. Table 5. The number of occurrences of  $R_1=17$  should be 2 and  
for  $R_1=58$ , should be 6.

Page 54. Line 9. The word "eleven" should be "nine".

Page 67. On the next to the last line, the word "six" should be "seven".

Page 68. Line 3. "five" should be "six".

Line 4. "21" should be "20".

Line 7. "45" should be "48" and "four" should be "five".

Line 8. "37" should be "43".

Page 70. Table 8. There are two additional transitions: an ambiguous  
2 (O-T), 3 (O-T) transition which occurs at an  $E_2$  event  
so that the frequency window width narrows; and  
a 3 (C-O) transition at which the LOF increases and,  
hence, the frequency window width narrows. Numbers  
35 and 45 are both "2 (C-O)" transitions rather than  
"3 (C-O)" transitions. Therefore, on page 67, on the  
fifth line from the bottom, the word "usually" should  
replace the word "always"

Page 72. Third line from the bottom, the number "151" should be "141".

Page 74. Fourth line from the bottom, the number "14" should be "15", and  
on the next line, the number "15" should be "14"



Unclassified

SECURITY CLASSIFICATION OF THIS PAGE (When Data Entered)

REPORT DOCUMENTATION PAGE		READ INSTRUCTIONS BEFORE COMPLETING FORM
1. REPORT NUMBER	2. GOVT ACCESSION NO.	3. RECIPIENT'S CATALOG NUMBER
AFGL-TR-77-0102, AFGL-ERP-596		
4. TITLE (and Subtitle)	5. TYPE OF REPORT & PERIOD COVERED	
ANALYSIS OF SWEEP FREQUENCY OBLIQUE POLAR REGION HIGH FREQUENCY RADIO PROPAGATION MEASUREMENTS	Scientific. Interim.	
7. AUTHOR(s)	6. PERFORMING ORG. REPORT NUMBER	
Alfred E. Reilly	ERP No. 596	
9. PERFORMING ORGANIZATION NAME AND ADDRESS		8. CONTRACT OR GRANT NUMBER(s)
Air Force Geophysics Laboratory (PHI) Hanscom AFB, Massachusetts 01731		
10. PROGRAM ELEMENT, PROJECT, TASK AREA & WORK UNIT NUMBERS		
62101F 76630901		
11. CONTROLLING OFFICE NAME AND ADDRESS		12. REPORT DATE
Air Force Geophysics Laboratory (PHI) Hanscom AFB, Massachusetts 01731		27 April 1977
13. NUMBER OF PAGES		14. MONITORING AGENCY NAME & ADDRESS (if different from Controlling Office)
101		
15. SECURITY CLASS. (of this report)		15a. DECLASSIFICATION/DOWNGRADING SCHEDULE
Unclassified		
16. DISTRIBUTION STATEMENT (of this Report)		
Approved for public release; distribution unlimited.		
17. DISTRIBUTION STATEMENT (of the abstract entered in Block 20, if different from Report)		
Environmental research papers,		
18. SUPPLEMENTARY NOTES		
19. KEY WORDS (Continue on reverse side if necessary and identify by block number)		
HF propagation Polar region Auroral oval		
20. ABSTRACT (Continue on reverse side if necessary and identify by block number)		
The Chapman-Davies-Littlewood technique for the computation of the equivalent path of an ionospherically propagated High Frequency (HF) radio signal was used to determine the most probable modes of oblique propagation and the corresponding frequency windows that existed during six experimental aircraft flights in the polar region. In comparison to these results, the Elkins-Rush HF Polar Predictive Model has been found to be inadequate for short-term propagation predictions.		

DD FORM 1 JAN 73 1473 EDITION OF 1 NOV 65 IS OBSOLETE

Unclassified

SECURITY CLASSIFICATION OF THIS PAGE (When Data Entered)

409 578

Unclassified

SECURITY CLASSIFICATION OF THIS PAGE(When Data Entered)

20. (Cont)

These oblique propagation measurements have verified Feldstein and Starkov's conclusion that the magnetic Index Q is a good indicator of the position, shape, and size of the Instantaneous Auroral Oval as they have defined it on the basis of ground-based optical measurements which they subjected to statistical analyses.

An approach has been developed which sheds new light on the behavior of HF signals propagating via the polar ionosphere. On the basis of the results achieved using this approach, it is recommended that an attempt be made to develop a new method of predicting short-term polar region HF' propagation conditions well in advance (that is, an hour or more in advance in real time). A hypothetical example of an application of such a method is given. Action should be taken soon to exploit this possibility.

Additional work could extend the applicability of this approach beyond anything that has seemed feasible before. New understanding of the physics of the polar ionosphere could result. It is hoped that this report will stimulate the experimental and theoretical research that will result in this increased understanding of the polar ionosphere.

Unclassified

SECURITY CLASSIFICATION OF THIS PAGE(When Data Entered)

## Preface

The Magnetic Indices Q and AE were secured from the Institute for Telecommunication Sciences and Aeronomy, Environmental Science Services Administration, Boulder, Colorado

ACCESSION for		
NTIS	White Section	<input checked="" type="checkbox"/>
DDC	Buff Section	<input type="checkbox"/>
UNANNOUNCED		<input type="checkbox"/>
JUSTIFICATION		
BY		
DISTRIBUTION/AVAILABILITY CODES		
Dist.	AVAIL.	and/or SPECIAL
A		

## Contents

1. INTRODUCTION	9
2. DETERMINATION OF THE MOST PROBABLE MODES OF PROPAGATION	10
2.1 The Elkins-Rush HF Polar Predictive Model	18
3. GEOPHYSICAL CONDITIONS	26
3.1 The One-Hop E Mode of Ionospheric Propagation	26
3.1.1 Statistical Studies	26
3.1.2 Definition of Propagation Events	26
3.1.3 Temporal Changes in Relevant Parameters	27
3.1.4 Instantaneous Auroral Oval	36
3.1.5 Example-Experiment 141	51
3.1.6 All Relevant Propagation Events - One-Hop E Mode	53
3.1.7 S and E Events	55
3.1.8 Frequency Window Widths for $r_1$ Conditions	59
3.1.9 Conclusions Based on the Analysis of the One-Hop E Mode Events	63
3.1.10 Additional Comments	63
3.1.11 Hypothetical Illustration	67
3.1.12 $R_1$ Associated Transitions of the Instantaneous Q Oval Boundaries for the One-Hop E Mode for Six Experiments	67
3.1.13 Specific Geophysical Event	70
3.1.14 Supplementary Note	72
4. ANALYSIS OF THE ELKINS-RUSH HF POLAR PREDICTIVE MODEL	73
4.1 Preliminary Comments	73
4.2 Input Parameters	73
4.3 Output Parameters	74
4.4 Numerical Analysis Results	74
5. CONCLUSIONS AND RECOMMENDATIONS	77



## Contents

REFERENCES	79
APPENDIX A: Analysis of the Less Extensive Observed Modes	81

## Illustrations

1. Geographical Flight Path of Experiment 58	11
2. Geographical Flight Path of Experiment 60	11
3. Geographical Flight Path of Experiment 141	12
4. Geographical Flight Path of Experiment 142	12
5. Geographical Flight Path of Experiment 193	13
6. Geographical Flight Path of Experiment 196	13
7. Flight Path of Experiment 58 in Corrected Geomagnetic Coordinates	14
8. Flight Path of Experiment 60 in Corrected Geomagnetic Coordinates	14
9. Flight Path of Experiment 141 in Corrected Geomagnetic Coordinates	15
10. Flight Path of Experiment 142 in Corrected Geomagnetic Coordinates	15
11. Flight Path of Experiment 193 in Corrected Geomagnetic Coordinates	16
12. Flight Path of Experiment 196 in Corrected Geomagnetic Coordinates	16
13. Timing Cycle	17
14. 1-E Modes Observed at Aircraft	19
15. Elkins-Rush HF Polar Predictive Model, Service Probability = 0.70, 1-E Modes	23
16. 1-E Modes Observed at Aircraft Showing Instantaneous Changes in the Index AE	28
17. 1-E Modes Observed at Aircraft Showing Q-Transition Times	31
18. Histogram of Percentage of Occurrence of All Significant and Relevant Events for the One-Hop E Mode for All Experiments Compared Temporally with Q-Transition Occurrences	37
19. Histogram of Percentage of Occurrence of S and E Events for the One-Hop E Mode Compared Temporally with Q-Transition Occurrences	37
20. Instantaneous Auroral Oval for Geomagnetic Activity Level Q = 3	39
21. Composite Instantaneous Auroral Oval for Experiment 58	44
22. Composite Instantaneous Auroral Oval for Experiment 60	44
23. Composite Instantaneous Auroral Oval for Experiment 141	45
24. Composite Instantaneous Auroral Oval for Experiment 142	45
25. Composite Instantaneous Auroral Oval for Experiment 193	46
26. Composite Instantaneous Auroral Oval for Experiment 196	46

## Illustrations

27.	1-E Modes Observed at Aircraft Showing $r_1$ -Conditions and $R_1$ Indices	47
28.	Experiment 141 as an Example of the Events that Can Occur and the Occurrences of $R_1$ Indices	52
29.	Deviation in Minutes (Experiment 141 as an example)	53
30.	Histogram of Percentage of Occurrence of All Significant and Relevant Events for the One-Hop E Mode for All Experiments Compared Temporally with $R_1$ Occurrences as Appropriate	54
31.	Histogram of Percentage of Occurrence of S and E Events for the One-Hop E Mode Compared Temporally with $R_1$ Occurrences	58
32.	Histogram of the Frequency Window Widths for Each $r_1$ -Condition for the One-Hop E Mode for All Six Experiments	60
33.	1-E Modes Observed at Aircraft Showing Randomly Selected Temporal Indices	64
34.	Histogram of Percentage of Occurrence of All Significant and Relevant Events for the One-Hop E Mode for All Experiments Compared to Randomly Selected Times	67
35.	HF Signal Observed at Aircraft in the One-Hop E Mode During an Auroral Substorm - Experiment 58	71
36.	Great Whale River H-Component Magnetogram During Auroral Substorm - Experiment 58	71
37.	3 dB - Goose Bay Riometer (30 MHz-Zenith) - Experiment 58	72
38.	Plots of $P$ vs $\frac{\Sigma \Delta o}{\Sigma \Delta o}$ and $P$ vs $\frac{\Sigma \Delta o}{\Sigma \Delta p}$	75
39.	Plots of $P$ vs $\frac{\Sigma \Delta o - \Sigma \Delta o}{\Sigma \Delta o}$ and $P$ vs $\frac{\Sigma \Delta p - \Sigma \Delta o}{\Sigma \Delta o}$	76
A1.	Elkins-Rush HF Polar Predictive Model, Service Probability = 0.70, 1-F Modes	82
A2.	1-F Modes Observed at Aircraft Showing Q-Transition Times	83
A3.	1-F Modes Observed at Aircraft Showing $r_1$ -Conditions and $R_1$ Indices	84
A4.	Histogram of Percentage of Occurrence of All Significant and Relevant Events for the One-Hop F Mode Compared Temporally with $R_1$ Occurrences	85
A5.	Histogram of Percentage of Occurrence of All Significant and Relevant Events for the One-Hop F Mode Compared Temporally with Q-Transition Occurrences	85
A6.	Elkins-Rush HF Polar Predictive Model, Service Probability = 0.70, 2-E Modes	88
A7.	2-E Modes Observed at Aircraft Showing Q-Transition Times	89
A8.	2-E Modes Observed at Aircraft Showing $r_2$ -Conditions and $R_2$ Indices	90
A9.	Histogram of Percentage of Occurrence of All Significant and Relevant Events for the Two-Hop E Mode for All Experiments Compared Temporally with $R_2$ Occurrences	91
A10.	Histogram of Percentage of Occurrence of All Significant and Relevant Events for the Two-Hop E Mode for All Experiments Compared Temporally with Q-Transition Occurrences	91

## Illustrations

A 11.	Elkins-Rush HF Polar Predictive Model, Service Probability = 0.70, 2-F Modes	92
A 12.	2-F Modes Observed at Aircraft Showing Q-Transition Times	93
A 13.	2-F Modes Observed at Aircraft Showing $r_2$ -Conditions and $R_2$ Indices	96
A 14.	Histogram of Percentage of Occurrence of All Significant and Relevant Events for the Two-Hop F Mode for All Experiments Compared Temporally with $R_2$ Occurrences	98
A 15.	Histogram of Percentage of Occurrence of All Significant and Relevant Events for the Two-Hop F Mode for All Experiments Compared Temporally with Q-Transition Occurrences	98
A 16.	Histogram of Percentage of Occurrence of All Significant and Relevant Events for All Modes and All Experiments Compared Temporally with $R_1$ and $R_2$ Occurrences as Appropriate	99
A 17.	Histogram of Percentage of Occurrence of All Significant and Relevant Events for All Modes and All Experiments Compared Temporally with Q-Transition Occurrences	99
A 18.	Histogram of Percentage of Occurrence of All S and E Events for All Modes and All Experiments Compared Temporally with $R_1$ and $R_2$ Occurrences	100
A 19.	Histogram of Percentage of Occurrence of All S and E Events for All Modes and All Experiments Compared Temporally with Q-Transition Occurrences	100

## Tables

1.	Dates and Times When the Experiments Were Conducted	17
2.	Definitions of the Reilly Conditions, $r_1$ , for One-Hop Modes of HF Propagation	40
3.	Definitions of the Reilly Indices, $R_1$ , in Terms of All Possible $r_1$ -Condition Transitions	41
4.	Values of the Index Q During each 15-min Interval During each Experiment	43
5.	Relevant $R_1$ Indices Which Occurred During the One-Hop E Mode in All Six Experiments	50
6.	Description of Each S and E Event for All Six Experiments for the One-Hop E Mode	57
7.	Mean Value of the Frequency Window Width for Each Value of $r_1$ for the One-Hop E Mode for All Six Experiments	59
8.	Observed Characteristics of Each Instantaneous Auroral Oval Edge Transition	69
A 1.	Definitions of the Reilly Conditions, $r_2$ , for Two-Hop Modes of HF Propagation	86
A 2.	Definitions of the Reilly Indices, $R_2$ , in Terms of All the Possible $r_2$ -Condition Transitions	87

## Analysis of Sweep Frequency Oblique Polar Region High Frequency Radio Propagation Measurements

### 1. INTRODUCTION

Sweep frequency HF radio observations of the ionosphere have been carried out at vertical incidence for a long time. These measurements have been used to calculate the maximum usable frequencies for oblique radio communication purposes and, in general, the relationships developed between vertical and oblique propagation data have been verified.

In the polar region, where the experiments analyzed in this report have been conducted, the short-term variations in HF propagation conditions have never been explained adequately. As far as the models that have been developed to describe the ionosphere at these latitudes are concerned, the question as to how successfully these models account for short-term HF propagation conditions or whether they can be employed to make useful predictions of these conditions has not been answered as yet.

This report is an analysis of the measurements made during six oblique HF sweep frequency experiments conducted in the polar region during 1974 in the months of February, March, May and July. Each experiment involved the use of a pair of identical sweep frequency sounding systems; one on the ground at the Goose Bay Ionospheric Observatory, Labrador, and the other installed aboard the Airborne Ionospheric Observatory—USAF NKC-135 jet aircraft.

---

(Received for publication 26 April 1977)



The six experiments analyzed in this report were designated by their Julian Day numbers: 58, 60, 141, 142, 193, and 196. Figures 1 to 6 are geographical plots of the flight paths followed during each of the experiments while Figures 7 to 12 are plots of the same six flight paths in corrected geomagnetic coordinates.<sup>1</sup> In addition to the flight path, which is indicated by the inner line, the midpoint of the path is indicated by the outer line, and the position of Goose Bay is indicated, at regular intervals, by the dots just outside of the outermost latitude circle shown (65°N).

As the aircraft flew northward from Goose Bay during all six of the experiments analyzed in this study, simultaneous ionospherically propagated oblique soundings between Goose Bay and the aircraft in both directions were made at 5-min intervals. Each sweep extended either from 4 to 14 MHz or from 6 to 16 MHz but was one or the other throughout each experiment. The maximum great circle distance in any experiment between Goose Bay and the aircraft was 2945 km. The experiments lasted for approximately eight hours each.

## 2. DETERMINATION OF THE MOST PROBABLE MODES OF PROPAGATION

In this report, the most probable propagation modes of the received signals have been identified for the six airborne experiments mentioned above. The frequency window for each mode at each instant of time was also measured. In an 8-hr experiment, there would be a total of 192 oblique incidence ionograms and, in six such experiments, a total of 1152 of them. From this large number of ionograms, those that indicated the emergence of new modes and the disappearance of old modes were selected along with enough intermediate ionograms to insure continuity. Only ionospherically propagated modes were considered.

The major tools used in this study to determine the most probable observed modes of propagation were: The Chapman-Davies-Littlewood<sup>2</sup> technique for the determination of group-path delays between unsynchronized bistatic pulsed transmitters at an arbitrary separation in distance; group-path calculations based on a geometrical-optics specular reflection model consisting of two perfectly conducting spheres concentric with a spherical earth and located at heights representative of the E layer and the F layer; and the group path delay calculations of the Elkins-Rush HF Polar Predictive Model. The appearance of the individual traces as well as the continuity from ionogram to ionogram were also valuable tools.

1. Whalen, J.A. (1970) Auroral Oval Plotter and Nomograph for Determining Corrected Geomagnetic Local Time, Latitude, and Longitude for High Latitudes in the Northern Hemisphere, AFCRL ERP No. 327.
2. Chapman, J.H., Davies, E., and Littlewood, C.A. (1955) Radio observations of the ionosphere at oblique incidence, Can. J. Phys. 33:713-722.

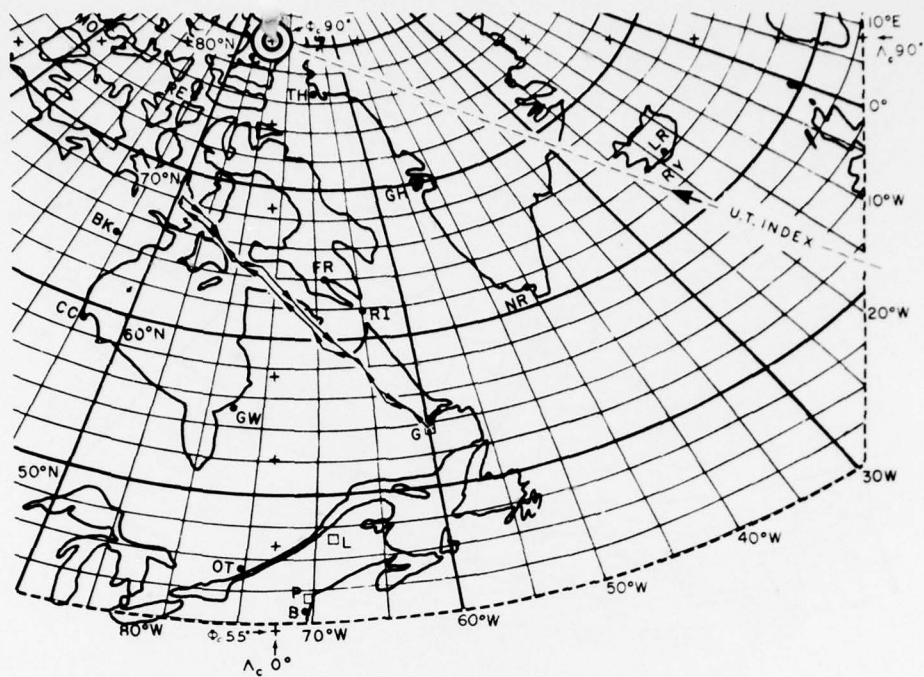


Figure 1. Geographical Flight Path of Experiment 58

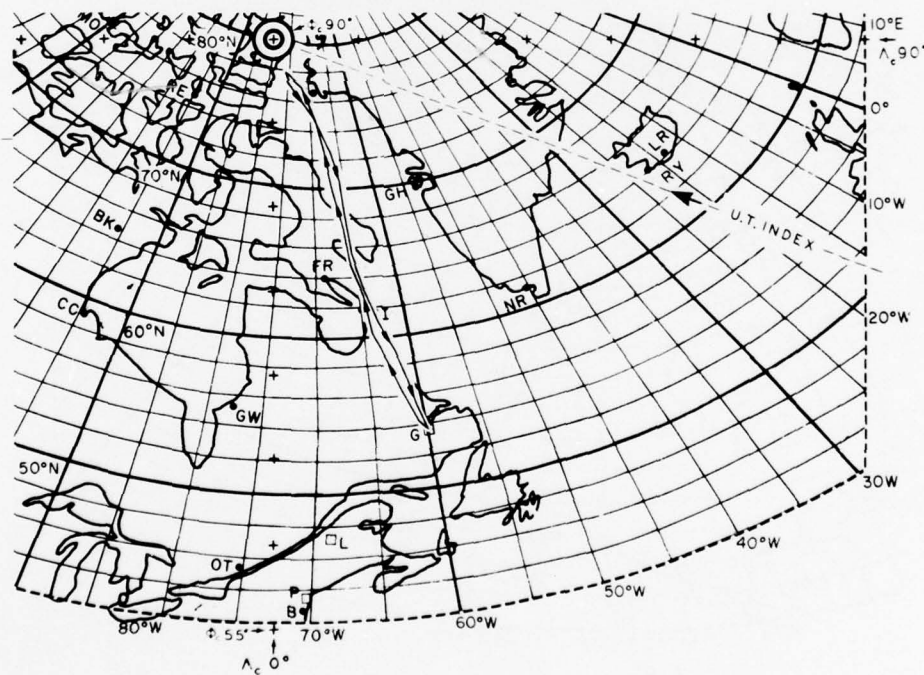


Figure 2. Geographical Flight Path of Experiment 60

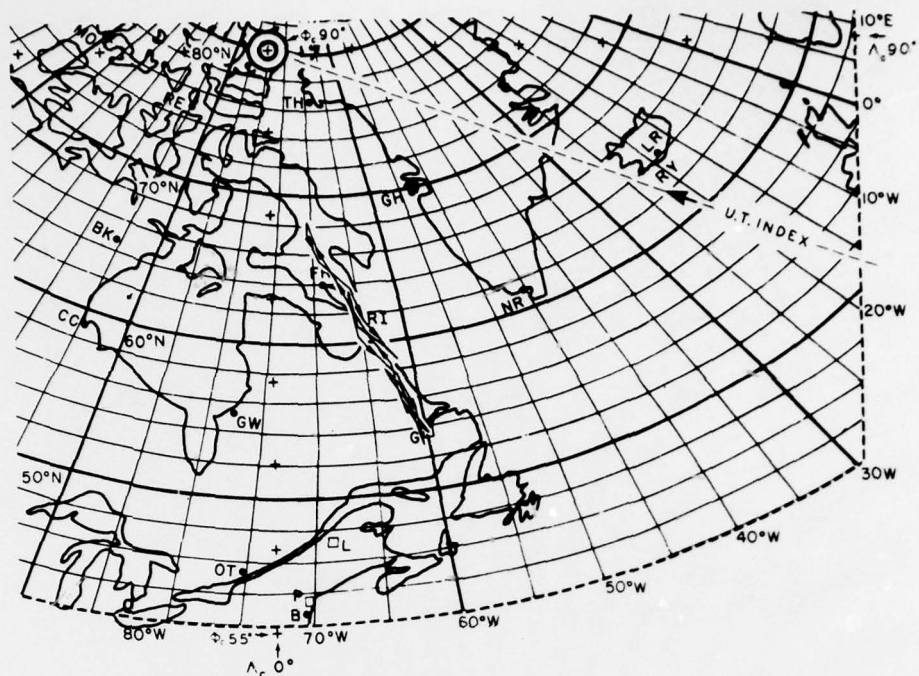


Figure 3. Geographical Flight Path of Experiment 141

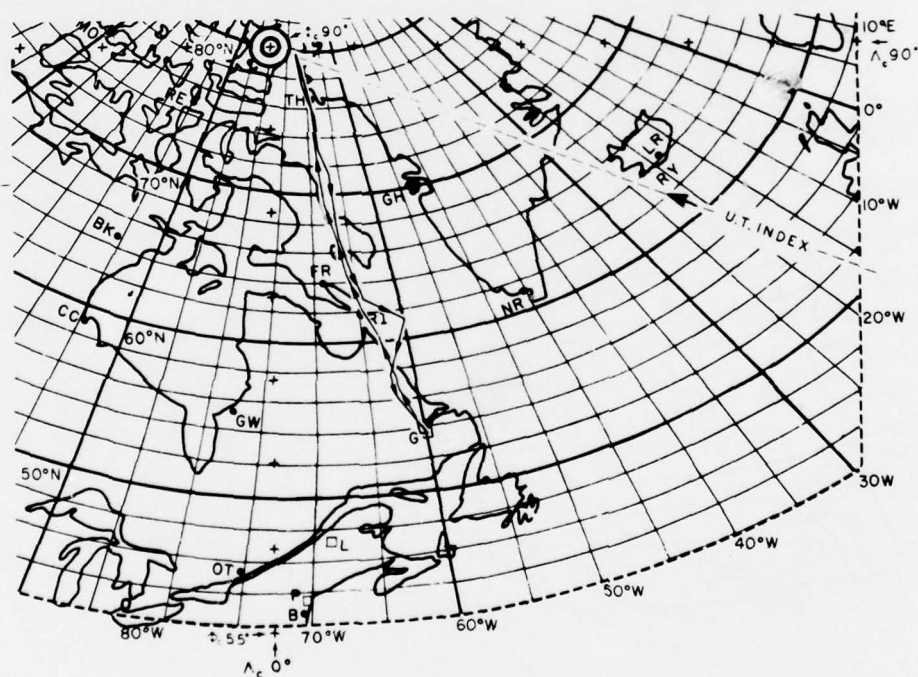


Figure 4. Geographical Flight Path of Experiment 142



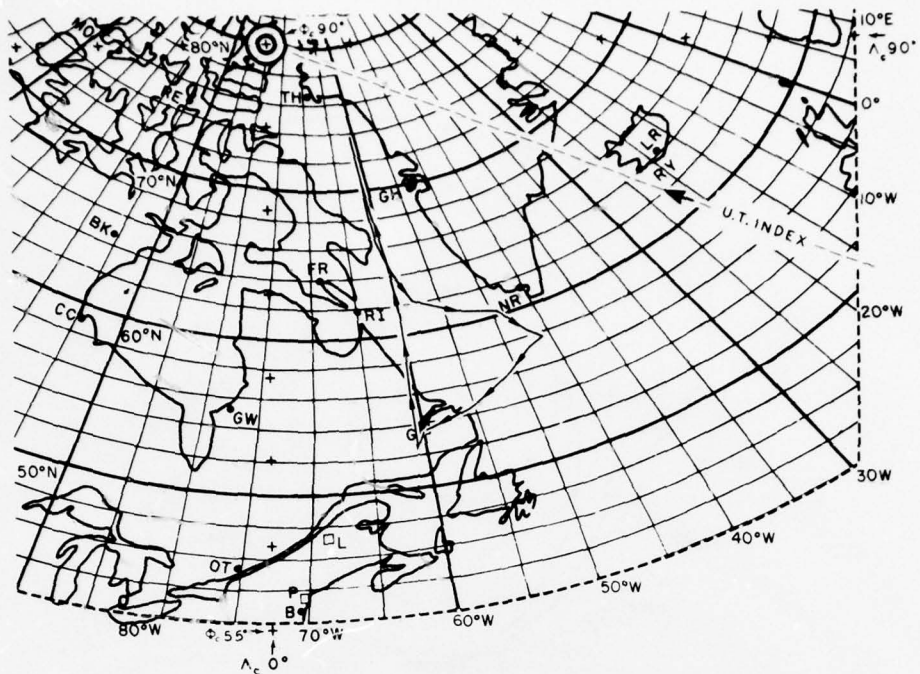


Figure 5. Geographical Flight Path of Experiment 193

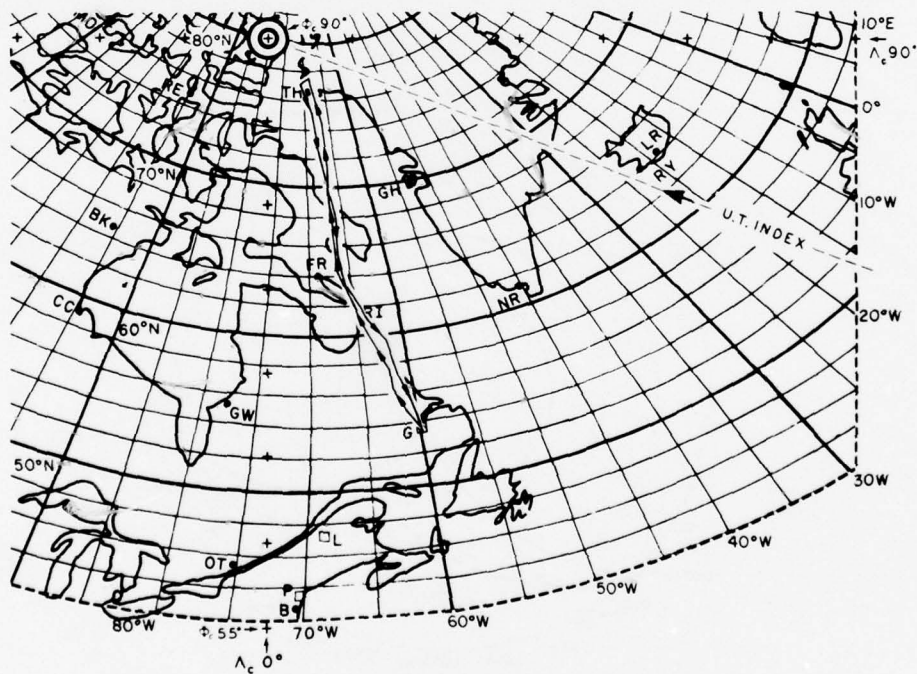


Figure 6. Geographical Flight Path of Experiment 196



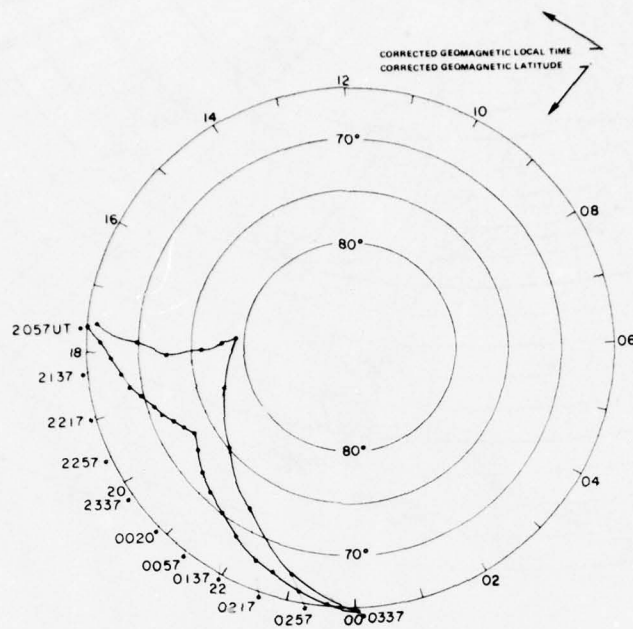


Figure 7. Flight Path of Experiment 58 in Corrected Geomagnetic Coordinates

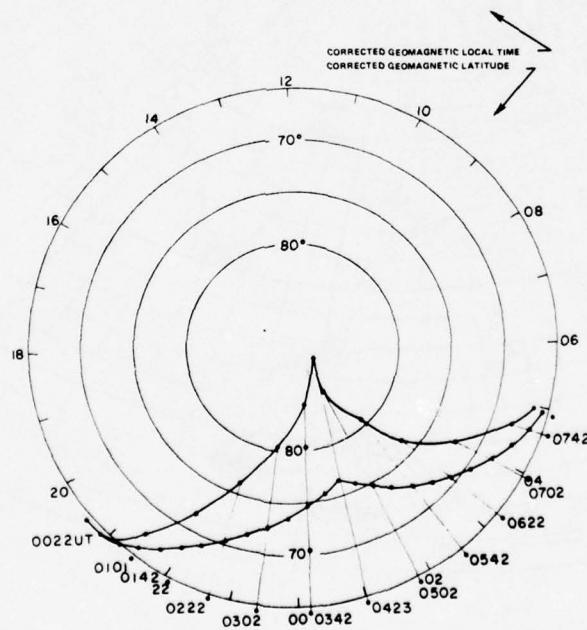


Figure 8. Flight Path of Experiment 60 in Corrected Geomagnetic Coordinates

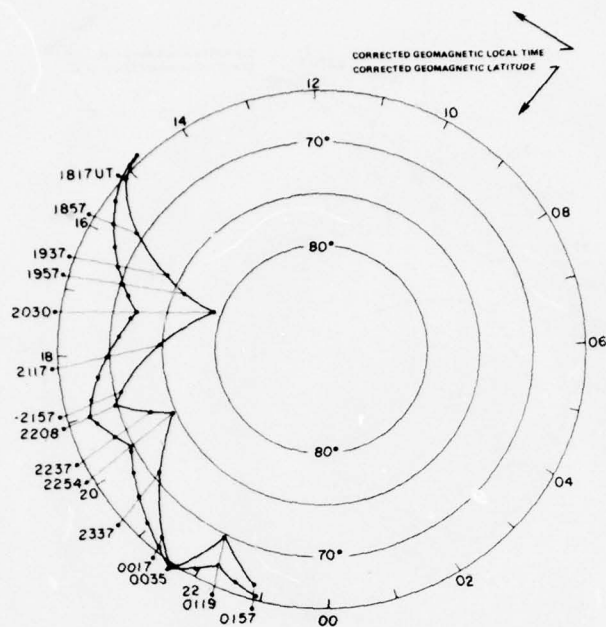


Figure 9. Flight Path of Experiment 141 in Corrected Geomagnetic Coordinates

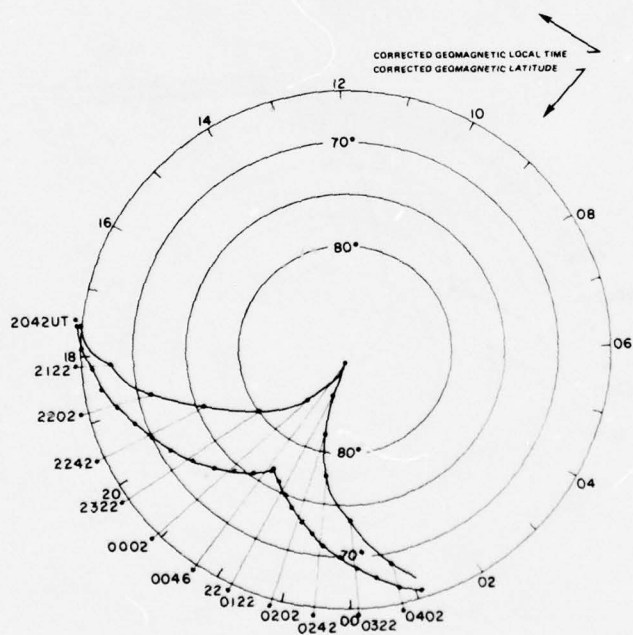


Figure 10. Flight Path of Experiment 142 in Corrected Geomagnetic Coordinates

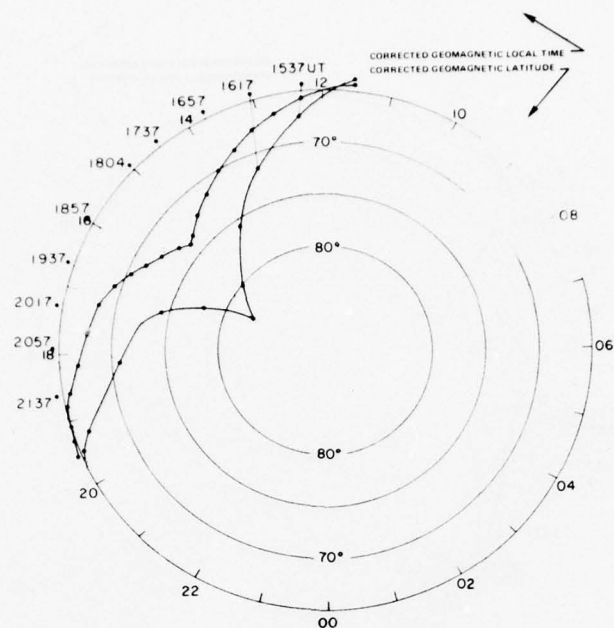


Figure 11. Flight Path of Experiment 193 in Corrected Geomagnetic Coordinates

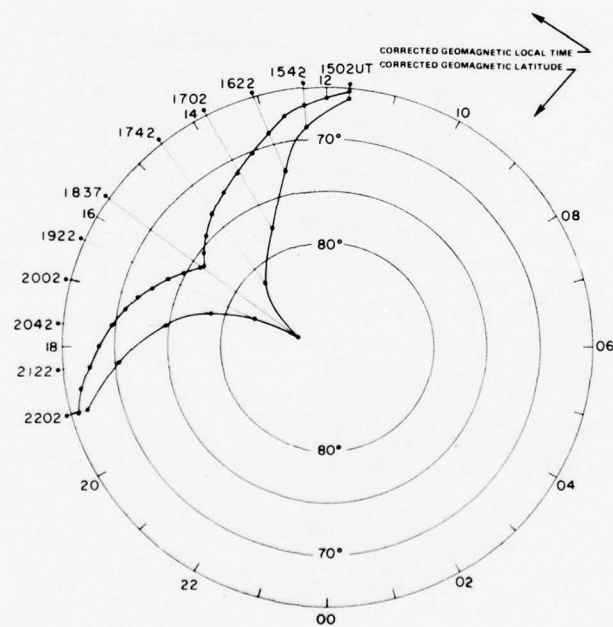


Figure 12. Flight Path of Experiment 196 in Corrected Geomagnetic Coordinates

Briefly, the Chapman-Davies-Little-wood technique for the computation of the equivalent path of a signal in a bistatic configuration is shown in Figure 13.

$P_A$  = the interval between the triggering of the equipment at A and the reception of the signal from B at A.

$P_B$  = the interval between the triggering of the equipment at B and the reception of the signal from A at B.

$P_{AB}$  = the equivalent path between A and B.

$P_{BA}$  = the equivalent path between B and A.

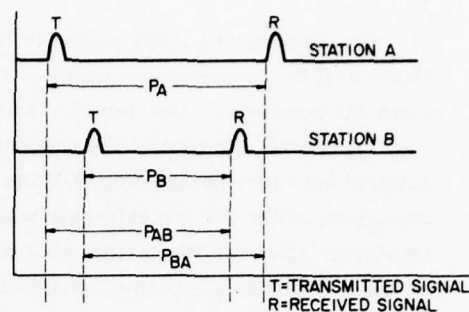


Figure 13. Timing Cycle

From the figure,

$$P_A + P_B = P_{AB} + P_{BA}.$$

Assuming the validity of the theory of reciprocity,

$$P_{AB} = P_{BA}$$

and therefore,

$$P_{AB} = P_{BA} = \frac{1}{2}(P_A + P_B).$$

The results of these calculations have been plotted as functions of time for comparison with geophysical phenomena.

The exact dates and times at which the six experiments were conducted, all in 1974, are as follows.

Table 1. Dates and Times When the Experiments Were Conducted

Experiment Number	Date and Universal Time of Start of Experiment	Date and Universal Time of End of Experiment
58	2100, 27 February	0320, 28 February
60	0005, 01 March	0802, 01 March
141	1749, 21 May	0158, 22 May
142	2036, 22 May	0433, 23 May
193	1448, 12 July	2225, 12 July
196	1445, 15 July	2206, 15 July



Henceforth, the most probable modes determined in the manner described above will be referred to simply as the observed modes. The observed modes were all one-hop E, one-hop F, two-hop E, or two-hop F.

Figure 14 is a plot of the frequency windows observed during all six of these experiments for the one-hop E Mode. This mode was observed very extensively during all of the six experiments whereas the other three observed modes were relatively sparse both in time and in frequency bandwidth. This fact is of interest in itself and has led to an emphasis in this analysis on the one-hop E mode of ionospheric propagation.

In Figure 14, the distances of the aircraft from Goose Bay at the time when the signal was first detected at the aircraft, at the turning points of the flights, and at the time when the signal finally ceased to be detected are indicated in parentheses. The final loss of the signal at the aircraft in these experiments was due either to the fact that the distance between the transmitter and the receiver exceeded the possible distance usually consistent with a one-hop E mode of propagation or because the aircraft was approaching Goose Bay. Also shown by crosses along the horizontal axis are the times when various types of equipment malfunction prevented any transmission from being detected. Other anomalous events are also indicated by special notations; such as the letter T (for Turn); C (for Circle); or S (for Auroral Substorm).

Generally speaking, the observed signals are characterized by an abrupt onset with many total breaks in reception not associated with equipment malfunctions, with sudden variations of the LOF and MOF, and an abrupt termination of reception as the aircraft approached Goose Bay on the final leg of each flight.

It would be very desirable to account for all of these characteristics. Do existing models account for them or is additional research required?

## 2.1 The Elkins-Rush HF Polar Predictive Model

An intensive effort has been made to compare the observed results of the six experiments discussed above with results calculated a-posteriori under identical conditions for the same six experiments by the Elkins-Rush HF Polar Predictive Model.<sup>3,4</sup> The same identical flight paths were used in all six of the experiments and the prescribed calculations were also made at 5-min intervals to match the precision of the observations mentioned above.

3. Elkins, T. J., and Rush, C. M. (1973) A statistical predictive model of the polar ionosphere, Air Force Survey in Geophysics, (No. 267):1-100.
4. Barkhausen, A. F., Finney, J. W., Proctor, L. L., and Schultz (1969) Predicting Long-Term Operational Parameters of High-Frequency Sky-Wave Telecommunications System, ESSA Technical Report ERL 110-17878.

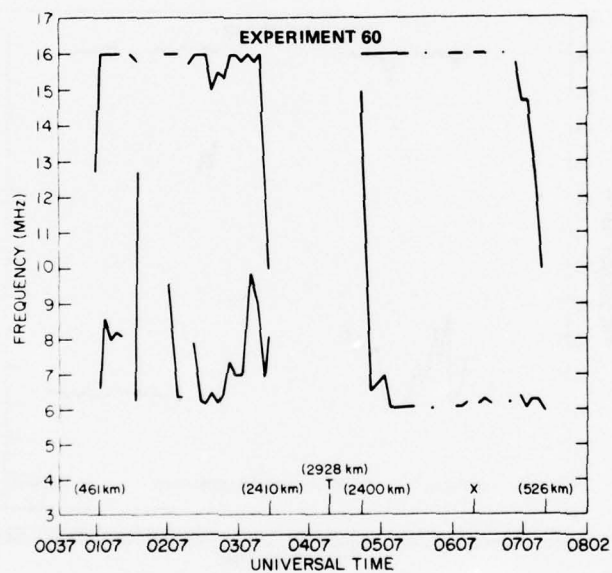
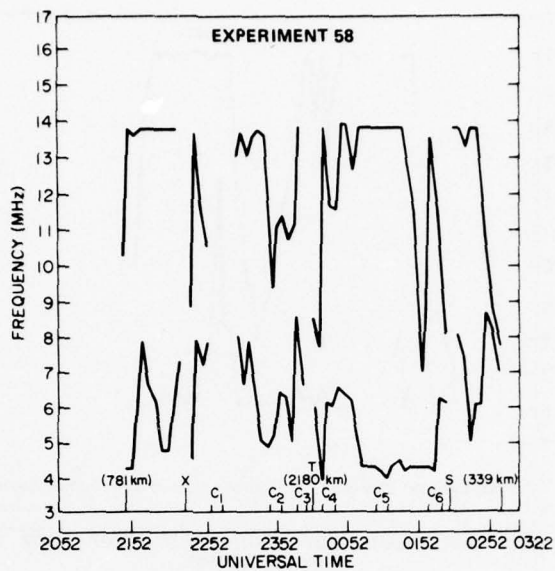


Figure 14. 1-E Modes Observed at Aircraft

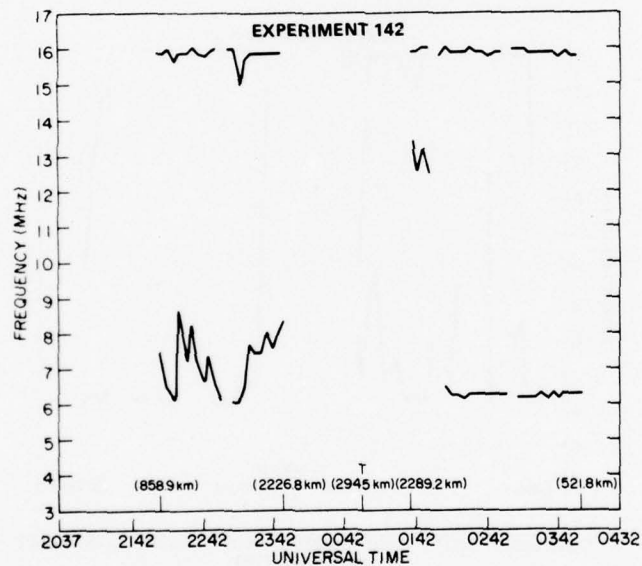
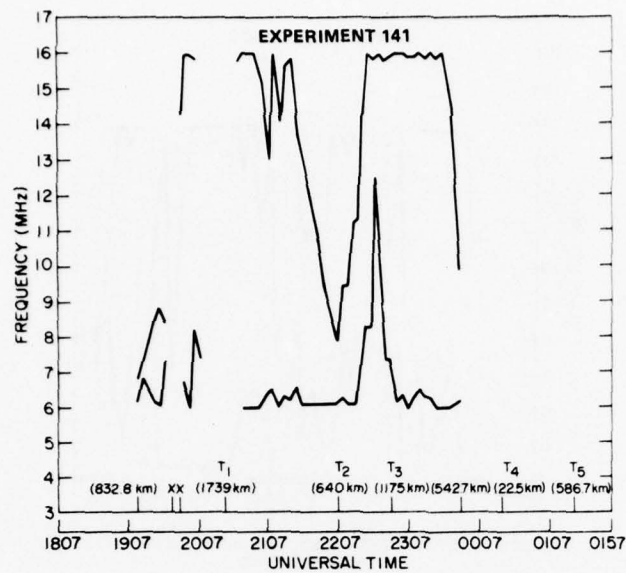


Figure 14. 1-E Modes Observed at Aircraft (Cont)

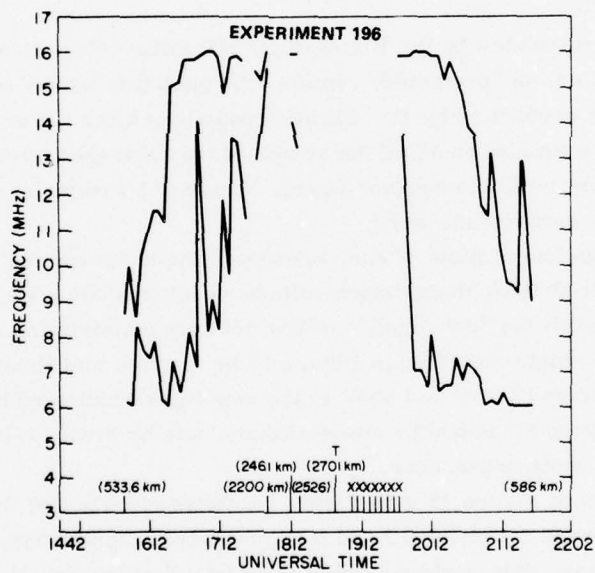
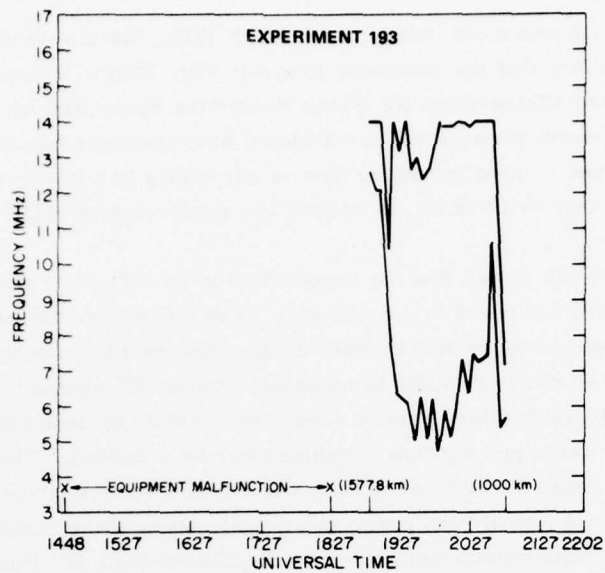


Figure 14. 1-E Modes Observed at Aircraft (Cont)



Dr. Elkins,<sup>5</sup> in a document dated 3 September 1975, has stated that one must "Recognize the fact that the computer program (Dr. Elkins is here referring to the computerized Elkins-Rush HF Polar Predictive Model and its ability to make accurate short-term propagation predictions) addresses median conditions only, and that some use of supplementary data is necessary to apply to an actual scenario (for example, what value of  $fE_s$  is needed to explain certain MUF data, and is it a reasonable one)."

This report has shown that the supposition of Dr. Elkins (quoted above) in his 3 September 1975 document is not correct. It is clear from the results of the analysis of these six experiments that results computed by means of the Elkins-Rush HF Polar Predictive Model in an actual "scenario" cannot be adjusted by the application of supplementary data in such a way that an accurate description of the observed short-term propagation conditions can be achieved. The application of supplementary data to actual scenarios, such as the six scenarios examined extensively in this study, would not result in a modification of the results produced by performing the calculations designated by the Elkins-Rush HF Polar Predictive Model so as to make them accurately predictive of the observed short-term HF Propagation conditions. An analysis that proves this will be presented in Section 4 of this report.

The results calculated by the Elkins-Rush HF Polar Predictive Model will henceforth be called the "predicted" results—the quotation marks indicating that the calculations were performed by Dr. Elkins' group long after the experiments were conducted and at a time when all of the values of the solar-geophysical input parameters were already available and were used. Hence the results were not predictions in the true sense of the word.

Figure 15 consists of plots of each one-hop E mode "predicted" by the Elkins-Rush HF Polar Predictive Model under optimal conditions for all six of these experiments. Although the "predicted" results actually maintain the same LOF and MOF between the points indicated in Figure 15 by the dots and abruptly change the value of the "predicted" LOF and MOF to the new values indicated by these dots, these plots have been smoothed by connecting the dots by straight-line segments in order to improve their appearance.

A comparison of Figure 15 with Figure 14 shows clearly that there is essentially no similarity between the observed and the "predicted" signals and, therefore, the use of supplementary data could not bring them into conformity. A perusal of references (3) and (4) as well as a study of Figures 38 and 39 will make this statement abundantly clear. Comparison of Figure A1 with Figure A2, Figure A6 with Figure A7 and Figure A11 with Figure A12 will erase all residual doubts.

5. Elkins, T.J. (1975) Private Communication.

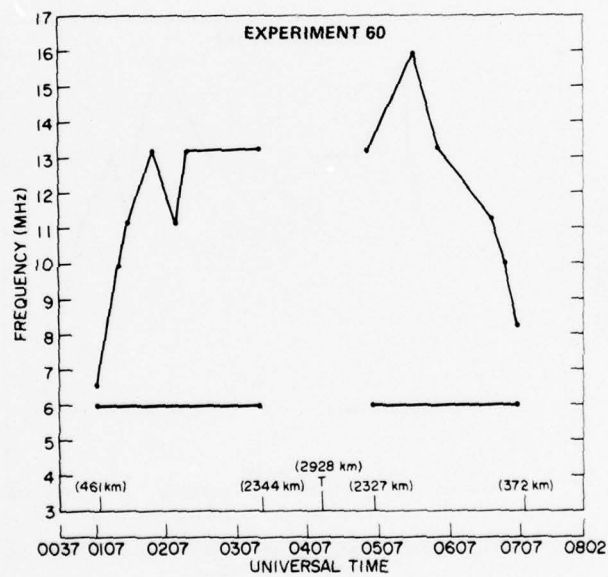
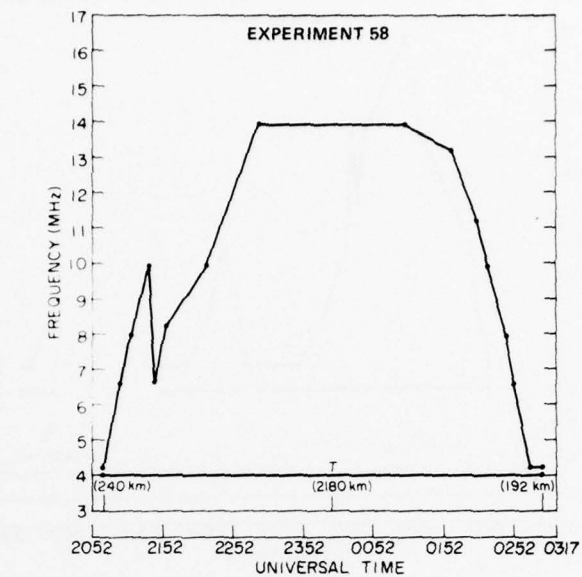


Figure 15. Elkins-Rush HF Polar Predictive Model, Service Probability = 0.70, 1-E Modes

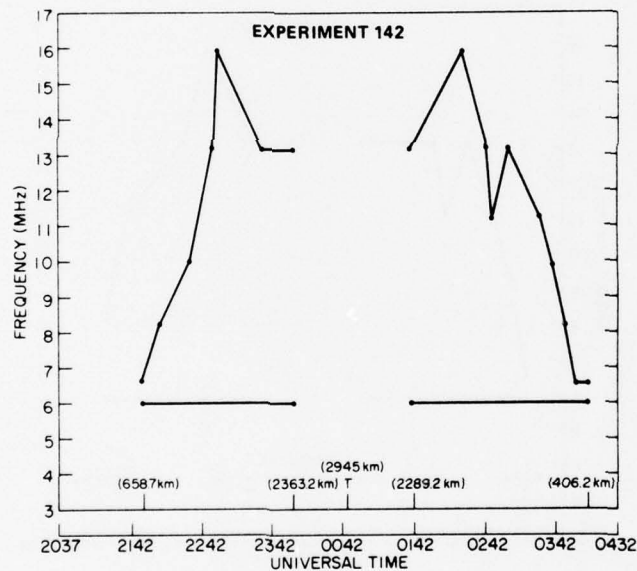
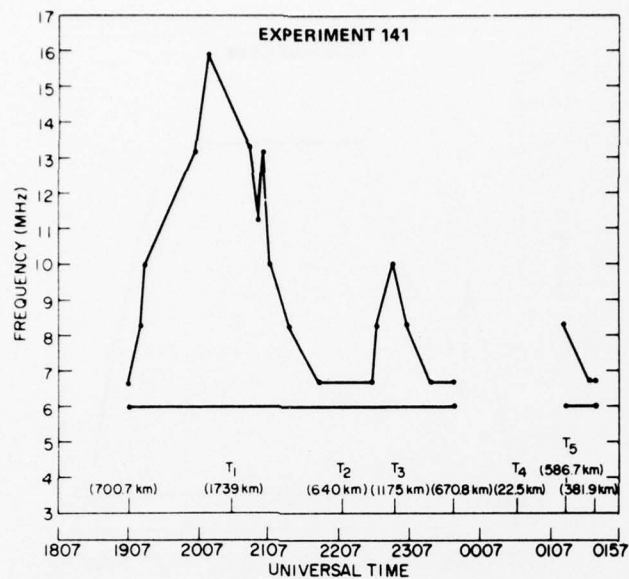


Figure 15. Elkins-Rush HF Polar Predictive Model, Service Probability = 0.70, 1-E Modes (Cont)

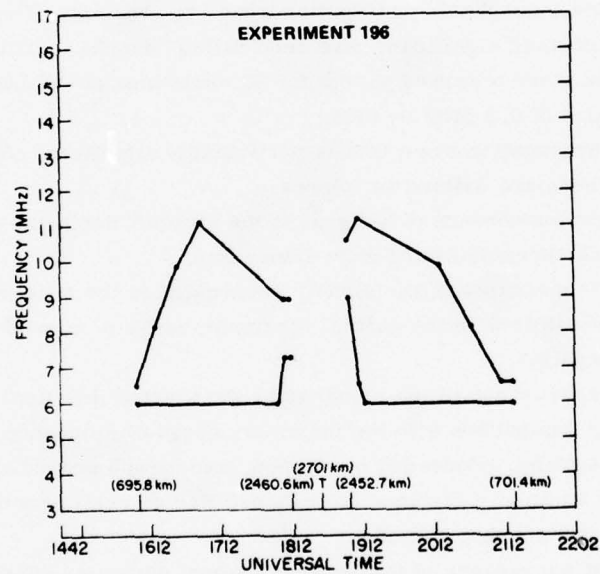
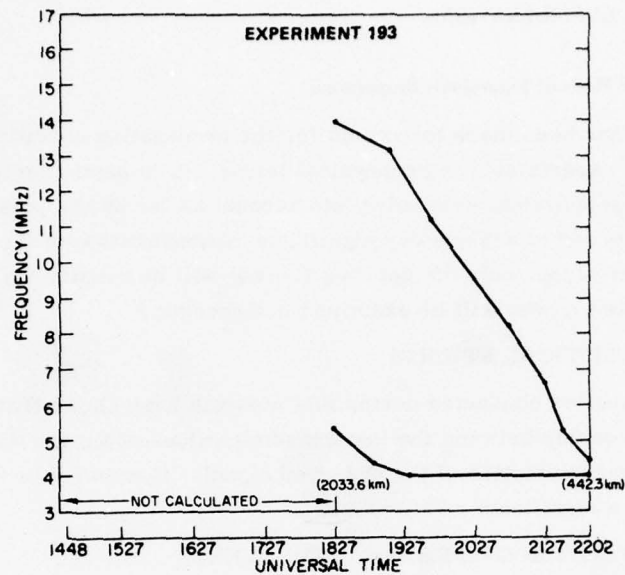


Figure 15. Elkins-Rush HF Polar Predictive Model, Service Probability = 0.70, 1-E Modes (Cont)



### 3. GEOPHYSICAL CONSIDERATIONS

#### 3.1 The One-Hop E Mode of Ionospheric Propagation

An attempt has been made to account for the propagation conditions observed during these six experiments in geophysical terms. It is particularly important to take existing geophysical knowledge into account as far as the polar ionosphere is concerned in order to achieve any significant rationalization of the observations. In this part of the study, only the one-hop E mode will be considered. The less extensive observed modes will be examined in Appendix A.

##### 3.1.1 STATISTICAL STUDIES

Statistical studies conducted during this analysis have shown that there is no significant relationship between the instantaneous values of Kp and AE and the instantaneous characteristics of the observed signal. However, the magnetic Q Index does have a significant relationship.

##### 3.1.2 DEFINITION OF PROPAGATION EVENTS

In the course of these six experiments, the characteristics of the observed signal received via ionospheric propagation were not constant. Those variations which have been deemed significant have been called "events." This includes all of the variations that were observed except for 32 variations of the LOF and the MOF that had magnitudes of 0.5 MHz or less.

One type of propagation event that is particularly significant consists of the S and E events. These are defined as follows.

$S_1$  = The first appearance of a signal at the aircraft during an experiment subsequent to its departure northward from Goose Bay.

$E_1$  = The disappearance of the signal, subsequent to the occurrence of an  $S_1$ , at a distance compatible with the normal maximum range of a one-hop E mode of ionospheric propagation.

$S_2$  = The reappearance of the signal after the aircraft has gone beyond the distance normally compatible with the maximum range of a one-hop E mode of ionospheric propagation, proceeded northward, and turned around moving southward so that it is again at a distance from Goose Bay compatible with the usual maximum range of a one-hop E mode.

$E_2$  = The last appearance of the observed signal during an experiment at the end of a southward leg of a flight path as the aircraft approaches Goose Bay toward the end of the experiment.

(When any of these subscripted letters is primed, it means that there is something anomalous about the event and this anomalous characteristic will be explained within this report.)

All other propagation events must occur between the times of occurrence of particular S and E events. The other propagation events which occurred during these six experiments include the total disappearance and the subsequent return of the signal at any time between  $S_1$  and  $E_1$ , or  $S_2$  and  $E_2$ ; or just between  $S_1$  and  $E_1$  in the event that the aircraft never went beyond the usual maximum range for a one-hop E mode of propagation. This latter circumstance happened in Experiments 58 and 141 but not in Experiments 60, 142, or 196. Experiment 193 is special because, although the aircraft went beyond the normal one-hop E mode propagation distance, the data for the outgoing leg and part of the ingoing leg are not available. Therefore, it only has an  $S_2$  and  $E_2$ . Any increase or decrease in the value of the LOF or MOF that was  $> 0.5$  MHz was also considered to be an event. This includes all of the fluctuations of the LOF and the MOF except for the 32 cases mentioned above. The inclusion of these variations would not affect the results of the study to any noticeable degree and, by excluding them, the probability of including random fluctuations is diminished.

There was a grand total of 174 events, as defined above, during these six experiments in all of the observed modes. Later in this report, some of these events will be excluded from consideration for reasons that will be explained at the time.

### 3.1.3 TEMPORAL CHANGES IN RELEVANT PARAMETERS

An investigation was made of the behavior of the observed HF signal at the times of changes in geophysical parameters that might be expected to produce significant changes in the observed results in an attempt to discover a significant temporal correlation.

Figures 16, 17, and 27 are identical to Figure 14 except that the temporal changes in various parameters are marked along the horizontal axis at the time at which they occurred.

Figure 16 shows the times, during all six of the experiments studied, when the geomagnetic index AE changed, within five min, by a value between  $50 \gamma$  and  $100 \gamma$  (shown by short lines perpendicular to the horizontal axis); the times when AE changed, within five min, by a value between  $100 \gamma$  and  $200 \gamma$  (shown by longer lines perpendicular to the horizontal axis); and the times when AE changed, within five min, by an amount greater than  $200 \gamma$  (shown by very long lines perpendicular to the horizontal axis). These changes are not significantly related to the behavior of the observed signal.

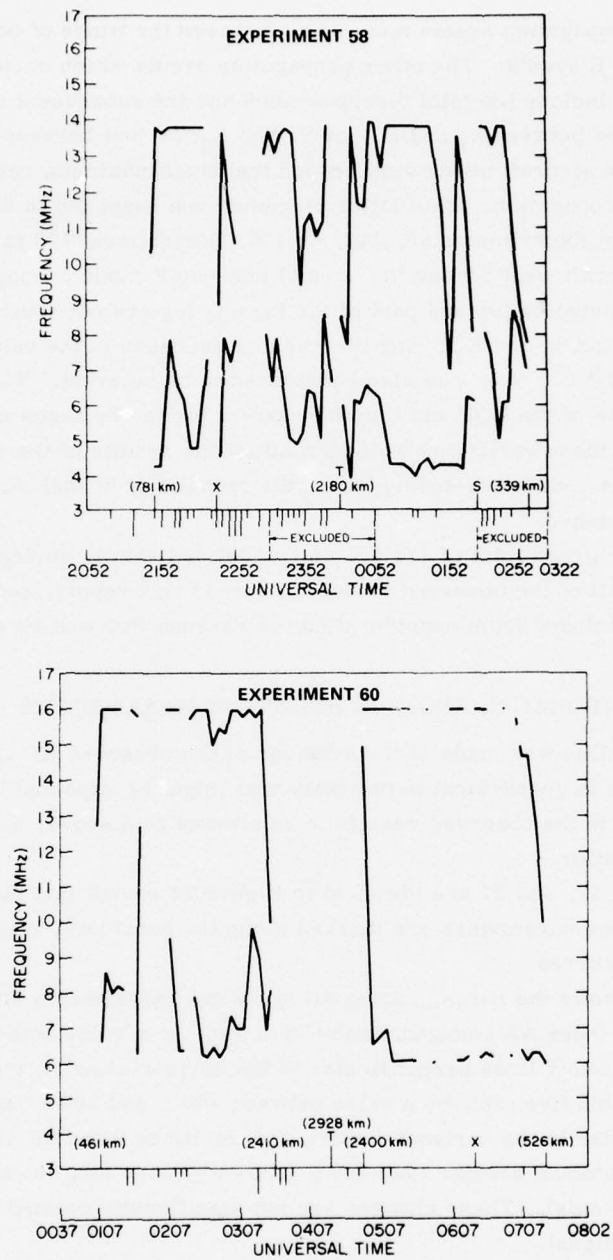


Figure 16. 1-E Modes Observed at Aircraft Showing Instantaneous Changes in the Index AE

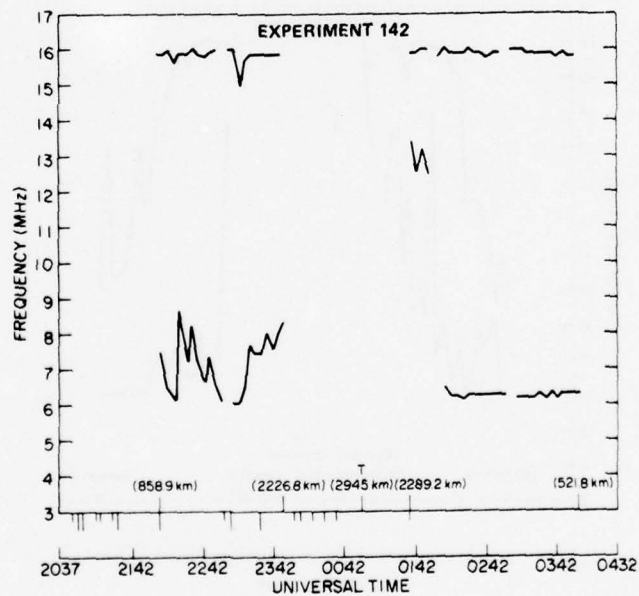
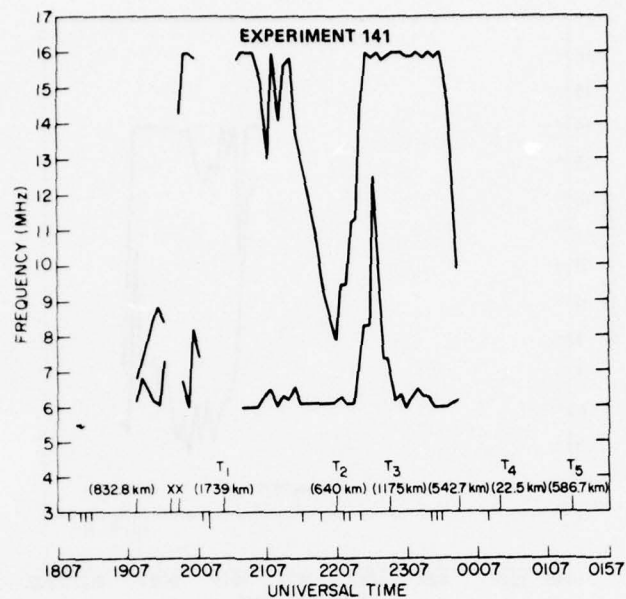


Figure 16. 1-E Modes Observed at Aircraft Showing Instantaneous Changes in the Index AE (Cont)



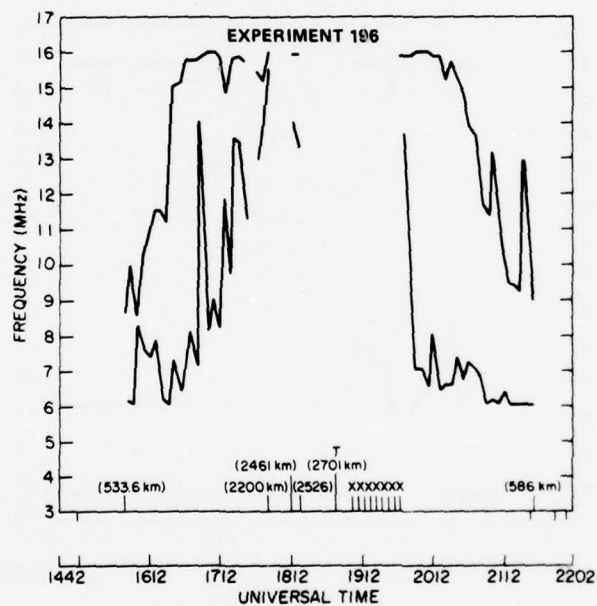
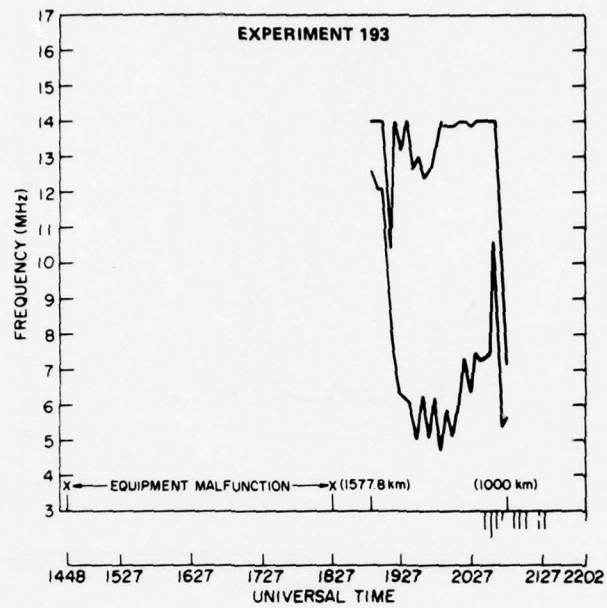


Figure 16. 1-E Modes Observed at Aircraft Showing Instantaneous Changes in the Index AE (Cont)

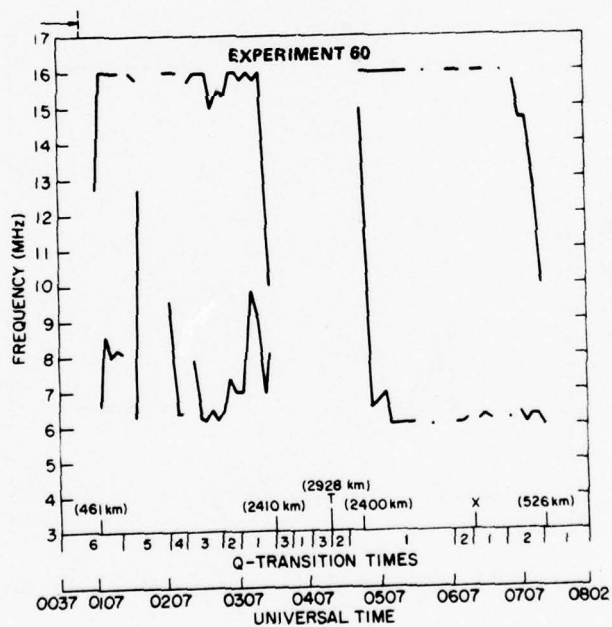
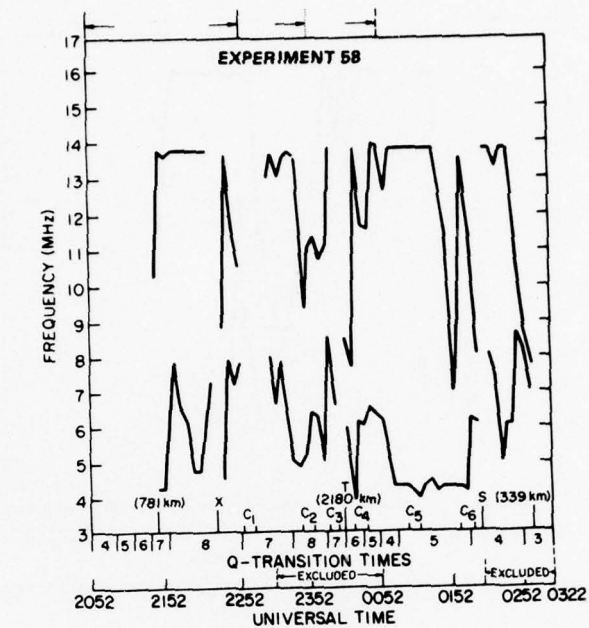


Figure 17. 1-E Modes Observed at Aircraft Showing Q-Transition Times

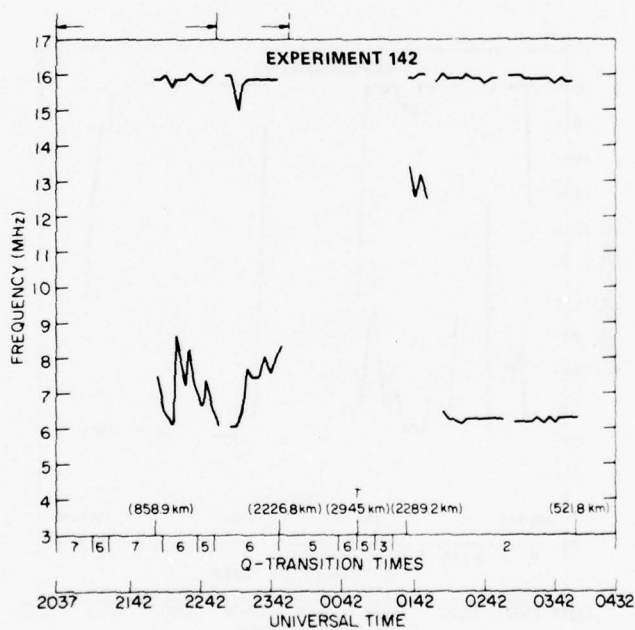
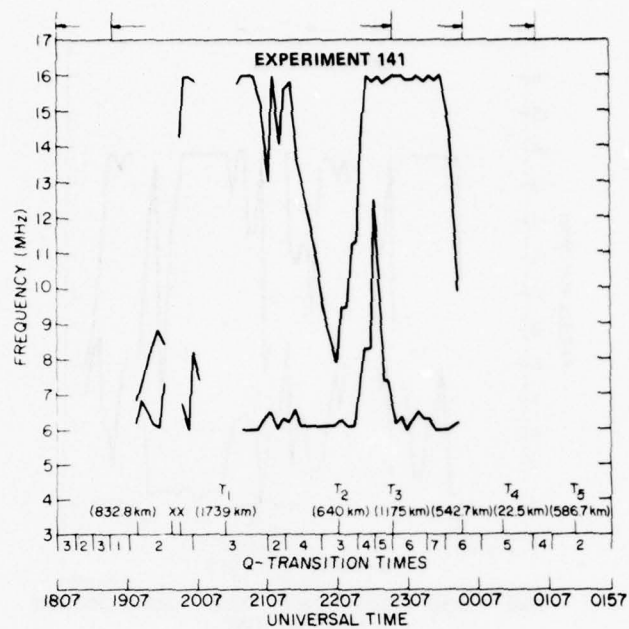


Figure 17. 1-E Modes Observed at Aircraft Showing Q-Transition Times (Cont)

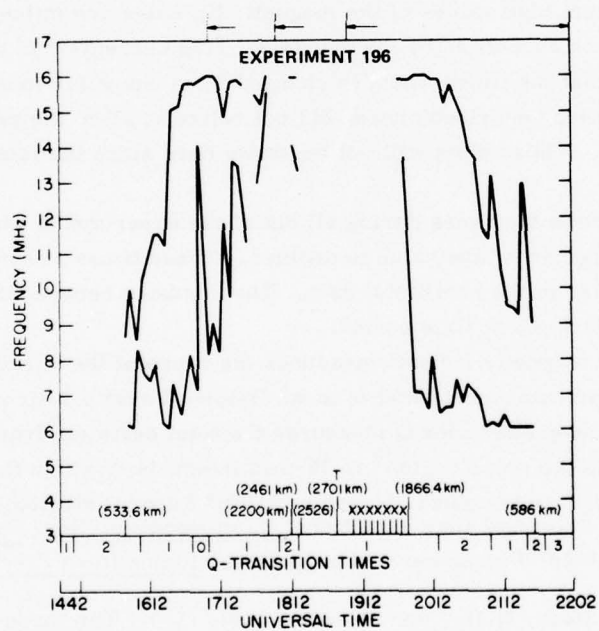
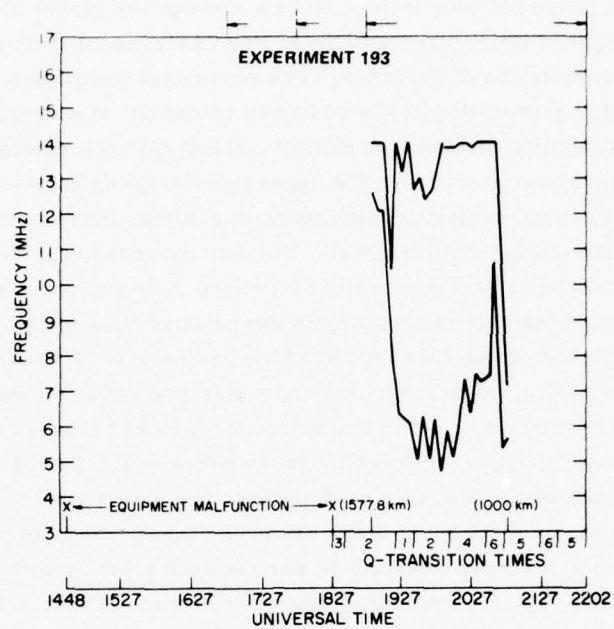


Figure 17. 1-E Modes Observed at Aircraft Showing Q-Transition Times (Cont)



The Magnetic Index AE was devised to be a measure of global electrojet activity.<sup>6</sup> At any given time, anywhere from five to eleven auroral zone stations contribute to the calculation of the Index. The horizontal component of the geomagnetic field (after elimination of the quiet day variation) at each 2.5-min interval at each of the contributing stations is plotted against UT on a common scale. Two envelopes are then drawn to embrace the upper and the lower points. The AE Index then consists of the numerical difference in gammas between the lower and upper envelopes at each 2.5-min interval. For our purposes, the 2.5-min value can be considered to be instantaneous (that is, there is no practical necessity to take into account any possible uncertainty in the putative time of their occurrence).

It has already been stated that the planetary Kp Index<sup>7,8</sup> did not correlate significantly, in a statistical sense, with the characteristics of the observed signals during these six experiments. Kp is the mean standardized K index from 12 observatories lying in northern and southern latitudes between 47° and 63° geomagnetic latitude. The K Indices for the individual stations are determined from the largest of the maximum ranges of the most disturbed of the three components of the geomagnetic field during the 3-hr intervals at each station starting with the interval 0000 UT to 0300 UT. Kp is essentially a measure of mid-latitude activity but, during periods of great magnetic activity, the auroral electrojets may move equatorward so that high values of the magnetic Kp Index are influenced by the auroral electrojets as well as by the equatorial ring currents. In this report, it was also shown that the times when Kp changed from one value to another, according to the convention described above, did not relate at all to the propagation events mentioned above. These plots will not be shown here since the lack of correlation is so obvious.

Figure 17 shows the times during all six of the experiments when the values of the Index Q changed from one value to another. These times are indicated by short lines perpendicular to the horizontal axis. The numbers between the lines indicate the values of Q during that time period.

Whereas the magnetic Index K measures the range of the variation of one of the three magnetic components that is most disturbed over a 3-hr period as stipulated above, the magnetic Index Q measures the total deviation from the normal quiet day curve in the polar region<sup>9</sup> in 15-min intervals of which the first for

6. Davis, T. Neil, and Sugiura, Masuhisa (1966) Auroral electrojet activity index AE and its universal time variations, J. of Geophys. Res. 71(No. 3).
7. Bartels, J. (1938) Potsdamer erdmagnetische Kennziffern Ztschr. f. Geophysik, 14:68-78.
8. Bartels, J., Heck, N.H., and Johnson, H.R. (1939) The three-hour-range index measuring geomagnetic activity, Terr. Magn. 41:411-454.
9. Bartels, J., and Fukushima, N. (1956) A Q index for the geomagnetic activity in quarter-hourly intervals, Akad. Wiss. Gothingen. Math-Phys. Klasse. Sonderhoft, No. 3.

each universal day is centered on 0000 UT (that is, it extends from 2352.5 UT of the previous UT day to 0007.5 UT of the current day). The 96 successive 15-min intervals follow one another continuously until the last one which is centered at 2345 UT and terminates at 2352.5 UT. The sequence for the next UT day then starts — ad infinitum. There is only one scale for all stations that calculate the Index Q which has 12 steps from 0 to 11. From my own perusal of years of these data, it is apparent that the values 9, 10 and 11 rarely occur. A further distinction between K and Q is that Q measures the total deviation from the quiet day normal curve of the most disturbed of the two horizontal components of the geomagnetic field only and not the Z component at all. Furthermore, it is very easy to determine the absolute level of the normal quiet day curve at the latitudes where Q is measured as has been pointed out in Reference (10).

During the IGY-IGC, 19 stations calculated Q at some time. However, shortly afterward, all but two stations terminated this calculation. Since 1966 only Sodankyla, Finland has made this calculation.

There was a grand total of 70 changes in Q during these six experiments. Their occurrence times will be referred to as Q-transition times.

One must realize that the Index Q is calculated during 15-min intervals starting, on each UT day, with the interval centered at 0000 UT and continuing one after the other until the interval centered at 2345 UT. If the convention was to start the initial interval elsewhere in UT time, the times when Q could change would be correspondingly different as would some of the Q values observed. If three or more consecutive 15-min intervals have the same Q value at a particular station, then the non-terminal intervals will retain the same value of Q regardless of the starting convention. However, the putative Q-transition times, which are the only times indicated in Figure 17, have an uncertainty associated with them which is assumed here to be  $\pm 7.5$  min — clearly a generous estimate (that is, the uncertainty is probably less than this).

Because of the fact that the sweep frequency ionospheric measurements were made at 5-min intervals, it is necessary to restrict this range to  $\pm 5.0$  min in practice.

What is meant by this is that when any defined event occurs within  $\pm 5$  min of one of the putative Q-transition times marked on Figure 17, then the two occurrences are considered to be simultaneous. Should a defined event occur +10 min after one of the putative Q-transition times marked in Figure 17, then it is considered to have occurred +5 min after the putative Q-transition time in question. This convention is followed throughout this phase of the analysis for both positive and negative deviations of the time of event occurrences from the time of the

10. Lincoln, J.V. (1967) *Geomagnetic Indices, Physics of Geomagnetic Phenomena*, Academic Press, pp 67-100.

putative Q-transition times. Naturally, the closest temporal correlation is chosen in every case.

Based on the above considerations, Figure 18 is a histogram which indicates the temporal correlation of the occurrences of Q-transitions with the 113 events defined above which occurred during these six experiments in the one-hop E modes. A plus deviation indicates that the event occurred after the most appropriate Q-transition time while a minus deviation indicates that it occurred before the most appropriate Q-transition time.

Nineteen Q-transitions occurred outside of S and E pairs and three that occurred within S and E events could not be correlated optimally with any event. These 22 Q-transitions are thus irrelevant.

The distribution of the deviations of events from the Q-transition times is quite pronounced and indicates a high degree of correlation as, indeed, does the same histogram when the putative transition points themselves are used—although the degree of correlation is understandably diminished in the latter case.

In this study, Q-transitions were also considered not to be relevant if they occurred during an auroral substorm or some other event or sequence of events such as an extended period of receiver instability as occurred during Experiment 58 between 2322 UT and 0005 UT.

Figure 19 is a histogram identical to the one described above but indicating only the temporal correlation of Q-transitions with S and E events which, after all, are very important propagation characteristics. It, too, indicates a high degree of temporal correlation between the Q-transition times and the times of occurrence of the S and E events. The similar histogram, based on the putative Q-transitions also indicates a high degree of correlation but, naturally, diminished in comparison to the one in Figure 19.

The list of all the S and E events that occurred during these six experiments is given in Section 3.1.7.

#### 3.1.4 INSTANTANEOUS AURORAL OVAL

It has been shown by Feldstein and Starkov<sup>11</sup> on the basis of ground-based optical observations, that the value of Q, which is calculated at a station ideally located at a geomagnetic latitude of 67° 50'N is highly correlated with the position shape, and size of the auroral oval. They performed their correlations with the Q Index measured in the so-called midnight sector from 2200 to 0200 local time.

11. Felstein, Y. I., and Starkov, G. V. (1967) Dynamics of auroral belt and polar geomagnetic disturbances, Planet. Space Sci. 15:209-229.

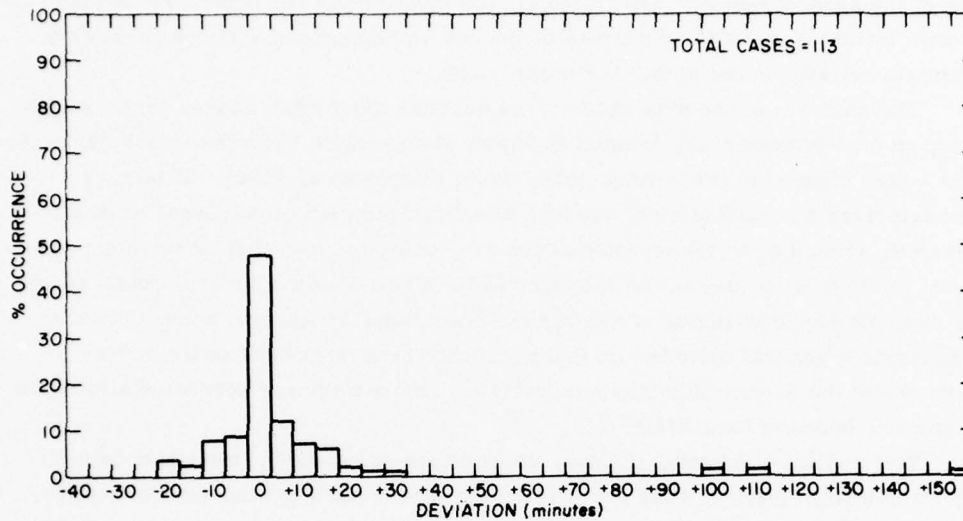


Figure 18. Histogram of Percentage of Occurrence of All Significant and Relevant Events for the One-Hop E Mode for All Experiments Compared Temporally with Q-Transition Occurrences

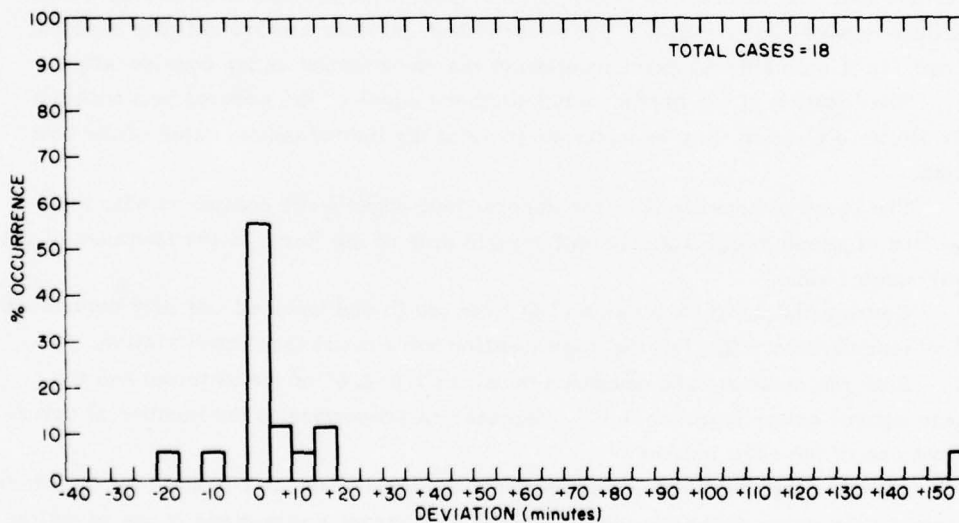


Figure 19. Histogram of Percentage of Occurrence of S and E Events for the One-Hop E Mode Compared Temporally with Q-Transition Occurrences



To quote directly from the Feldstein and Starkov paper mentioned in the previous paragraph,

"Using IGY-IGC all-sky camera films from many stations, the width and location of the auroral belt are determined. The positions of the edges are defined, at 15-min intervals for different times of the day and compared with the Q-index of magnetic activity on the night side of the Earth.

"The analysis of the data showed that aurorae most often appear in the zenith along an oval-shaped zone, located at higher geomagnetic latitudes on the day side than on the night side (Feldstein, 1960, 1963; Khorosheva, 1962). This zone characterizes a distribution of aurorae at a fixed moment of universal time and is oriented, according to the position of the Sun, in such a way that on the night side of the Earth it is located at the latitudes of the Fritz-Vestine auroral zone, and on the day side at the latitudes of the inner Alfven-Nikolsky auroral zone. Thus it represents a general distribution embracing the separate cases of the Fritz-Vestine and the Alfven-Nikolsky auroral zones characterizing aurorae distribution at specific hours of local time.

"The method of locating the oval-shaped zone is based on statistical data on the latitudinal variation of the auroral occurrence frequency, the zone being provisionally taken to be the region where this exceeds a nominal value [taken to be 0.6 by Sandford (1964) and Feldstein (1966a)]. It does not however give us precise information about the latitude interval in which aurorae are observed directly in the zenith, that is, the width of the auroral belt. In this paper the term 'zone' will denote the region of latitudes in which aurorae most often appear and the term 'auroral belt' will denote the region of latitudes, with precise boundaries, where aurorae appear in the zenith. The auroral belt has thus a more definite physical sense, as it indicates an exact location of the phenomenon under consideration.

"The location of the northern and southern edges of the auroral belt within a 15-min time interval may be assumed to yield the instantaneous value of the belt width.

"The observed positions of the auroral belt edges were compared with the Q-index of geomagnetic activity on the night side of the Earth at the latitudes of the oval-shaped zone.

"Corresponding to each value of Q from ten to one hundred and fifty determinations (usually about fifty) of the edge location were made from each station.

"Both the mean square deviation (equal to  $1.0-1.5^\circ$  of the latitude) and the mean square error (equal to  $0.2^\circ$ ), decrease in proportion to the number of determinations of the edge location."

Feldstein and Starkov have proven that the instantaneous auroral oval is determined by the value of the magnetic Index Q concurrently measured in the so-called midnight sector.

This section addresses the geometry of this Instantaneous Oval in relation to the geometry of the propagation path and temporal changes which occur in this relationship. It adopts the model of Feldstein and Starkov as to the dependence of

the Instantaneous Oval on the magnetic Index  $Q$  and, by showing that the adoption of this model in an entirely different study than the one conducted by Feldstein and Starkov leads to the solution of an important problem, indicates that they are very likely correct in their description of the position, size and shape of the Instantaneous Oval as a function of the magnetic Index  $Q$  except that they probably have imposed an unnecessary restriction on their model.

Figure 20<sup>12</sup> shows the  $Q$  oval for  $Q = 3$  which is often used in polar studies both for analytical and illustrative purposes. Since the edges of these ovals have been determined statistically, there is some uncertainty as to their exact location. However, the uncertainty is small.

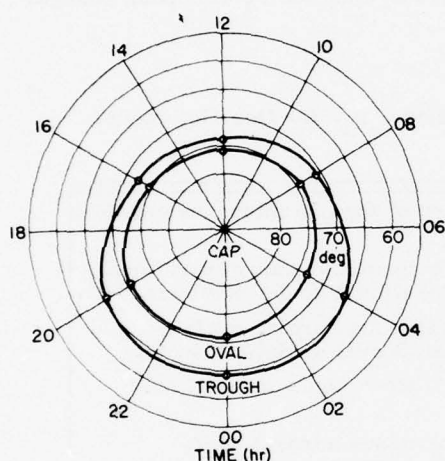


Figure 20. Instantaneous Auroral Oval for Geomagnetic Activity Level  $Q = 3$

Figure 20 shows the three regions that exist in the polar region. North of the poleward edge of the  $Q$  oval is the polar cap region. Then there is the  $Q$  oval itself. Finally, there is the region south of the equatorward edge of the  $Q$  oval known as the trough whereupon the polar ionosphere merges with the mid-latitude ionosphere. The location of the southern edge of the trough is not precisely known as a function of geophysical and temporal parameters at this time. The trough can be quite narrow or, apparently, can be over  $10^\circ$  of latitude in extent.

Each of these three polar regions has its own ionospheric characteristics as do the boundaries of the oval itself. The existence and geometry of the oval is defined by the precipitation of energetic particles which probably originate in the solar wind.<sup>13</sup> The geometry of the oval may be related to the direction of the

12. Comfort, R. H. (1972) Auroral Oval Kinematics Program, NASA CR-613-73.

13. Thorne, R. (1975) Ionospheric-magnetospheric coupling, Review of Geophysics and Space Physics, 13(No. 3).

Interplanetary Magnetic Field, but this relationship is not well understood at this time.<sup>14</sup>

The geographical points of interest in a one-hop mode of ionospheric propagation are the transmitter location, the receiver location, and the location of the reflection point (which is considered to be at the midpoint of the path for a one-hop mode). In this study, nine conditions (the  $r_1$ -conditions) have been defined in which these three points have been considered in relation to the location of the auroral oval, the polar cap, and the sub-auroral region from the poleward trough wall southward.

In Table 2 are listed the definitions of each of the nine possible values of the  $r_1$ -condition which could occur during these six experiments. Table 3 indicates the 72 theoretically possible values of the Index  $R_1$  that could arise due to all possible  $r_1$ -condition changes. The  $r_1$ -conditions persist over a period of time while the  $R_1$  indices occur instantaneously when the  $r_1$ -condition changes from one value to another. For example the  $R_1 = 10$  Index occurs when the  $r_1$ -condition changes from 2 to 3.

Table 2. Definitions of the Reilly Conditions,  $r_1$ , for One-Hop Modes of HF Propagation

$r_1 = 1$	GB, MP, A/C all equatorward of the instantaneous auroral oval as defined by Q.
$r_1 = 2$	GB and MP equatorward of the instantaneous auroral oval; A/C in the instantaneous auroral oval as defined by Q.
$r_1 = 3$	GB equatorward of the instantaneous auroral oval; MP and A/C in the instantaneous auroral oval as defined by Q.
$r_1 = 4$	GB, MP, and A/C all in the instantaneous auroral oval as defined by Q.
$r_1 = 5$	GB equatorward of the instantaneous auroral oval; MP in the instantaneous auroral oval; and A/C in the polar cap poleward of the instantaneous auroral oval as defined by Q.
$r_1 = 6$	GB and MP in the instantaneous auroral oval; A/C in the polar cap poleward of the instantaneous auroral oval as defined by Q.
$r_1 = 7$	GB in the instantaneous auroral oval; MP and A/C in the polar cap poleward of the instantaneous auroral oval as defined by Q.
$r_1 = 8$	GB and MP equatorward of the instantaneous auroral oval; A/C in the polar cap poleward of the instantaneous auroral oval as defined by Q.
$r_1 = 9$	GB equatorward of the instantaneous auroral oval; MP and A/C in the polar cap poleward of the instantaneous auroral oval as defined by Q.

GB = Goose Bay      MP = Midpoint      A/C = Aircraft

14. Evans, J.V. (1975) A review of F region dynamics, Review of Geophysics and Space Physics, 13(No. 3).

Table 3. Definitions of the Reilly Indices,  $R_1$ , in Terms of all Possible  $r_1$ -Condition Transitions

$R_1$	$r_1$ -Condition Transition	$R_1$	$r_1$ -Condition Transition	$R_1$	$r_1$ -Condition Transition
1	1-2	25	4-1	49	7-1
2	1-3	26	4-2	50	7-2
3	1-4	27	4-3	51	7-3
4	1-5	28	4-5	52	7-4
5	1-6	29	4-6	53	7-5
6	1-7	30	4-7	54	7-6
7	1-8	31	4-8	55	7-8
8	1-9	32	4-9	56	7-9
9	2-1	33	5-1	57	8-1
10	2-3	34	5-2	58	8-2
11	2-4	35	5-3	59	8-3
12	2-5	36	5-4	60	8-4
13	2-6	37	5-6	61	8-5
14	2-7	38	5-7	62	8-6
15	2-8	39	5-8	63	8-7
16	2-9	40	5-9	64	8-9
17	3-1	41	6-1	65	9-1
18	3-2	42	6-2	66	9-2
19	3-4	43	6-3	67	9-3
20	3-5	44	6-4	68	9-4
21	3-6	45	6-5	69	9-5
22	3-7	46	6-7	70	9-6
23	3-8	47	6-8	71	9-7
24	3-9	48	6-9	72	9-8

We have stated above that the Index  $Q$  can have values from zero to eleven. However, values above eight did not occur during these six experiments. We have given an example in Figure 20 of the auroral oval defined for  $Q = 3$ . There are ovals defined for all values of  $Q$  from zero to eight and they vary in size and shape considerably.

It has been common in studies of HF Polar Propagation to assume that one particular value of  $Q$  and, hence, one particular configuration of the oval persists throughout the experiment. However, in an 8-hr experiment  $Q$  could conceivably change 32 times from one value to another. However, the magnetic Index  $Q$  actually has a high degree of persistence.



This high degree of persistence is evident in Table 4 in which are listed, in order, all of the values of the magnetic Index  $Q$  that were computed during these six experiments. There were long periods (up to 195 minutes) when the published value of  $Q$  remained constant. In all 169 of the relevant conventional 15-min periods listed in Table 4,  $Q$  changed by zero from one period to the next 92 times; by an increment of only one numerical category 68 times; by an increment of only two numerical categories nine times; and never by more than an increment of two numerical categories. There are 42 hours and 5 minutes within 169  $Q$  intervals out of which only nine consecutive  $Q$ -transitions changed by more than one numerical value; never changing by more than two.

The approach taken here has been to create a composite instantaneous auroral oval consisting of the concatenation of the positions of the edges of the Feldstein and Starkov ovals corresponding, for each time period, to the value of the magnetic Index  $Q$  which existed over that period during each of the six experiments. This produced the results shown in Figures 21 to 26. The composite ovals are quite different from any single oval associated with any single value of  $Q$ . Thus, the dynamic character of the auroral oval is explicitly taken into account.

Figure 27 is a reproduction of Figure 14 with lines perpendicular to the horizontal axis which indicate the times at which the  $R_1$  Index occurred during these six experiments. The value of the prevailing  $r_1$ -condition is indicated between the dark lines. The subscript 1 indicates that a one-hop mode is being considered. When the two-hop modes are considered, the subscript 2 is used.

In Table 5, we have listed the relevant  $R_1$  values which actually occurred for the one-hop E mode in all six of these experiments and have indicated the location and changes in location of the transmitter, the midpoint, and the receiver which occurred at such times relative to the composite instantaneous oval.

All  $R_1$  Indices are considered to be relevant and significant except those that occur prior to the first  $R_1$  Index associated with an  $S_1$ , between the  $R_1$  Indices associated with an  $E_1$  and the following  $S_2$ , after the last  $R_1$  Index associated with an  $E_2$ , or during an extended period of equipment malfunction.

In the case of the  $R_1$  Indices, not all of the events defined to be significant for the  $Q$ -transition analysis are relevant. Such events are relevant providing they did not occur during an  $r_1 = 1$  condition or an  $r_1 = 4$  condition prior to the occurrence of the first  $R_1$  Index of the experiment or after the last  $R_1$  Index. The other restrictions with respect to extraordinary conditions also apply in this case as in the  $Q$  transition case.

In the  $r_1 = 1$  condition, all three of the relevant propagation points are in the region south of the equatorward edge of the instantaneous  $Q$  oval. This is an ordinary propagation problem. This occurs only at the start of Experiment 196.

Table 4. Values of the Index Q During Each Fifteen-Min Interval During Each Experiment

Experiment 58	Experiment 60	Experiment 141	Experiment 142	Experiment 193	Experiment 196
Time (UT) Q	Time (UT) Q	Time (UT) Q	Time (UT) Q	Time (UT) Q	Time (UT) Q
2100 4	0000 7	1745 4	2030 7	1800 4	1445 1
2115 5	0015 7	1800 4	2045 7	1815 4	1500 2
2130 6	0030 6	1815 3	2100 7	1830 3	1515 2
2145 7	0045 6	1830 2	2115 6	1845 2	1530 2
2200 8	0100 6	1845 3	2130 7	1900 2	1545 2
2215 8	0115 6	1900 1	2145 7	1915 2	1600 1
2230 8	0130 6	1915 2	2200 7	1930 1	1615 1
2245 8	0145 5	1930 2	2215 6	1945 2	1630 1
2300 7	0200 5	1945 2	2230 6	2000 2	1645 0
2315 7	0215 4	2000 2	2245 5	2015 4	1700 1
2330 7	0230 3	2015 3	2300 6	2030 4	1715 1
2345 8	0245 3	2030 3	2315 6	2045 6	1730 1
0000 8	0300 2	2045 3	2330 6	2100 5	1745 1
0015 7	0315 1	2100 3	2345 6	2115 5	1800 2
0030 6	0330 1	2115 2	0000 5	2130 6	1815 1
0045 5	0345 3	2130 4	0015 5	2145 5	1830 1
0100 4	0400 1	2145 4	0030 5	2200 5	1845 1
0115 5	0415 3	2200 3	0045 6	2215 3	1900 1
0130 5	0430 2	2215 3	0100 5	2230 2	1915 1
0145 5	0445 1	2230 4	0115 3		1930 1
0200 5	0500 1	2245 5	0130 2		1945 1
0215 4	0515 1	2300 6	0145 2		2000 1
0230 4	0530 1	2315 6	0200 2		2015 2
0245 4	0545 1	2330 7	0215 2		2030 2
0300 3	0600 1	2345 6	0230 2		2045 2
0315 3	0615 2	0000 6	0245 2		2100 1
0330 3	0630 1	0015 5	0300 2		2115 1
	0645 1	0030 5	0315 2		2130 2
	0700 2	0045 5	0330 2		2145 3
	0715 2	0100 4	0345 2		2200 3
	0730 1	0115 2	0400 2		
	0745 1	0130 2	0415 2		
	0800 1	0145 2	0430 2		
		0200 2			

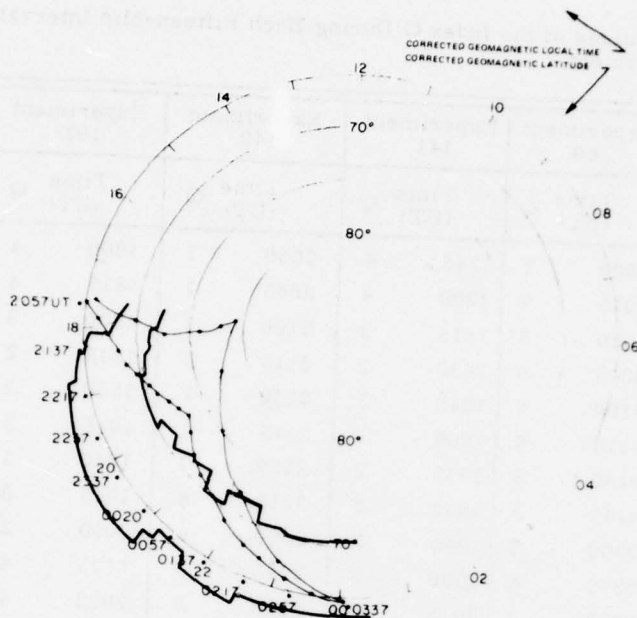


Figure 21. Composite Instantaneous Auroral Oval for Experiment 58

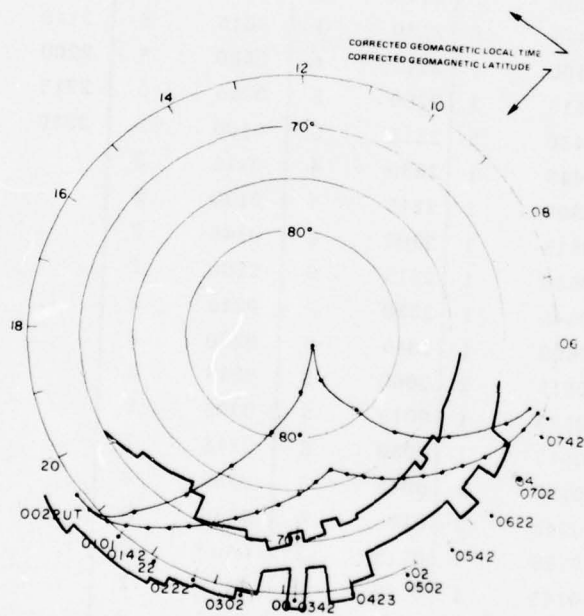


Figure 22. Composite Instantaneous Auroral Oval for Experiment 60

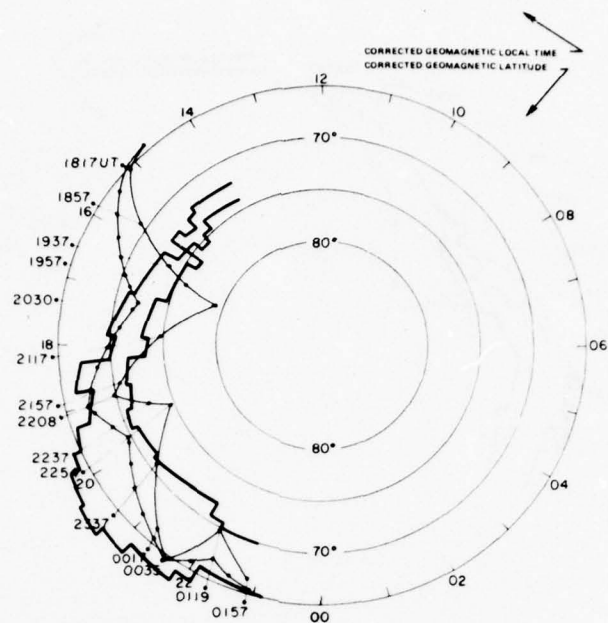


Figure 23. Composite Instantaneous Auroral Oval for Experiment 141

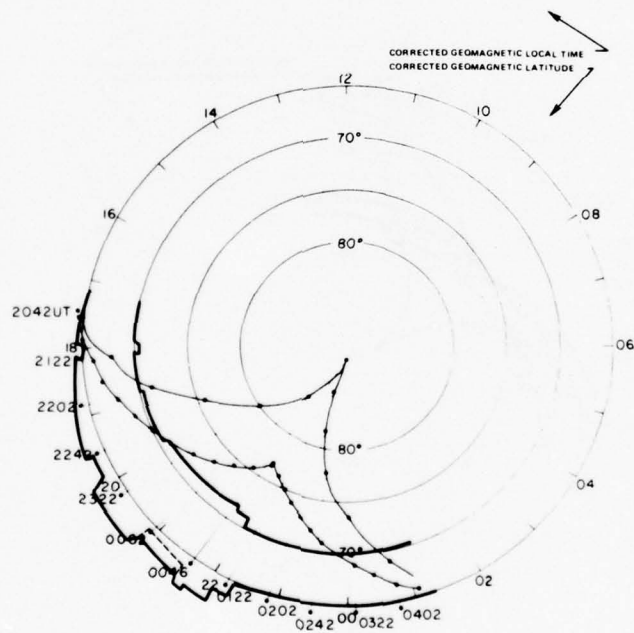


Figure 24. Composite Instantaneous Auroral Oval for Experiment 142



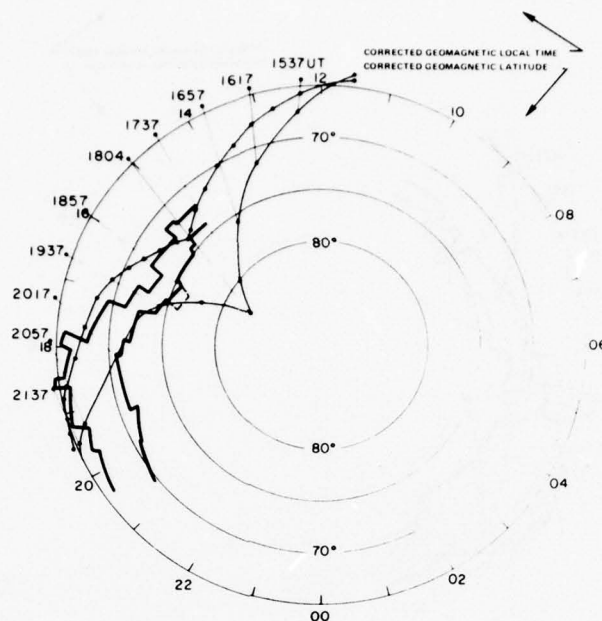


Figure 25. Composite Instantaneous Auroral Oval for Experiment 193

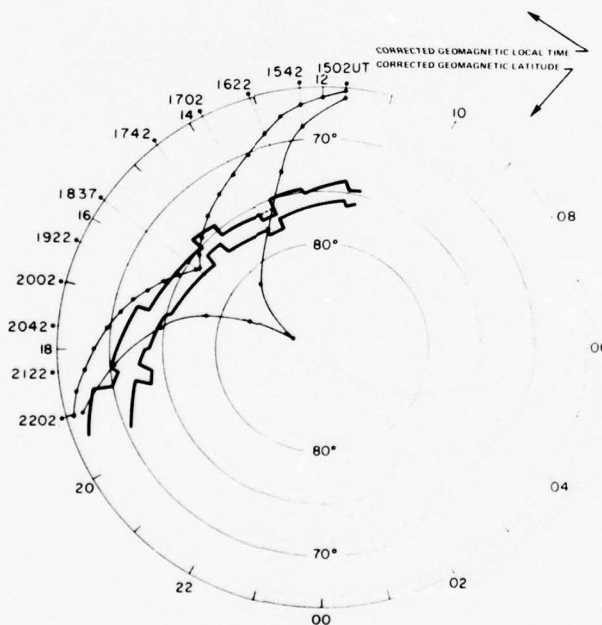


Figure 26. Composite Instantaneous Auroral Oval for Experiment 196

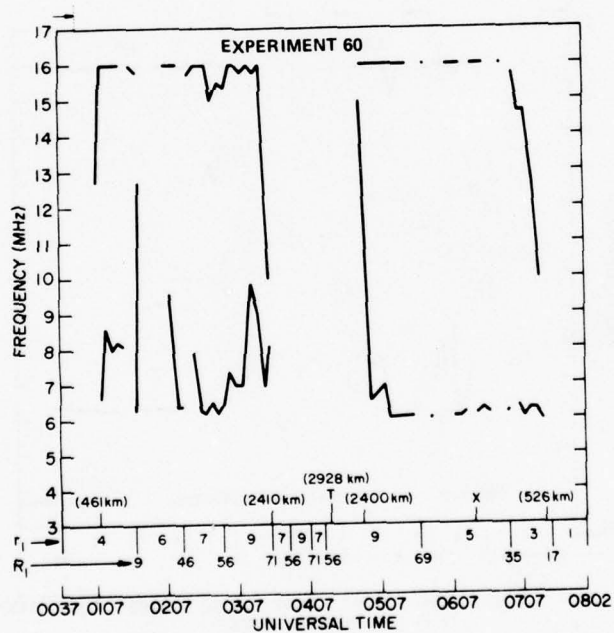
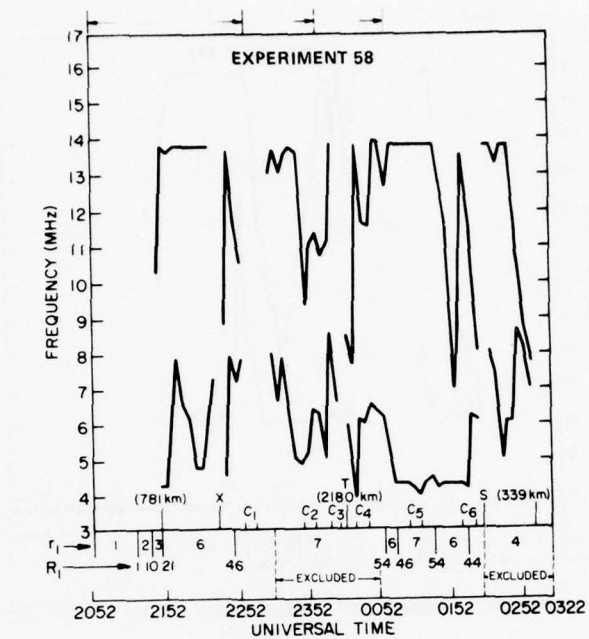


Figure 27. 1-E Modes Observed at Aircraft Showing  $r_1$ -Conditions and  $R_1$  Indices

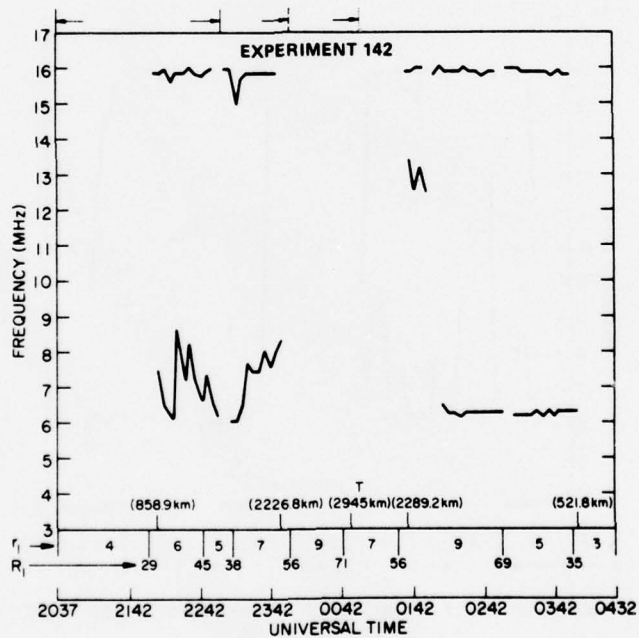
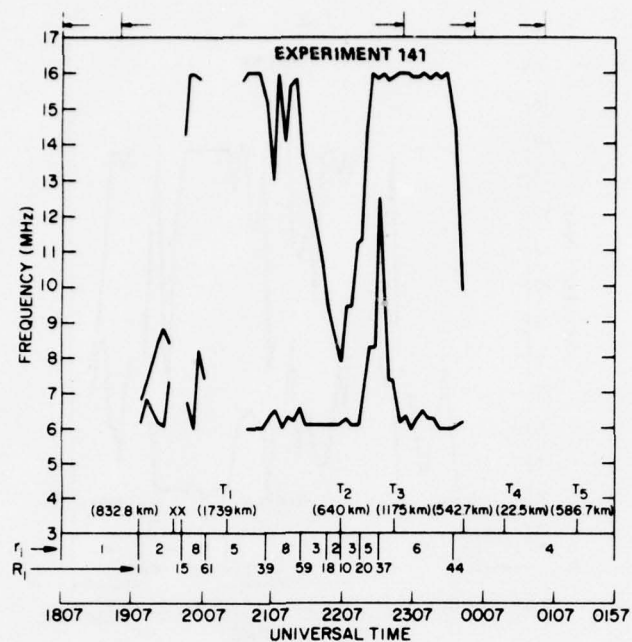


Figure 27. 1-E Modes Observed at Aircraft Showing  
r<sub>1</sub>-Conditions and R<sub>1</sub> Indices (Cont)

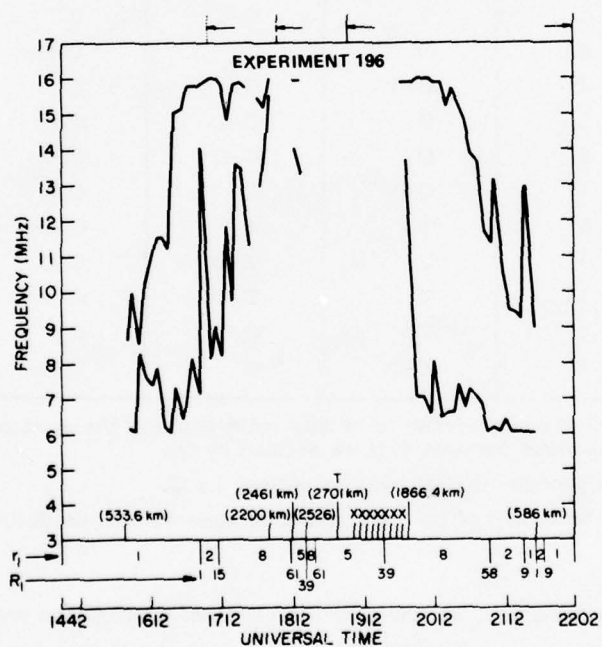
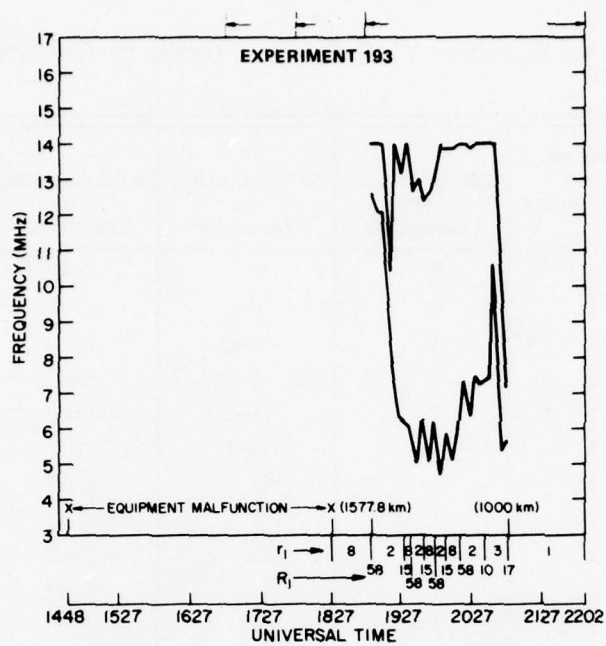


Figure 27. 1-E Modes Observed at Aircraft Showing  $r_1$ -Conditions and  $R_1$  Indices (Cont)



Table 5. Relevant  $R_1$  Indices Which Occurred During the One-Hop E Mode in All Six Experiments

$R_1$	Number of Relevant Occurrences of $R_1$	GB Location or Transition	MP Location or Transition	A/C Location or Transition	Transitions: 1 = GB 2 = MP 3 = A/C
1	3	T	T	T-O	3
9	1	T	T	O-T	3
10	2	T	T-O	O	2
15	5	T	T	O-C	3
17	1	T	O-T	O-T	2, 3
18	1	T	O-T	O	2
20	1	T	O	O-C	3
21	1	T-O	O	O-C	1, 3
29	2	O	O	O-C	3
35	2	T	O	C-O	3
37	1	T-O	O	C	1
38	1	T-O	O-C	C	1, 2
39	1	T	O-T	C	2
44	2	O	O	C-O	3
45	1	O-T	O	C	1
46	3	O	O-C	C	2
54	2	O	C-O	C	2
56	4	O-T	C	C	1
58	5	T	T	C-O	3
59	1	T	T-O	C-O	2, 3
61	1	T	T-O	C	2
69	2	T	C-O	C	2
71	1	T-O	C	C	1

T = "Trough" (here considered to be any point south of the equatorward edge of the instantaneous auroral oval as defined by Q).

O = The instantaneous auroral oval as defined by Q.

C = Polar Cap poleward of the instantaneous auroral oval as defined by Q.

In the  $r_1 = 4$  condition, all three of the relevant propagation points are within the instantaneous Q oval. If this situation persists, as it does for  $E_1$  of Experiment 58 and  $S_1$  of Experiment 60, then the first appearance or final disappearance of the signal can occur at a time when an  $r_1$ -condition transition could not possibly occur.

Its occurrence then depends upon the properties of the polar ionosphere that is completely contained within the instantaneous Q oval in relation to the flight path involved.

Note the dashed bracket in Figure 24 which indicates that allowance has been made during this 45-min period for an uncertainty of  $1^\circ$  in latitude for the equatorward edge of the instantaneous Q oval. Q was equal to 5 during this period. In Figure 25, the dashed bracket indicates that, for a period of about 20 min, allowance has been made for an uncertainty of  $1^\circ$  in latitude of the poleward edge of the instantaneous Q oval. Q was equal to 2 during this period. In Figure 26, the dashed bracket indicates that, for a period of about 20 min, allowance has been made for a  $0.5^\circ$  uncertainty in the latitude of the poleward edge of the instantaneous Q oval. Q was equal to zero during this period.

The results produced in the immediately following analysis justify the assumption of these three brief periods of uncertainty in the latitude of the instantaneous Q oval.

### 3.1.5 EXAMPLE-EXPERIMENT 141

In Figure 28, Experiment 141 has been isolated in order to demonstrate the high degree of temporal correlation between the  $R_1$  Indices and the characteristics of the HF signal. A histogram will be shown later in this report that indicates the temporal deviation of all relevant and significant propagation events from relevant  $R_1$  Indices for all of the one-hop E modes observed during all six of the experiments being considered.

For now, Figure 28 will serve to demonstrate the general relationship. Note that the signal first is detected when the aircraft is 832.8 km from the Goose Bay transmitter at 1917 UT and is last detected when the aircraft is 542.7 km from the Goose Bay transmitter. There are three turns: at 1739 km, 640 km, and 1175 km north of Goose Bay in between the above two points. The flight path of the aircraft is always either northward or southward of Goose Bay (see Figure 3).

Ten  $R_1$  Indices occurred during this experiment as has been shown in Figure 28. In chronological order, they were:  $R_1 = 1$ ,  $R_1 = 15$ ,  $R_1 = 61$ ,  $R_1 = 39$ ,  $R_1 = 59$ ,  $R_1 = 18$ ,  $R_1 = 10$ ,  $R_1 = 20$ ,  $R_1 = 37$ , and  $R_1 = 44$ . The noteworthy propagation events were: the first and last detection of the signal; a 10-min period of signal blackout caused by equipment malfunction; a sudden increase in the total frequency window width; and a number of significant variations in the Maximum Observable Frequency (MOF) and the Lowest Observable Frequency (LOF) greater than 0.5 MHz as well as a 35-min period of total signal blackout.

The signal first appears at 1917 UT at the same time that the  $R_1 = 1$  Index occurs. A rationale will be given later in the report for the anomalously narrow frequency window width at this time. The slope of the MOF immediately starts to

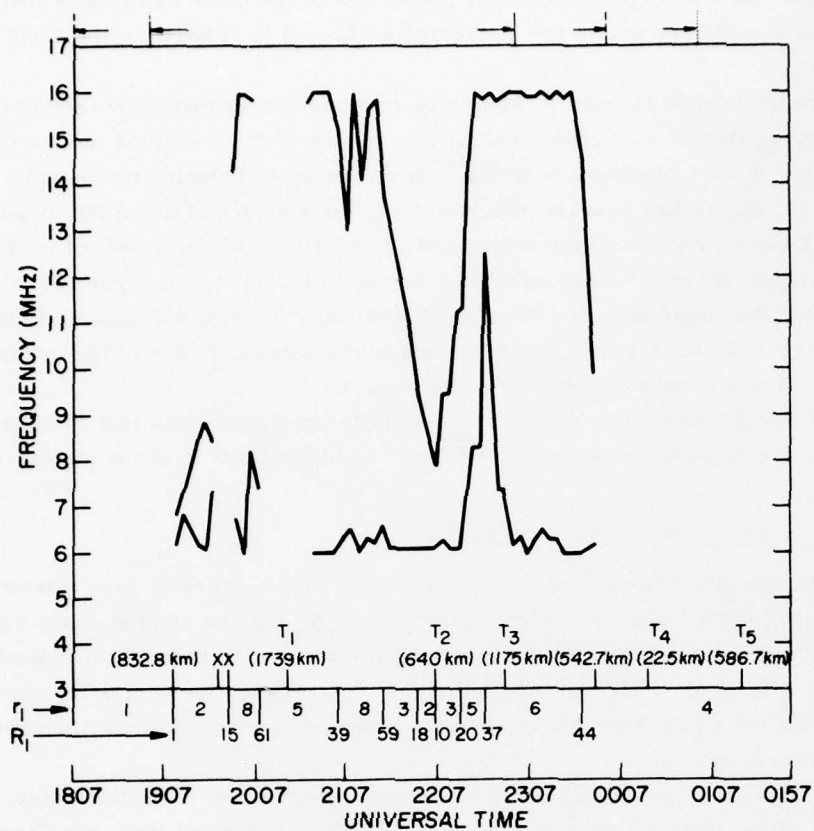


Figure 28. Experiment 141 as an Example of the Events that Can Occur and the Occurrences of  $R_1$  Indices

rise while the slope of the LOF increases and then decreases. The frequency window width suddenly widens very significantly at 1957 UT while the  $R_1 = 15$  Index occurs at 1952 UT. A 35-min period of total signal blackout starts at 2012 UT and the  $R_1 = 61$  Index occurs at 2012 UT also. At 2102 UT, a period of fluctuations of the MOF and the LOF starts which ends at 2132 UT. The  $R_1 = 39$  Index occurs at 2102 UT and the  $R_1 = 59$  Index occurs at 2132 UT. At 2132 UT, the MOF begins a very long-lived and deep decrease. The  $R_1 = 59$  Index occurs at 2132 UT also. The decrease in the MOF stops at 2207 UT and a rapid increase begins. The  $R_1 = 10$  Index occurs at 2207 UT. At 2222 UT, the LOF starts to rise rapidly and the  $R_1 = 20$  Index occurs at the very same time. At 2237 UT the slope of this increase in the LOF changes markedly and the  $R_1 = 37$  Index occurs at the very same time.

At 2342 UT, the MOF starts a rapid decrease and, 10 min later, the signal is last seen during this experiment. The  $R_1 = 44$  Index occurs at 2342 UT.

So far we have not mentioned the  $R_1 = 18$  Index which occurred at 2157 UT. At this time, a minor change in the slope of the decreasing MOF occurred that is not considered to be significant at this time.

All of the  $R_1$  Indices that occurred during this experiment were relevant and significant. Also, all of the propagation events mentioned above were relevant and significant except the event that occurred at 2157 UT. This is not considered to be significant at this time. There were no other propagation events that were not considered significant that were simultaneous with the occurrence of an  $R_1$  Index in any of the six experiments.

On the basis of Figure 28 and the above discussion, we can construct the histogram in Figure 29 which shows the percentage of the total number of relevant and significant propagation events which deviated from an  $R_1$  Index by the amount of time indicated. This histogram shows how highly correlated temporally the  $R_1$  Indices are with the propagation events. A plus sign means that the event occurred after the  $R_1$  Index while a minus sign indicates that the event occurred before the  $R_1$  Index.

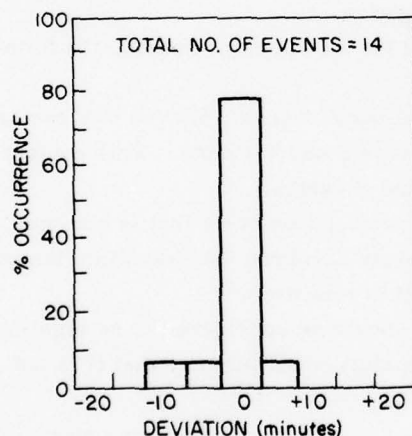


Figure 29. Deviation In Minutes  
(Experiment 141 as an example)

### 3.1.6 ALL RELEVANT PROPAGATION EVENTS - ONE-HOP E MODE

A histogram is shown in Figure 30 which shows the way in which the relevant and significant  $R_1$  Indices which occurred between the various  $S_1-E_1$ ,  $S_2-E_2$  combinations were correlated with significant and relevant propagation events.



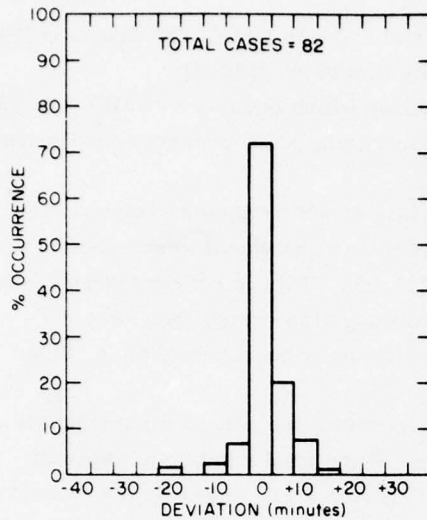


Figure 30. Histogram of Percentage of Occurrence of All Significant and Relevant Events for the One-Hop E Mode for All Experiments Compared Temporally with  $R_1$  Occurrences as Appropriate

The  $r_1 = 1$  and  $r_1 = 4$  conditions are special for geographical reasons as explained above. The  $r_1 = 5, 8$ , and  $9$  conditions are characterized by special propagation conditions. The  $r_1 = 5$  condition is characterized by numerous total signal outages. The  $r_1 = 8$  condition is characterized by numerous significant fluctuations in both the LOF and the MOF. The  $r_1 = 9$  condition is often characterized by anomalously long-range one-hop E mode propagation.

As far as the one-hop E mode is concerned for all six experiments, the following is a resume of the situation.

(1) There were a grand total of 55  $R_1$  Index occurrences. Eleven of these are not relevant at all because they did not fall between S and E events. This compares to 19 Q-transitions which did not fall between S and E events.

(2) One  $R_1$  Index was simultaneous with a propagation event that is not considered significant at this time. No other  $R_1$  Index occurred that was simultaneous with an event that was not considered significant at this time.

Future study could indicate that this event should be considered to be significant so that one should not term it insignificant prematurely but just say that it is not considered to be significant at this time.

(3) Two relevant and significant propagation events occurred during an  $r_1 = 9$  condition which accounts for their occurrence and renders a temporal comparison with the occurrence of an  $R_1$  Index meaningless.

(4) The fluctuations of the LOF and MOF that constitute the characteristic feature of an  $r_1 = 8$  condition are, in each of the three relatively extensive cases which occurred, counted as a single event.

One fact should be emphasized here. Not all  $R_1$  Indices occurred during those six experiments contemporaneously with a Q-transition. (The obverse case is even

more pronounced.) The  $R_1$  Indices, by definition, are indicative of a change from one  $r_1$ -condition to another which necessarily involves at least one transition of the boundaries of the instantaneous Q oval by the transmitter, the path midpoint, or the receiver. But the transition can occur because of the motion of the receiver and, hence, the midpoint as well as by changes in the instantaneous Q oval dimensions associated with a coincident Q transition. In fact, this was the case in 20 of the 45 relevant and significant  $R_1$  conditions that occurred during all six of these experiments.

This indicates that it is the  $r_1$ -condition transitions that are the more important rather than the Q-transitions as far as the occurrence of  $R_1$  Indices is concerned. Of course, the prevailing Q will determine the time, in the course of a given flight path, when an  $r_1$ -condition will occur (an  $r_1$ -condition transition corresponds exactly to one or more transitions of a Q oval edge).

The same uncertainty of  $\pm 0.5$  min should be invoked in those 25  $r_1$ -transitions which coincide with Q transitions. This has been done in the analysis of the temporal correlation of  $R_1$  Index occurrence with all events and with S and E events separately just as it was done in the case of Q transitions.

The histogram of the temporal correlation of the  $R_1$  Index occurrences with all propagation events is shown in Figure 30.

The superior precision of the  $R_1$  Index, in terms of temporal correlation with propagation events, as compared to the magnetic Q Index is clear from a comparison of Figure 30 with Figure 18.

### 3.1.7 S AND E EVENTS

The following is a list of all of the S and E events which occurred during all six of these experiments. Table 6 describes each such event in some detail including those in the following three lists that are primed.

Experiment 58:  $S_1, E_1$   
 Experiment 60:  $S_1, E_1, S_2, E_2$   
 Experiment 141:  $S_1, E_1$   
 Experiment 142:  $S_1, E_1, S_2, E_2$   
 Experiment 193:  $S_2, E_2$   
 Experiment 196:  $S_1, E_1, S'_1, E'_1, S_2, E_2$

There is a grand total of 20 cases of this type of event. The following is a list of events that were associated with an  $R_1$  Index.

Experiment 58:  $S_1$   
 Experiment 60:  $E_1, E_2$   
 Experiment 141:  $S_1, E_1$   
 Experiment 142:  $S_1, E_1, E_2$   
 Experiment 193:  $S_2, E_2$   
 Experiment 196:  $S'_1, E'_1, E_2$

There were 13 of these events associated with an  $R_1$  Index out of a total of 20.

Finally, the following is a list of the total number of these events that were not associated with an  $R_1$  Index.

Experiment 58:  $E_1$   
Experiment 60:  $S_1, S_2$   
Experiment 141: NONE  
Experiment 142:  $S_2$   
Experiment 193: NONE  
Experiment 196:  $S_1, E_1, S_2$

There were seven of these events that were not associated with an  $R_1$  Index. Each of these seven particular events will now be considered individually.

(1)  $S_1$  in Experiment 58 occurred during an auroral substorm so that its occurrence at this time is not considered relevant to this discussion. This extraordinary occurrence will be discussed in detail later in this report.

(2)  $S_1$  in Experiment 60 occurred during an  $r_1 = 4$  condition which lasted from 0037 UT until 0142 UT (65 min). In an  $r_1 = 4$  condition, all three of the relevant propagation points (transmitter location, reflection point, and receiver location) are within the auroral oval. This is an ordinary propagation situation and merely indicates that the ionosphere could not support a one-hop E mode at a shorter distance than this between transmitter and receiver. Its occurrence is not relevant to this discussion since the transition of an oval edge is not involved and, hence, no  $R_1$  Index could occur. The occurrence of  $S_1$  at this time and distance during an  $r_1 = 4$  condition is a natural result of the properties of the part of the ionosphere contained completely within the instantaneous Q oval.

(3)  $S_2$  in Experiment 60 occurred at a distance of 2400 km from Goose Bay, that is, about 180 km further than a one-hop E signal would normally be expected to come in. This is undoubtedly a characteristic of the very unusual  $r_1 = 9$  condition during which this  $S_2$  occurred. The occurrence of  $E_1$  at 2410 km during an  $r_1 = 9$  condition during this same experiment substantiates this supposition.

(4)  $S_2$  in Experiment 142 occurred at a distance of 2289.2 km from Goose Bay or almost 70 km further than a one-hop E mode signal would be expected to occur. This too occurred during an  $r_1 = 9$  condition.

(5)  $S_1$  in Experiment 196 occurred during an  $r_1 = 1$  condition that lasted from 1542 UT to 1647 UT (85 min). During an  $r_1$  condition, the transmitter, reflection point, and the receiver are all equatorward of the oval either in the trough or in the mid-latitude ionospheric region. In either case, it is not relevant to this discussion. There is nothing uniquely polar about it.

(6)  $E_1$  in Experiment 196 occurred at a normal one-hop E mode distance from the transmitter and hence is not relevant to this discussion.

(7)  $S_2'$  in Experiment 196 occurred immediately after a 40-min period of equipment malfunction and hence is not relevant to this discussion either.

In summary, one of these events occurred during an auroral substorm, one occurred after a period of equipment malfunction, one is explicable in terms of the characteristics of the ionosphere contained completely within the instantaneous Q-oval, two did not involve any unique polar region conditions, and two occurred during a particular  $r_1$ -condition which explains them.

Table 6. Description of Each S and E Event for All Six Experiments for the One-Hop E Mode

Experiment 58	$S_1$	- 781 km from GB; 2147 UT; 4.2 MHz to 10.3 MHz. Signal appeared just when the $R_1 = 10$ Index occurred.
	$E_1$	- 339 km from GB; 0302 UT; 7.0 MHz to 7.8 MHz. Last $R_1 = 44$ at 0207 UT. This $E_2$ occurred during an $r_1 = 4$ condition while an auroral substorm was in progress which dominated the behavior of the signal.
Experiment 60	$S_1$	- 461 km from GB; 0112 UT; 6.6 MHz to 12.8 MHz. Signal appears during an $r_1 = 4$ condition. The next $R_1 = 29$ occurred at 0142 UT.
	$E_1$	- 2410 km from GB; 0337 UT; 8.1 MHz to 10 MHz. Signal disappears just when $R_1 = 71$ .
	$S_2'$	- 2400 km from GB; 0457 UT; 15 MHz to 16 MHz. Signal appears during $r_1 = 9$ condition. Next $R_1 = 69$ at 0542 UT.
	$E_2$	- 526 km from GB; 0727 UT; 6 MHz to 10 MHz. Signal disappears just before $R_1 = 17$ .
Experiment 141	$S_1$	- 832.8 km from GB; 1917 UT; 6.2 MHz to 6.9 MHz. Signal appears just as an $R_1 = 1$ Index occurred.
	$E_1$	- 542.7 km from GB; 2352 UT; 6.2 MHz to 9.9 MHz. Signal window width was at the maximum of 10 MHz for the previous 55 min. At 2342 UT it started to drop precipitously just when an $R_1 = 44$ Index occurred.
Experiment 142	$S_1$	- 858.9 km from GB; 2207 UT; 7.5 MHz to 15.9 MHz. Signal appears just after $R_1 = 25$ Index occurred.
	$E_1$	- 2226.8 km from GB; 2352 UT; 8.4 MHz to 15.9 MHz. In this case we can utilize the probability that the equatorward edge of the Q oval is $1^\circ$ too far south and adjust it as shown by the dashed line in the figure. Then $R_1 = 56$ occurs at 2357 UT.
	$S_2'$	- 2289.2 km from GB; 0142 UT; 13.4 MHz to 15.9 MHz. Signal appears just after $R_1 = 36$ occurred at 0127 UT.
	$E_2$	- 521.8 km from GB; 0402 UT; 6.3 MHz to 15.8 MHz. Signal disappeared just after $R_1 = 35$ Index occurred at 0357 UT.



Table 6. Description of Each S and E Event for All Six Experiments for the One-Hop E Mode (Cont)

Experiment 193	$S_2$	- 1577.8 km from GB; 1907 UT; 12.6 MHz to 14.0 MHz. In this case we can use the probability that the poleward edge of the Q oval is $1^\circ$ too far south and adjust it as shown by the dashed line in the figure. The $R_1 = 38$ Index occurred at 1907 UT.
	$E_2$	- 1000 km from GB; 2057 UT; 5.6 MHz to 7.2 MHz. Signal disappeared just as an $R_1 = 17$ Index occurred.
Experiment 196	$S_1$	- 533.6 km from GB; 1547 UT; 6.2 MHz to 8.7 MHz. Signal appears during an $r_1 = 1$ condition. Next the $R_1 = 1$ Index occurs at 1637 UT.
	$E_1, S_1'$ and $E_1'$	- $E_1$ occurs at 2195.7 km from GB; 1752 UT; 15.8 MHz to 16 MHz. Signal disappears during an $r_1 = 8$ condition but reappears anomalously at 1812 UT 2461 km from GB just after an $R_1 = 61$ Index occurred. This is $S_1'$ . $E_1'$ occurs at 2576.7 km.
	$S_2'$	- 1866.4 km from GB; 1947 UT; 15.7 MHz to 15.8 MHz. Equipment malfunction makes it impossible to determine $S_2$ .
	$E_2$	- 586 km from GB; 2132 UT; 6 MHz to 9 MHz. Signal reappears just when an $R_1 = 9$ Index occurs.

In Figure 31 is shown a histogram which indicates the temporal correlation of the 13 relevant and significant S and E events with the occurrence of  $R_1$  Indices.

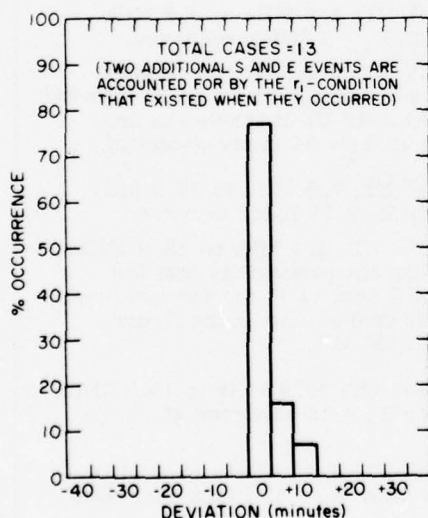


Figure 31. Histogram of Percentage of Occurrence of S and E Events for the One-Hop E Mode Compared Temporally with  $R_1$  Occurrences

Comparison of Figure 31 with Figure 19 clearly shows the superior precision of the  $R_1$  Index over the magnetic Q Index as far as temporal correlation with relevant and significant S and E events is concerned.

### 3.1.8 FREQUENCY WINDOW WIDTHS FOR $r_1$ -CONDITIONS

Table 7 indicates the mean value of the frequency window width for each value of  $r_1$  that occurred during these six experiments for the one-hop E mode. They range from 4.917 MHz to 9.078 MHz out of a possible 10.0 MHz. Also listed are the total number of complete signal blackouts. Note that the signal was completely blacked out during  $r_1$ -condition 5 for almost 40 percent of the time. Out of 3.67 hours during which the  $r_1 = 5$  condition existed during these experiments, the signal was blacked out for 1.62 hours.

Table 7. Mean Value of the Frequency Window Width for Each Value of  $r_1$  for the One-Hop E Mode for All Six Experiments

$r_1$	Positions of Transmitter, Reflection Point and Receiver Relative to the Instantaneous Auroral Oval	Total Signals Received at Aircraft For Each $r_1$ -Condition For All Six Experiments	Total Number of Signal Blackouts For Each $r_1$ -Condition (Artifacts and Abnormal States Excluded)	Total Number of Times Signal Could Have Been Received at Aircraft	Average Value of the Non-Zero Frequency Window Widths For Each $r_1$ -Condition For All Six Experiments
1	T, T, T	12	0	12	4.492 MHz
2	T, T, O	32	1	33	4.917 MHz
3	T, O, O	19	1	20	7.274 MHz
4	O, O, O	11	1	12	7.473 MHz
5	T, O, C	27	17	44	9.078 MHz
6	O, O, C	33	5	38	7.794 MHz
7	O, C, C	27	6	33	8.219 MHz
8	T, T, C	36	12	48	7.214 MHz
9	T, C, C	30	1	31	8.323 MHz

T = "Trough" (here considered to be any point south of the equatorward edge of the instantaneous auroral oval as defined by Q).

O = The instantaneous auroral oval as defined by Q.

C = Polar cap poleward of the instantaneous auroral oval as defined by Q.

Figures 32a to 32i are histograms of the frequency window widths of the one-hop E mode for each  $r_1$ -condition throughout these six experiments.

These histograms, by the nature of their distributions, indicate the likelihood of propagation during the existence of any particular  $r_1$ -condition during a one-hop E mode.

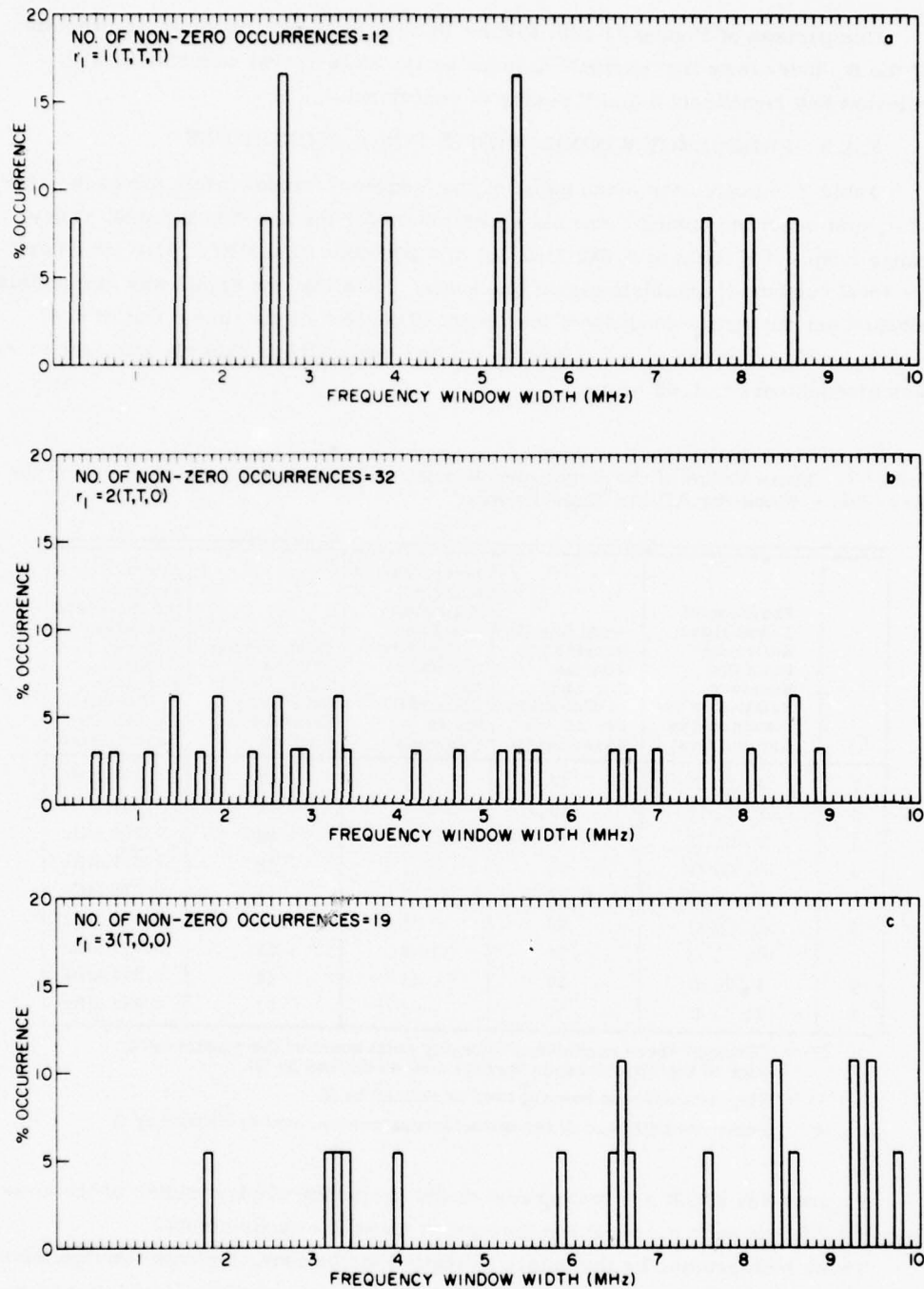


Figure 32. Histogram of the Frequency Window Widths for Each  $r_1$ -Condition for the One-Hop E Mode for All Six Experiments

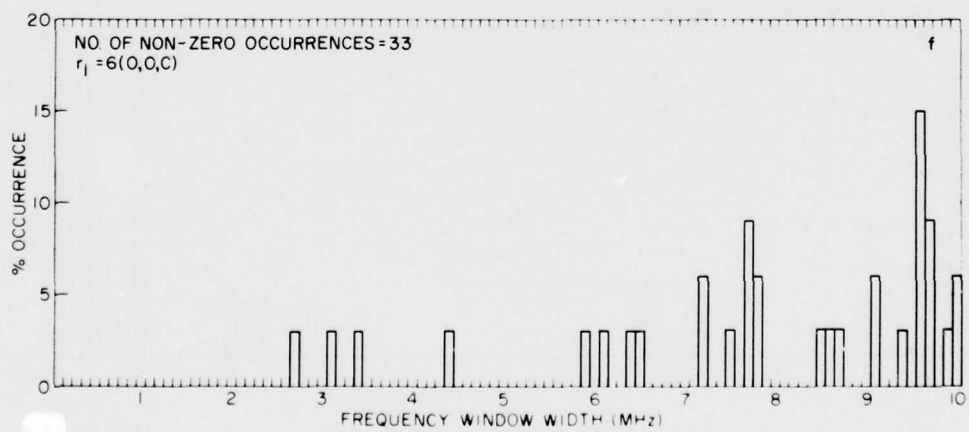
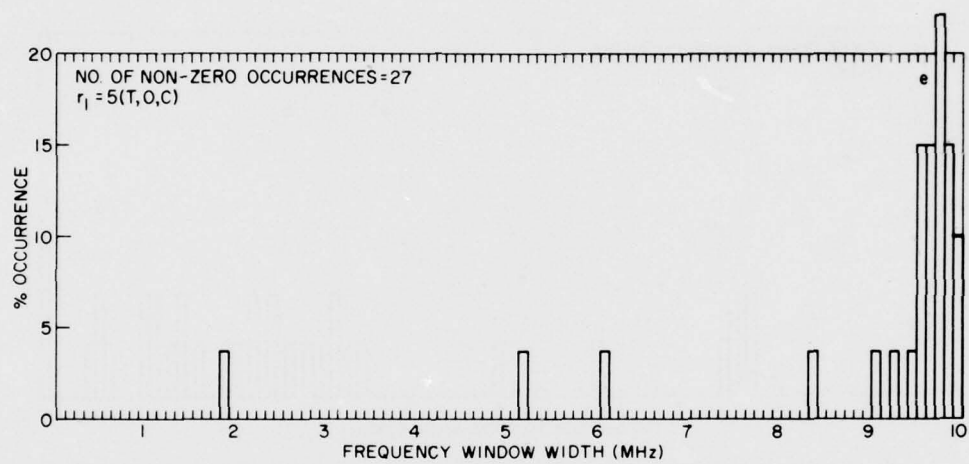
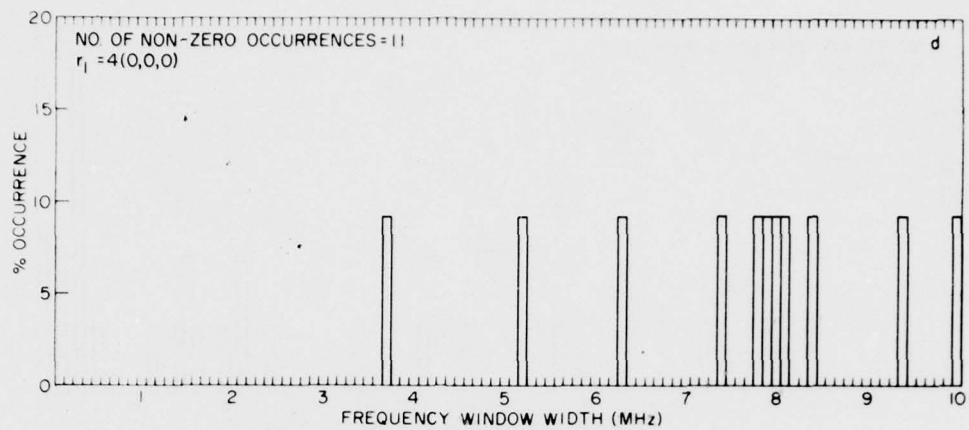


Figure 32. Histogram of the Frequency Window Widths for Each  $r_1$ -Condition for the One-Hop E Mode for All Six Experiments (Cont)



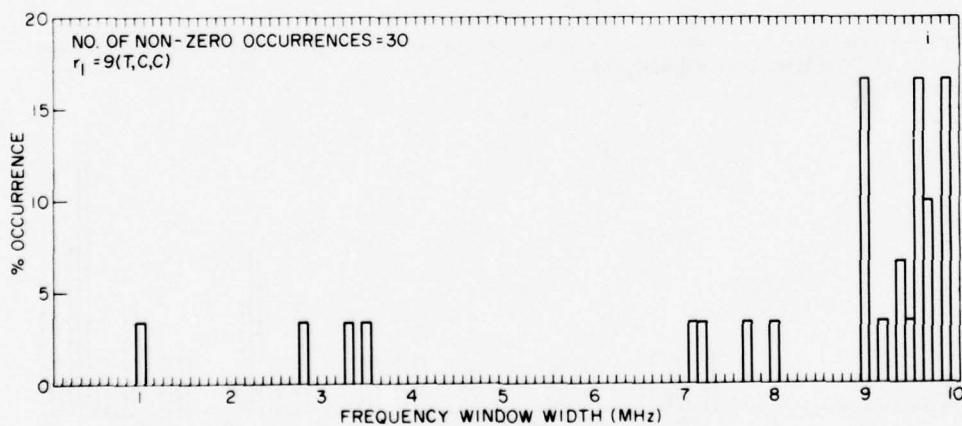
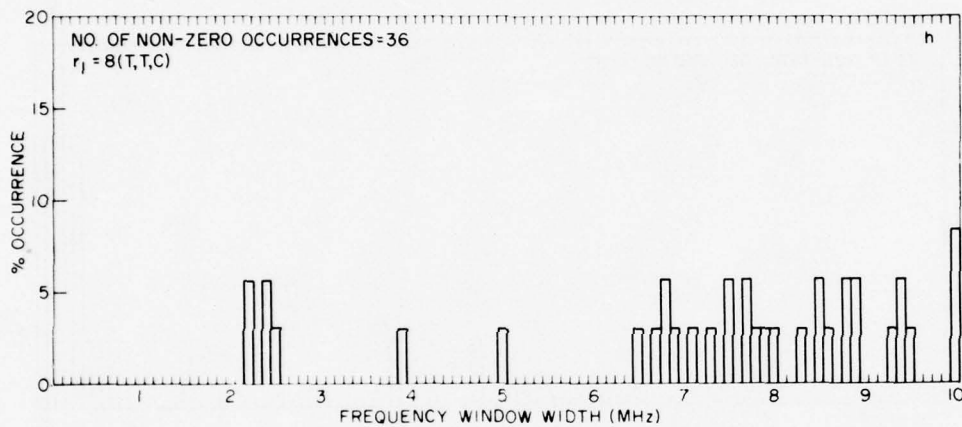
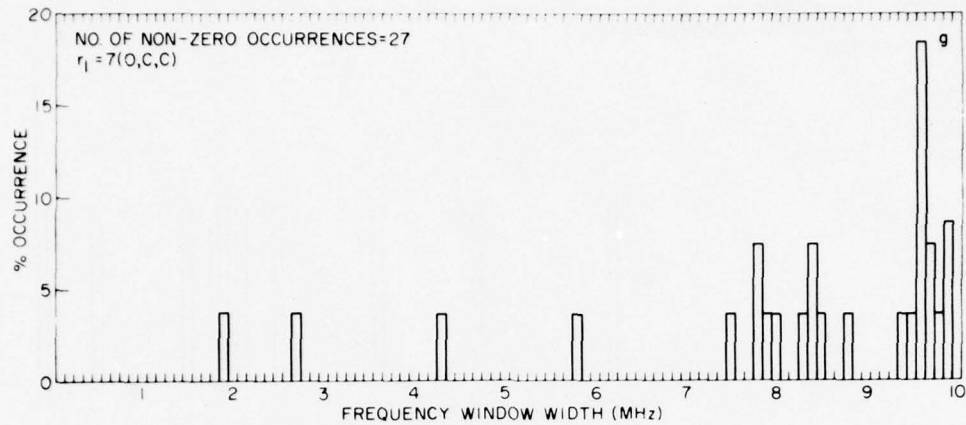


Figure 32. Histogram of the Frequency Window Widths for Each  $r_1$ -Condition for the One-Hop E Mode for All Six Experiments (Cont)

### 3.1.9 CONCLUSIONS BASED ON THE ANALYSIS OF THE ONE-HOP E MODE EVENTS

It is clear that the characteristics of a one-hop E HF signal propagated through the polar region by ionospheric reflection are strongly related to the  $r_1$ -conditions and the  $R_1$  Indices as defined above. It is also clear that the value of  $Q$ , which was originally correlated with the position, size, and shape of the auroral oval on the basis of ground-based optical observations also has significance in this regard on the basis of oblique HF measurements. The Instantaneous  $Q$  ovals provide an ordering principle for these observed signal characteristics. It follows that the success achieved in this study, which incorporated Feldstein and Starkov's  $Q$ -related Instantaneous Ovals as an ordering principle, indicates that the ovals have physical significance.

This method of analysis is well-defined and logical and it has produced results in these six experiments which could not have happened by chance. This is indicated in Figure 33 in which Figure 14 is again reproduced but with lines drawn perpendicular to the horizontal axis which indicate times selected at random during each of the six experiments. There were nine times selected at random for each experiment except for Experiment 193 for which five were selected. In three cases the same time was selected twice since the random selection was done with replacement. Figure 34 is a histogram of the deviation of the propagation events defined above from the times selected at random. The diagram speaks for itself.

### 3.1.10 ADDITIONAL COMMENT

In the original studies of Feldstein and Starkov,<sup>11</sup> based on optical observations made from the ground, the relationship between the instantaneous auroral oval and the magnetic index  $Q$  was studied using the values of  $Q$  within the so-called midnight sector. Since the IGY, when many polar stations measured  $Q$  routinely, interest in it has diminished rapidly and the number of stations measuring it has also decreased rapidly. Since 1966, only Sodanklyä, Finland (67° 22'N geomagnetic latitude) has made this calculation.

In Figure 27, the solid lines at the top of figure perpendicular to it, with the appropriate arrows, indicate the time period during which Sodanklyä was within the midnight sector during each experiment. The dashed lines indicate when it was within one hour of the midnight sector. The dotted lines indicate when it was within two hours of the midnight sector. At other times, Sodanklyä was more than two hours out of the midnight sector, but this did not make any difference in the results, indicating that this restriction is not necessary.

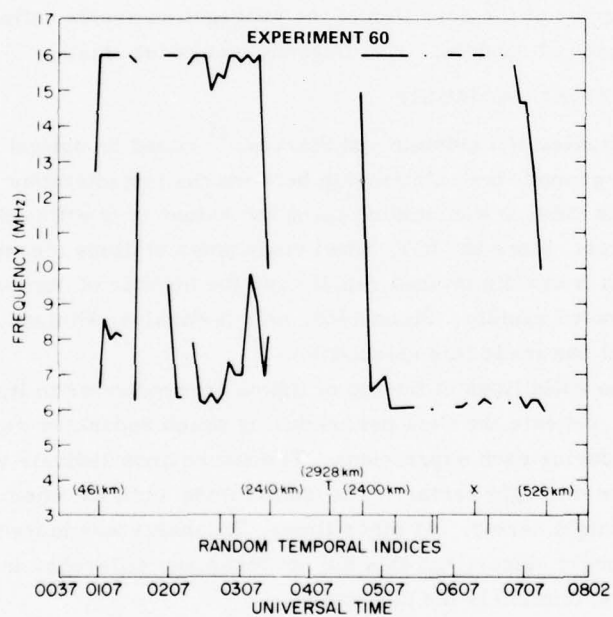
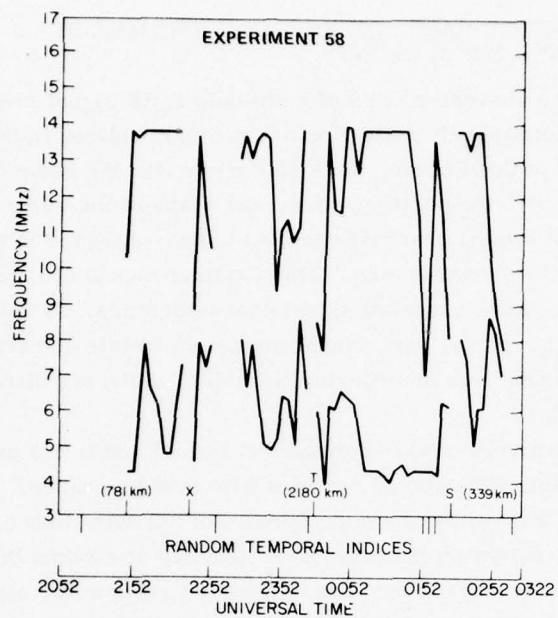


Figure 33. 1-E Modes Observed at Aircraft Showing Randomly Selected Temporal Indices

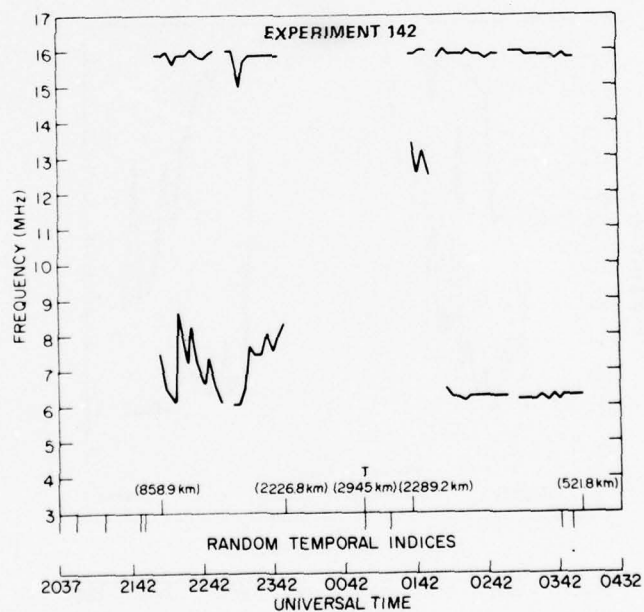
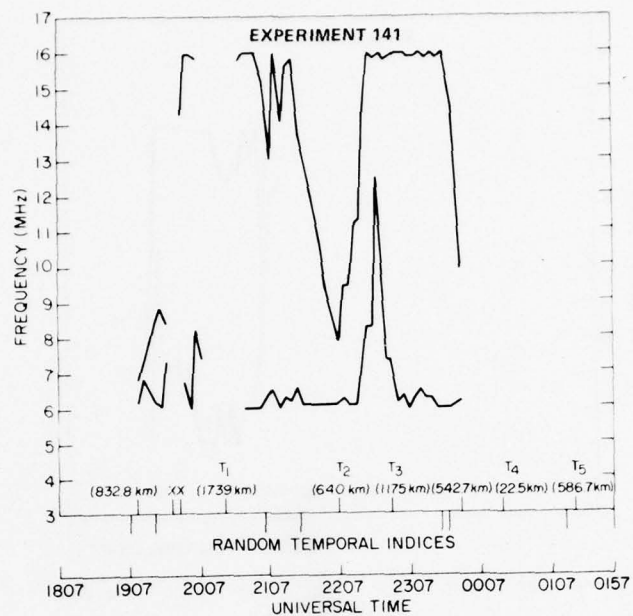


Figure 33. 1-E Modes Observed at Aircraft Showing Randomly Selected Temporal Indices (Cont)



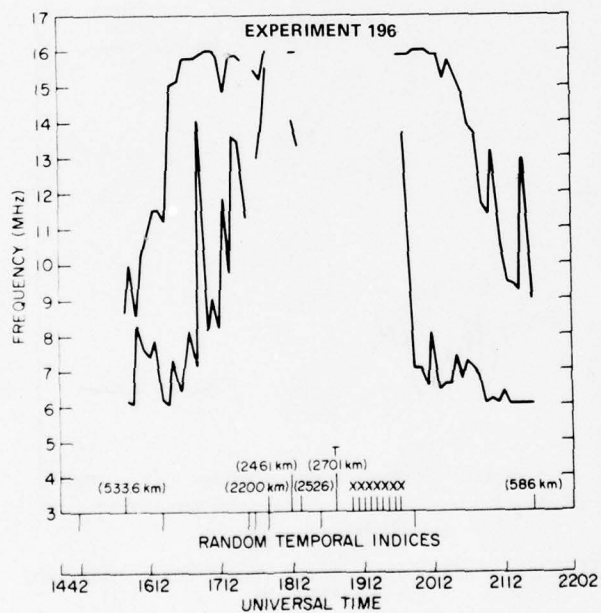
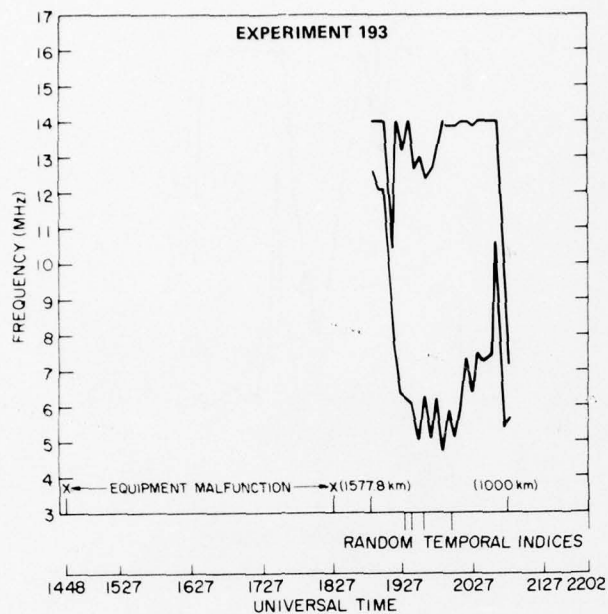


Figure 33. 1-E Modes Observed at Aircraft Showing Randomly Selected Temporal Indices (Cont)

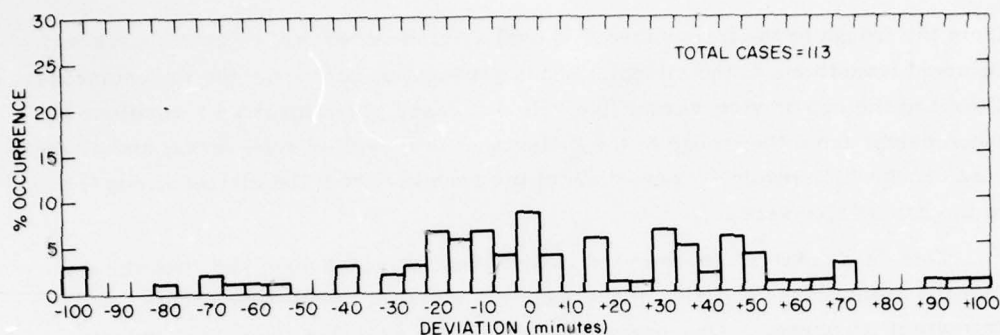


Figure 34. Histogram of Percentage of Occurrence of All Significant and Relevant Events for the One-Hop E Mode for All Experiments Compared to Randomly Selected Times

### 3.1.11 HYPOTHETICAL ILLUSTRATION

A particular hypothetical case of point-to-point transmission in the polar region might be illustrative of the possible utilization of the research reported on here.

If a transmitter was located just south of the southernmost probable extension of the oval and a receiver just to the north of the northernmost probable extension of the oval and it were desired to communicate regularly via HF ionospheric propagation between these two points, we can see that only the condition  $r_1 = 5, 8, \text{ or } 9$  could exist as far as the one-hop E mode is concerned.

From Table 7 we can see that when condition  $r_1 = 5$  exists, transmission would be possible at any of the frequencies considered here only 61 percent of the time. For condition  $r_1 = 8$ , it would be possible only about 75 percent of the time, and, for condition  $r_1 = 9$ , about 97 percent of the time.

However, from Figures 32e, 32h, and 32i we can see that, when transmissions can occur during an  $r_1 = 5$  condition, the window width will probably be  $\geq 5.0$  MHz 96 percent of the time and  $\geq 9.5$  MHz 78 percent of the time. When  $r_1 = 8$ , the window width will probably be  $\geq 5$  MHz 83 percent of the time and  $\geq 8.0$  MHz 44 percent of the time, and when  $r_1 = 9$ , the window width will probably be  $\geq 5.0$  MHz 83 percent of the time and  $\geq 9$  MHz 73 percent of the time. Other characteristic events will occur as the midpoint of the path passes from one polar region to another as will be explained below. The result will always be a temporary narrowing of the window width. There are other hypothetical cases that could be discussed.

### 3.1.12 $R_1$ ASSOCIATED TRANSITIONS OF THE INSTANTANEOUS Q OVAL BOUNDARIES FOR THE ONE-HOP E MODE FOR SIX EXPERIMENTS

There were seven relevant cases which involved transitions of the transmitter from the trough (as defined above) to the instantaneous Q oval or vice-versa; six relevant cases which involved transitions of the midpoint of the propagation path

from the trough to the instantaneous Q oval or vice-versa; six relevant cases which involved transitions of the midpoint of the propagation path from the instantaneous Q oval to the cap or vice-versa; five relevant cases which involved transitions of the receiver from the trough to the instantaneous Q oval or vice-versa; and 21 relevant cases which involved transitions of the receiver from the instantaneous Q oval to the cap or vice-versa.

This is a total of 45 relevant cases, four of which involved two simultaneous transitions. Thus, there were 37 relevant cases where only one transition occurred. One unambiguous case is excluded from the analysis because the propagation event that occurred is not considered significant at this time. Two relevant transitions marked the beginning of  $r_1$ -conditions that accounted for the observed events.

The overall results of an analysis of what happened at each type of transition is given in Table 8. In this table, the numbers 1, 2, and 3 refer respectively to the transmitter, the propagation path midpoint, and the receiver, while the letters T, O, and C refer respectively to the trough (as defined above), the instantaneous Q oval, and the cap. The notation used is illustrated by 2(O-C) which indicates a transition of the midpoint of the propagation path from the instantaneous Q oval into the cap. An indication is given in the next column of the figure as to whether the frequency window width widens or narrows in correlation with the particular transition and, in the next column, the specific nature of the event is indicated where MOF $\uparrow$  means that the MOF increased in frequency, MOF $\downarrow$  means that the MOF decreased in frequency, LOF $\uparrow$  means that the LOF increased in frequency, and LOF $\downarrow$  means that the LOF decreased in frequency. At times, both the MOF and the LOF were affected. The "Remarks" column provides information in special cases. The single and double asterisks are explained in the table. Only transition No. 45 is substantially inconsistent with its type.

An examination of Table 8 shows that the frequency window width narrows for virtually every transition except 3 (O - C) in which case it widens.

There must be heretofore unknown ionospheric features associated with the boundaries of Feldstein and Starkov's Q-related Instantaneous Ovals. The word "anchored" to them might be appropriate. Studies should be made to identify and describe these features and the physical mechanisms by means of which they influenced the results reported on in this report.

Whatever has already been gleaned from previous measurements in the polar region should be used as a starting point for these studies.

Table 8. Observed Characteristics of Each Instantaneous Auroral Oval Edge Transition

Number	Transition	Effect on Frequency Window Width	Specific Propagation Events	Remarks (* and ** Indicate Ambiguous Situations)
1	1 (T-O)	Narrows	$E_1$	-5 min LOF $\uparrow$ (1.1 MHz), MOF $\downarrow$ (6 MHz)
2	1 (T-O)	Narrows	LOF $\uparrow$	
3	1 (T-O)	Narrows	LOF $\uparrow$ , MOF $\downarrow$ *	Also 2 (O-C). Same as No. 16.
4	1 (T-O)	See remarks	$S_1$ , LOF $\uparrow$ , MOF $\uparrow$ *	Within 15 min of transition, frequency window width slightly narrowed (0.5 MHz). Same transition as No. 33 - 3 (O-C).
5	1 (O-T)	Narrows	LOF $\uparrow$ , MOF $\downarrow$	
6	1 (O-T)	Narrows	LOF $\uparrow$	
7	1 (O-T)	Narrows	$E_1$	
8	2 (T-O)	Narrows	MOF $\downarrow$ *	Also 3 (C-O). Same as No. 37. Decrease of MOF lasts 35 min until transition at same time as northward turn at 640 km away from transmitter.
9	2 (T-O)	Narrows	Start of total blackout	35-min duration
10	2 (T-O)	Narrows	LOF $\uparrow$	
11	2 (T-O)	Widens	MOF $\uparrow$ **	** For the 15 min before the next transition, MOF $\uparrow$ 3 MHz and WW $\uparrow$ 3 MHz. No. 11 coincided with turn at 640 km from transmitter from movement toward to movement away. Ambiguous. (WW = Frequency Window Width).
12	2 (O-T)	Narrows	$E_2$ *	Same transition as No. 23 - 3 (O-T). LOF $\uparrow$ , MOF $\downarrow$ 5 min before transition.
13	2 (O-T)	Narrows	LOF $\uparrow$ , MOF $\downarrow$	
14	2 (O-C)	Narrows	MOF $\downarrow$	
15	2 (O-C)	Narrows	Start of total blackout	10-min duration.
16	2 (O-C)	Narrows	LOF $\uparrow$ , MOF $\downarrow$ *	Also 1 (T-O). Same as No. 3.
17	2 (O-C)	Narrows	See remarks	At this transition, frequency window width stops widening - a virtual narrowing.
18	2 (C-O)	Narrows	Start of total blackout	120-min duration.
19	2 (C-O)	Narrows	Start of total blackout	10-min duration.
20	3 (T-O)	Narrows	LOF $\uparrow$	
21	3 (T-O)	Narrows	$E_2$	
22	3 (T-O)	Narrow	See remarks	At $S_1$ (833 km from transmitter), frequency window width (0.6 MHz) abnormally narrow for 25 min.
23	3 (O-T)	Narrows	$E_2$ *	Same transition as No. 12, LOF $\uparrow$ , MOF $\downarrow$ 5 min before transition.
24	3 (O-T)	Narrows	See remarks	5 min prior to transition, MOF starts increase, then decreases to $E_2$ 5 min after transition.
25	3 (O-C)	Widens	See remarks	Transition occurs at end of total blackout. Frequency window width instantaneously 9.8 MHz.
26	3 (O-C)	Widens	LOF $\downarrow$ , MOF $\uparrow$	
27	3 (O-C)	Widens	LOF $\uparrow$ , MOF $\uparrow$	$\Delta$ MOF > $\Delta$ LOF by 2.7 MHz.
28	3 (O-C)	Widens	$S_1$	$\Delta$ Frequency window width = 8.4 MHz.
29	3 (O-C)	Widens	LOF $\downarrow$ , MOF $\uparrow$	
30	3 (O-C)	Widens	LOF $\downarrow$	
31	3 (O-C)	Widens	LOF $\downarrow$	
32	3 (O-C)	Widens	LOF $\downarrow$	
33	3 (O-C)	Widens	$S_1$ *	$\Delta$ Frequency window width = 6.1 MHz at $S_1$ . Also 1 (T-O). Same transition as No. 14.



Table 8. Observed Characteristics of Each Instantaneous Auroral Oval Edge Transition (Cont)

Number	Transition	Effect on Frequency Window Width	Specific Propagation Events	Remarks (* and ** Indicate Ambiguous Situations)
34	3 (C-O)	Narrows	LOF ↑ MOF ↓	Also 2 (T-O)-same as No. 8. Decrease of MOF lasts 35 min until transition at the same time as north turn of A/C.
35	3 (C-O)	Narrows	MOF ↓	
36	3 (C-O)	Narrows	MOF ↓	
37	3 (C-O)	Narrows	MOF ↓ *	
38	3 (C-O)	Narrows	MOF ↓	E <sub>2</sub> occurs 5 min after transition.
39	3 (C-O)	Narrows	E <sub>2</sub>	
40	3 (C-O)	Narrows	LOF ↑	S <sub>2</sub> occurs when range from transmitter is 1577.8 km. Very narrow Q oval. Q=2. Frequency window width unusually narrow. Frequency window width stops widening. Virtual narrowing.
41	3 (C-O)	Narrow S <sub>2</sub>	See remarks **	
42	3 (C-O)	Narrow	See remarks	
43	3 (C-O)	Narrows	LOF ↓ MOF ↓	In 5 min after transition, $\Delta \text{MOF} > \Delta \text{LOF} = 0.5 \text{ MHz}$ .
44	3 (C-O)	Widens	LOF ↓ MOF ↓	$\Delta \text{MOF} < \Delta \text{LOF}$ by 0.2 MHz. Slight widening.
45	3 (C-O)	Widens	LOF ↓ MOF ↑	Net increase in frequency window width is 2.8 MHz. MOF increase is anomalous.

### 3.1.13 SPECIFIC GEOPHYSICAL EVENT

One specific geophysical event which occurred during one of these experiments occurred at the end of Experiment 58 starting at 0215 UT on 28 February. It was seen on the aircraft all sky camera film to be a well developed auroral substorm which lasted throughout the rest of the experiment

As shown in the expanded section of the propagation flight for this period in Figure 35, the recorded signal at the aircraft first experienced a 10-min total blackout. Then the MOF behaved normally but the LOF seems to have been controlled by the variable D-layer associated with the substorm. Figure 36 indicates the behavior of the H-component of the magnetometer trace at Great Whale River, Canada, during this same time period. There was an extremely pronounced decrease in the magnitude of this component coincident with the onset of the substorm. The geographical position of Great Whale River in relation to the aircraft and Goose Bay is shown in Figure 1.

Figure 37 shows that there was an absorption event lasting for about four minutes and of greater than 3 dB magnitude at the Goose Bay zenith just before 0200 UT on 28 February. Poleward expansion of this absorption region may account for the transmission blackout noted above.

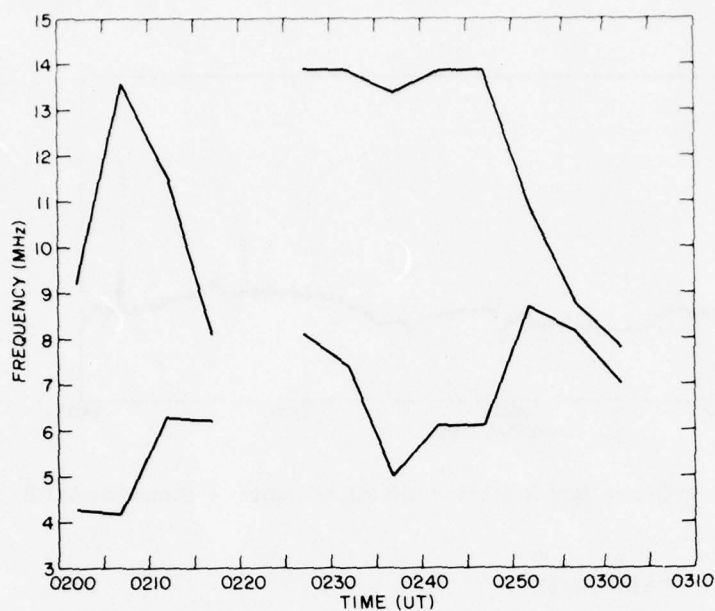


Figure 35. HF  
Signal Observed  
at Aircraft in the  
One-Hop E Mode  
During an Auroral  
Substorm -  
Experiment 58

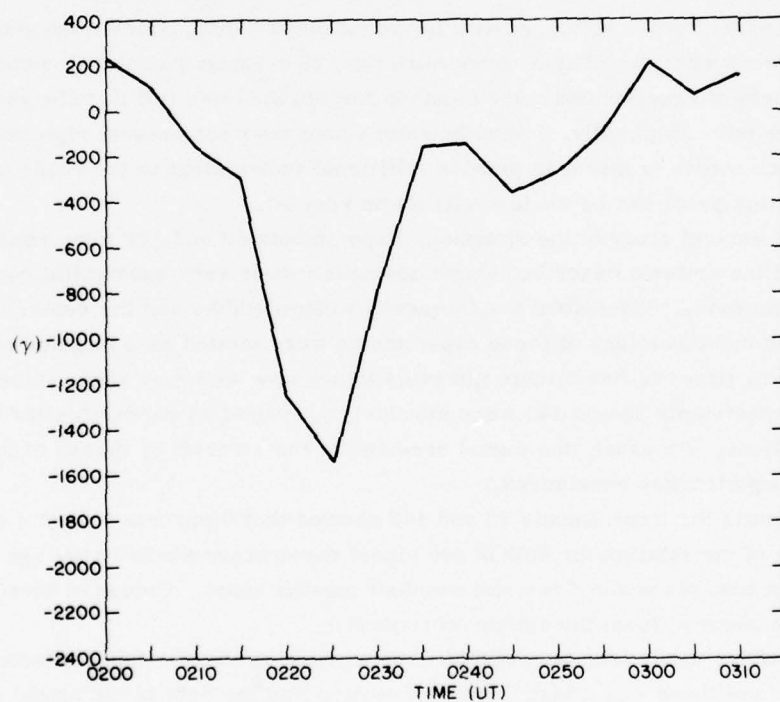


Figure 36. Great Whale River H-Component Magnetogram  
During Auroral Substorm - Experiment 58

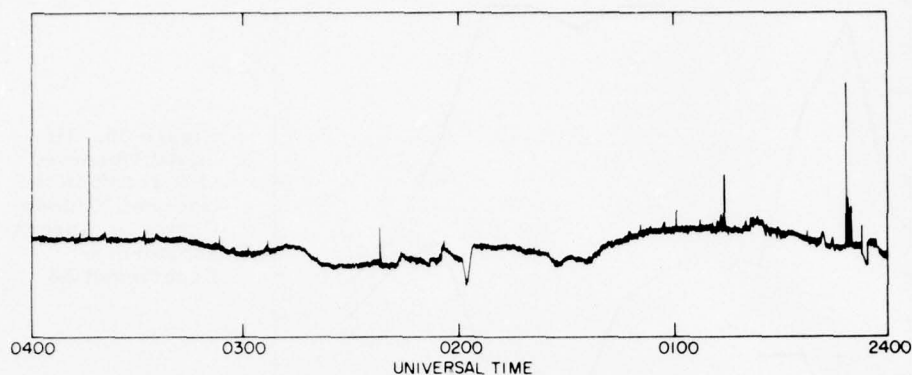


Figure 37. 3 dB Event — Goose Bay Riometer (30 MHz-Zenith) — Experiment 58

#### 3.1.14 SUPPLEMENTARY NOTE

All of this research indicates that the polar ionosphere is not completely chaotic and non-repetitive in nature. This supplementary note describes the results of an attempt that was made to find among the six experiments studied here any sets of experiments which had similar flight paths during times when geophysical conditions were similar. There were more than 25 a-priori possibilities out of which two sets of experiments were selected for which it was felt that the above conditions were met. Naturally, a supplementary note does not present rigorous proofs. Such a note is meant to provide additional information to the reader for which rigorous proof can be made available on request.

After a careful study of the situation, Experiments 60 and 142 were considered to have met the criteria described above adequately over very substantial portions of their flight paths. Therefore the frequency window widths and the center frequencies for these portions of these experiments were plotted as a function of the corresponding times in five minute intervals to see how well they were correlated. Parts of Experiments 58 and 141 were similarly identified as candidates for this type of analysis. As usual, the signal received at the aircraft by means of ionospheric propagation was considered.

The results for Experiments 60 and 142 showed that there was indeed a very high degree of correlation for both of the signal parameters studied although the experiments took place about two and one-half months apart. Copies of these results can be secured from the author on request.

On the other hand, four portions of Experiments 58 and 151 were selected for comparison and there was a high degree of correlation for both of the signal parameters studied, but this correlation was not nearly as good as in the case of the

previously described pair although these two experiments also occurred approximately two and one-half months apart. Copies of these results can also be received from the author on request.

The interesting thing to note here is that the geophysical parameter that differed quite a bit during the course of Experiment 58 as compared to Experiment 141 but which differed very little during the temporal sequence selected in both Experiments 60 and 142 was the Index Q. This result further verifies Feldstein and Starkov's conclusion that the Index Q is significant in the polar region. Here, as elsewhere in this report, we have found that this Index is also significant in the polar region as far as HF propagation is concerned.

#### **4. ANALYSIS OF THE ELKINS-RUSH HF POLAR PREDICTIVE MODEL**

##### **4.1 Preliminary Comments**

Under what conditions of the input and output parameters should a comparison between the "predictions" of the computerized model and the observed results be made? Most of the parameters of the model cannot be manipulated easily. However, in order to give the computerized model as good a chance as possible to prove itself to be a worthwhile tool in the prediction of actual propagation conditions in the polar region, it is desirable to vary, in an experimental manner, the readily available input and output parameters that are most likely to affect the computed results.

The primary input parameters that can easily be varied are the 10.7-cm solar flux, the value of Kp, the transmitted power, the local time, and the required signal-to-noise ratio. The output parameter that can produce a significant variation in the results is the so-called Service Probability.

##### **4.2 Input Parameters**

It has been determined that variation of the 10.7-cm flux, the local time, and the transmitted power have little effect upon the "predictions" made by the Elkins-Rush HF Polar Predictive Model. Variation of Kp has a major effect. Of course Kp was not originally designed for use in the polar region as we have noted above, but, since the model called for its use, the published values were used in computing the results plotted in Figure 15. Antenna pattern considerations could also be important at some times but the Elkins-Rush computerized model could not be modified to incorporate the desired patterns. Dr. Elkins himself acknowledged the desirability of doing this in Reference (5), subsequent to my suggestion dated 29 August 1975 which was brought to his attention but he was not able to achieve it with the resources at his disposal.



### 4.3 Output Parameters

Effort has been concentrated on the effect on the model "predictions", for the six experiments mentioned above, of varying the so-called Service Probability. The Service Probability (henceforth referred to as "P") is essentially the joint probability that, given the input parameters of the program (both those easily subject to control and those not so easily accessible), ionospheric conditions in the polar region are judged to be such at the time in question that a particular mode can be propagated between the two geographical points of interest and that the signal-to-noise ratio judged to exist at the receiving antenna is sufficient to produce a detectable signal for the given mode at the frequency under consideration. It is both logical to assume and has been shown empirically that the variation of this parameter very significantly affects the predictions made by the model.

Based on preliminary studies, a set of values of P were selected for intensive study and methods were developed to demonstrate which value of P is most likely to produce the desired result, that is, the most conformity between the "predicted" results and the observed results. This analysis also indicates the absolute capability of the Elkins-Rush computerized model in "predicting" the real world when the "best" value of P is used.

For these 6 experiments, there were 15 modes that were both observed and "predicted". There were 17 "predicted" modes that were never observed at all during the 6 experiments.

The 17 "predicted" modes that were never observed were as follows: for flight 58—two-hop E, two-hop F, four-hop F, and five-hop F; for flight 60—two-hop E, three-hop E, and one-hop F; for flight 141—one-hop F; for flight 142—three-hop E, one-hop F, three-hop F and four-hop F; for flight 193—two-hop E and three-hop F; and for flight 196—two-hop E, three-hop E, and three-hop F. More modes were "predicted" that were not observed than the total number of those that actually were observed.

### 4.4 Numerical Analysis Results

A considerable amount of numerical analytical work was done in order to answer the question as to which value of P would be most suitable in order to make the "predicted" results conform most exactly to the observed results. None of the analysis was at all encouraging. For now, one of the analytical results will be shown which, together with the plots of the results from each "predicted" model that was also observed, suffices to substantiate the conclusions reached. Refer to Figures 14, A1, A6, and A11 for the plots of the "predicted" modes that were also observed and compare them to the plots of the observed modes in Figures 15, A2, A7, and A12.

The definition of the output parameter P was given in Section 4.3.

In order to determine the optimum value of  $P$  to utilize in these comparisons and to reach a definitive conclusion as to the capability of this computerized model to make short-term "predictions" good enough to be correctable by the use of current supplementary data, the following approach was taken.

Let  $\Delta_o$  equal the observed frequency window at a particular instant;  $\Delta_p$  equal the "predicted" frequency window at the same instant; and  $\Delta_{ov}$  equal the total amount of overlap between the "predicted" frequency window and the observed frequency window at the same instant.

The  $\frac{\sum \Delta_{ov}}{\sum \Delta_o}$  for all six experiments for all modes that were both observed and "predicted" gives the proportion by which the observed frequency window was overlapped by the "predicted" frequency window.

Also  $\frac{\sum \Delta_{ov}}{\sum \Delta_p}$  for all six experiments for all modes that were both observed and "predicted" gives the proportion by which the "predicted" frequency window was overlapped by the observed frequency window.

Figure 38, shows that when these two parameters are plotted as a function of  $P$ , the crossover point is at about 0.80 which means that this is the optimum value of  $P$  to use. However, the value of the ordinate at that point is only 0.37 whereas if the model were perfect, the value would be unity. That is, a perfect model would produce results such that  $\sum \Delta_{ov} = \sum \Delta_o = \sum \Delta_p$  for at least one value of  $P$ .

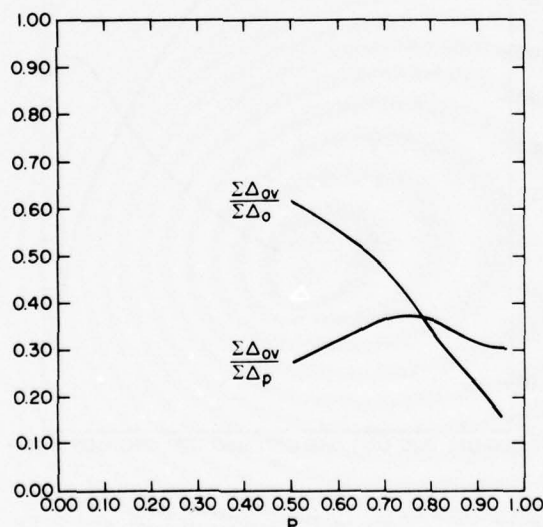


Figure 38. Plots of  $P$  vs  $\frac{\sum \Delta_{ov}}{\sum \Delta_o}$  and  $P$  vs  $\frac{\sum \Delta_{ov}}{\sum \Delta_p}$

Now,  $\frac{\Sigma \Delta_o - \Sigma \Delta_{ov}}{\Sigma \Delta_o}$  equals the total excess observed frequency window width as a proportion of the total observed frequency window width while  $\frac{\Sigma \Delta_p - \Sigma \Delta_{ov}}{\Sigma \Delta_o}$  equals the total excess "predicted" frequency window width as a proportion of the total observed frequency window width. Again, when these parameters are plotted as a function of P, as shown in Figures 39 the crossover point is about 0.80. But, the value of the ordinate at the crossover point is 0.65 whereas, if the computerized model were perfect, the value would be zero. That is, there would be no excess frequency window width and the numerator in both cases would be zero for at least one value of P. Only modes that were both observed and "predicted" were used.

It is obvious that the Elkins-Rush HF Polar Predictive Model is inadequate for making correct short-term predictions even if the optimum value of P is used and adjustments are made based on current supplementary data - as was pointed out in Section 2 of this report. As for the claim that it is accurate in the mean over long periods of time is concerned, an objective study would be worthwhile.

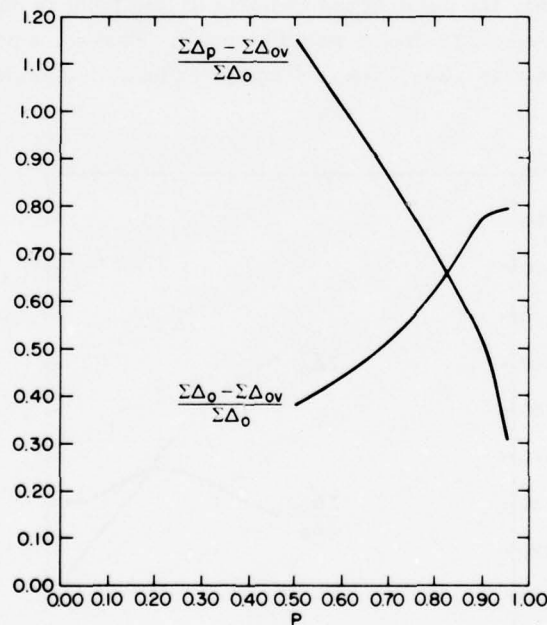


Figure 39. Plots of P vs  $\frac{\Sigma \Delta_o - \Sigma \Delta_{ov}}{\Sigma \Delta_o}$  and P vs  $\frac{\Sigma \Delta_p - \Sigma \Delta_{ov}}{\Sigma \Delta_o}$

## 5: CONCLUSIONS AND RECOMMENDATIONS

The conclusions and recommendations of this study are as follows:

- (1) The Elkins-Rush HF Polar Predictive Model, regardless of any adjustments that could possibly be made based on supplementary data as pointed out in Section 2.1 is inadequate for predicting short-term HF propagation conditions in the polar region or even for after-the-fact descriptions at a time when all the published values of the input parameters are definitely known.
- (2) The  $R_1$  Indices are highly correlated with the significant propagation events, defined above, observed in the polar region. In Appendix A the same correlation is shown to hold for the  $R_2$  Indices.
- (3) Consistent patterns of behavior for HF propagation in the polar region are associated with the  $r_1$ -conditions for the one-hop E mode.
- (4) Investigations of the ionospheric features and the physical mechanisms that account for the relationship of the  $r_1$ -conditions and the  $R_1$  Indices to propagation conditions in the polar region should be instituted. This also applies to the  $r_2$ -conditions and the  $R_2$  Indices.
- (5) These oblique HF measurements verify the discovery of Feldstein and Starkov that the Index Q is a good indicator of the position, size, and shape of the instantaneous auroral oval. The results shown in Appendix A provide further verification.
- (6) In view of the persistence of Q, which can easily be seen in Table 4, a method of predicting Q in advance should be sought thus making the prediction of short-term HF propagation conditions in the polar region possible (that is, an hour or more in advance in real time).
- (7) Serious consideration should be given to the possibility that only one magnetic observatory may be needed to calculate the Index Q if it is done at the proper latitude.



Preceding Page BLANK - FILM

## References

1. Whalen, J.A. (1970) Auroral Oval Plotter and Nomograph for Determining Corrected Geomagnetic Local Time, Latitude, and Longitude for High Latitudes in the Northern Hemisphere, AFCRL ERP No. 327.
2. Chapman, J.H., Davies, E., and Littlewood, C.A. (1955) Radio observations of the ionosphere at oblique incidence, Can. J. Phys. 33:713-722.
3. Elkins, T.J., and Rush, C.M. (1973) A statistical predictive model of the polar ionosphere, Air Force Survey in Geophysics, (No. 267):1-100.
4. Barkhausen, A.F., Finney, J.W., Proctor, L.L., and Schultz (1969) Predicting Long-Term Operational Parameters of High-Frequency Sky-Wave Telecommunications System, ESSA Technical Report ERL 110-17878.
5. Elkins, T.J. (1975) Private Communication.
6. Davis, T. Neil, and Sugiura, Masuhisa (1966) Auroral electrojet activity index AE and its universal time variations, J. of Geophys. Res. 71(No. 3).
7. Bartels, J. (1938) Potsdamer erdmagnetische Kennziffern Ztschr. f. Geophysik, 14:68-78.
8. Bartels, J., Heck, N.H., and Johnson, H.F. (1939) The three-hour-range index measuring geomagnetic activity, Terr. Magn. 41:411-454.
9. Bartels, J., and Fukushima, N. (1956) A Q index for the geomagnetic activity in quarter-hourly intervals, Akad. Wiss. Gothingen. Math-Phys. Klasse. Sonderhoft, No. 3.
10. Lincoln, J.V. (1967) Geomagnetic Indices, Physics of Geomagnetic Phenomena, Academic Press, pp 67-100.
11. Feldstein, Y.I., and Starkov, G.V. (1967) Dynamics of auroral belt and polar geomagnetic disturbances, Planet. Space Sci. 15:209-229.
12. Comfort, R.H. (1972) Auroral Oval Kinematics Programs, NASA CR-613-73.
13. Thorne, R. (1975) Ionospheric-magnetospheric coupling, Review of Geophysics and Space Physics, 13(No. 3).
14. Evans, J.V. (1975) A review of F region Dynamics, Review of Geophysics and Space Physics, 13(No. 3).

Preceding Page BLANK - F

## Appendix A

### Analysis of the Less Extensive Observed Modes

#### A1. RESULTS

As was mentioned earlier, the three other modes of ionospheric propagation that were observed during these six experiments - the one-hop F, the two-hop E, and the two-hop F were less extensive, both in time and in frequency window width than the one-hop E mode which was examined in some detail in Section 3 of this report.

For the one-hop F mode, the  $R_1$  Indices occurred at the same time as for the one-hop E mode since all of the  $r_1$ -conditions were the same and changed from one to the other at the same times.

From this point on, we are eliminating the propagation plots which show the temporal changes in the AE Index due to its obvious lack of significant correlation with the defined events. The discussion of the one-hop F, two-hop E, and two-hop F modes each includes a set of three curves: the appropriate smoothed version of the Elkins-Rush Model "predicted" propagation plots calculated under the same relatively optimal conditions used in the case of the one-hop E mode; the observed propagation plots with the times of the Q-transition occurrences indicated; and the observed propagation plots with the times of  $R_1$  or  $R_2$  Index occurrences indicated.

The observed propagation plots can easily be compared to the "predicted" propagation plots with this set of essential curves and there is no need to indicate the randomized curves since the results are essentially the same as was indicated for the one-hop E mode.

The one-hop F mode occurred only during Experiments 58, 193, and 196. Figures A1, A2, and A3 constitute the package mentioned above. The signals detected during Experiment 58 all occurred within the range excluded from consideration here because of the number of circles and turns that occurred during the period of detection.

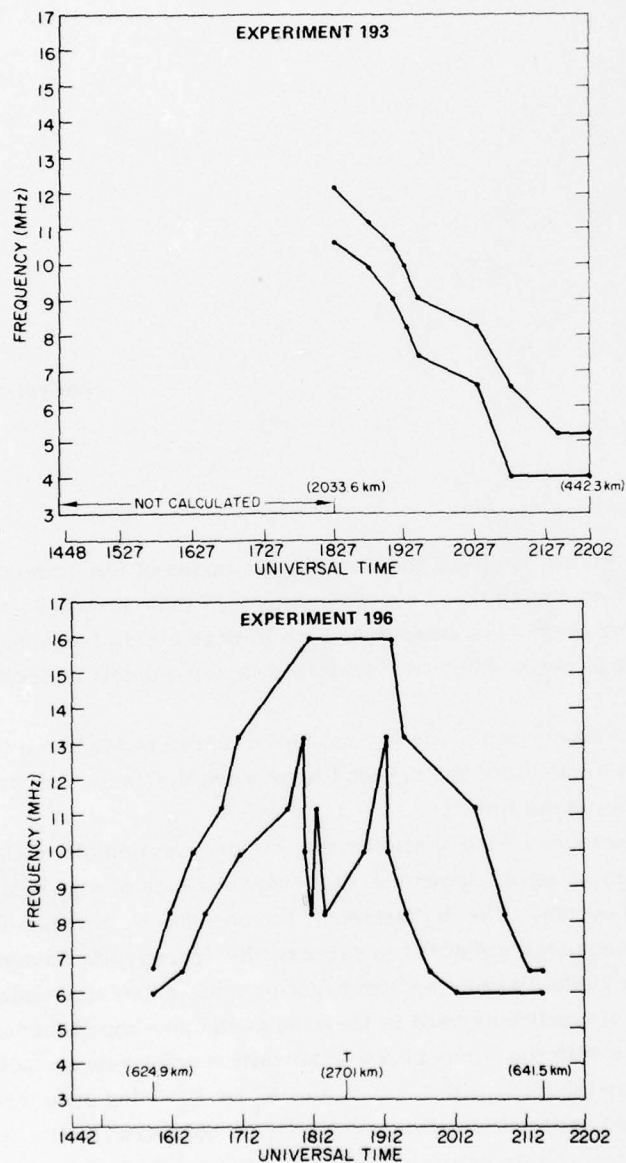


Figure A1. Elkins-Rush HF Polar Predictive Model, Service Probability = 0.70, 1-F Modes

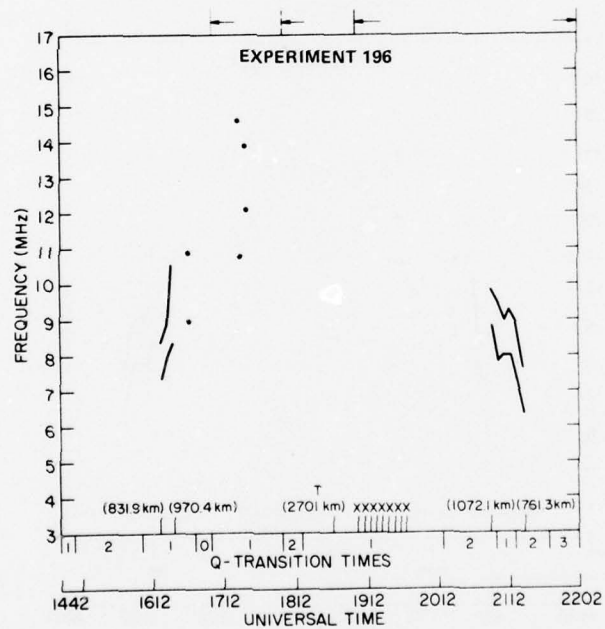
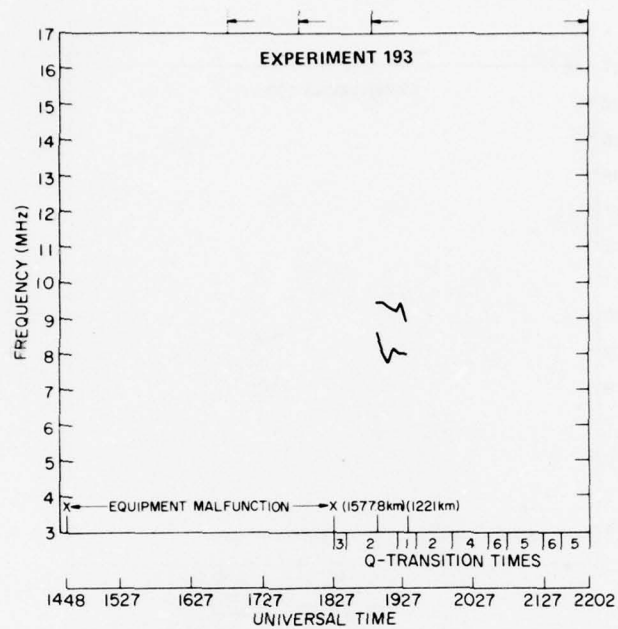


Figure A2. 1-F Modes Observed at Aircraft Showing Q-Transition Times



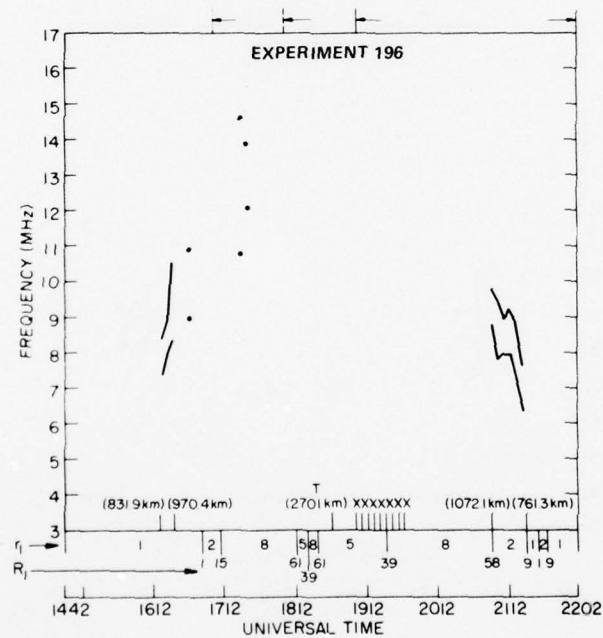
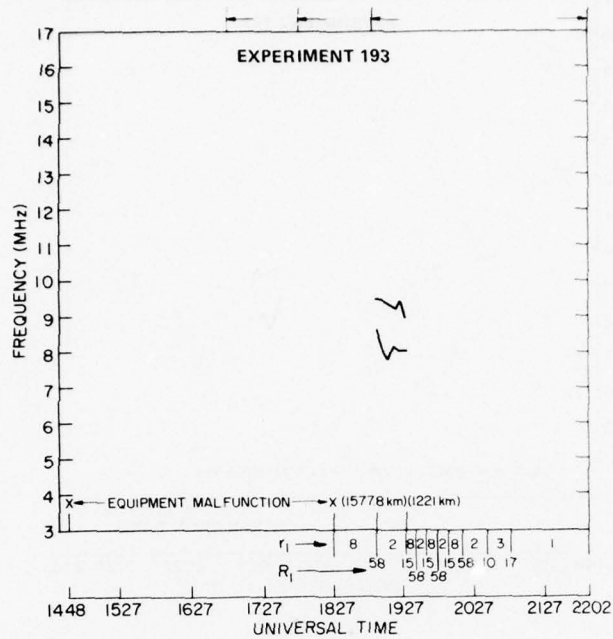


Figure A3. 1-F Modes Observed at Aircraft Showing  $r_1$ -Conditions and  $R_1$  Indices

Figure A4 is the histogram of the number of relevant and significant events that occurred during the one-hop F mode for all experiments. Figure A5 is the identical histogram with Q as the parameter. These are strictly analogous to the same type of histogram already shown for the one-hop E mode. Again,  $R_1$  is obviously a much more precise indicator of the occurrence of significant propagation events than is Q. These histograms are plotted as the percentage of the total of the significant and relevant observed events in each 5-min interval as in the one-hop cases. The zero column means no deviation while the + 5 box means deviation between  $>0$  and + 5 min, etc. There are a different total number of events for the case of  $R_1$  as compared to Q since the exclusions necessary in both cases are different.

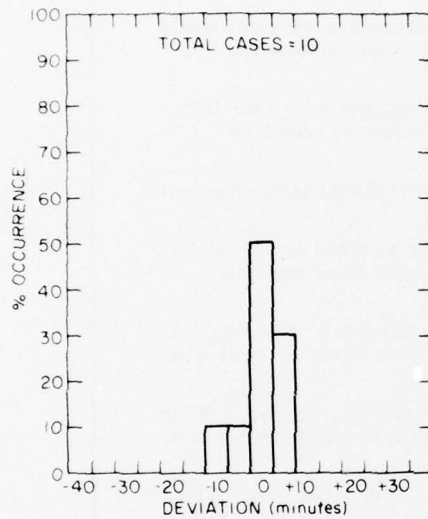


Figure A4. Histogram of Percentage of Occurrence of All Significant and Relevant Events for the One-Hop F Mode Compared Temporally with  $R_1$  Occurrences

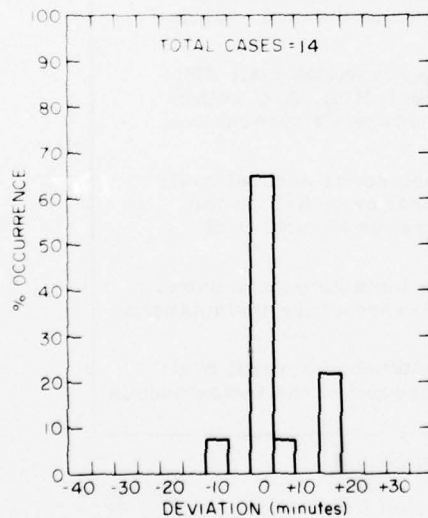


Figure A5. Histogram of Percentage of Occurrence of All Significant and Relevant Events for the One-Hop F Mode Compared Temporally with Q-Transition Occurrences

As far as the two-hop modes of ionospheric propagation observed during the six experiments is concerned, the times of occurrence of the  $r_2$ -conditions and the resulting  $R_2$  Indices that mark the times of transition from one  $r_2$ -condition to another are different from those of the  $r_1$ -conditions and the  $R_1$  Indices associated with the one-hop modes. These definitions are given in Tables A1 and A2.

Table A1. Definitions of the Reilly Conditions,  $r_2$ , for Two-Hop Modes of HF Propagation

$r_2 = 1$	GB, $RP_1$ , $RP_2$ , A/C all equatorward of the instantaneous auroral oval as defined by Q.
$r_2 = 2$	GB, $RP_1$ , $RP_2$ equatorward of the instantaneous auroral oval; A/C within the instantaneous auroral oval as defined by Q.
$r_2 = 3$	GB, $RP_1$ equatorward of the instantaneous auroral oval; $RP_2$ , A/C within the instantaneous auroral oval as defined by Q.
$r_2 = 4$	GB equatorward of the instantaneous auroral oval; $RP_1$ , $RP_2$ , A/C within the instantaneous auroral oval as defined by Q.
$r_2 = 5$	GB, $RP_1$ , $RP_2$ , A/C all within the instantaneous auroral oval as defined by Q.
$r_2 = 6$	GB, $RP_1$ , $RP_2$ in the instantaneous auroral oval; A/C in the polar cap poleward of the instantaneous auroral oval as defined by Q.
$r_2 = 7$	GB, $RP_1$ in the instantaneous auroral oval; $RP_2$ , A/C in the polar cap poleward of the instantaneous auroral oval as defined by Q.
$r_2 = 8$	GB in the instantaneous auroral oval; $RP_1$ , $RP_2$ , A/C in the polar cap poleward of the instantaneous auroral oval as defined by Q.
$r_2 = 9$	GB equatorward of the instantaneous auroral oval; $RP_1$ , $RP_2$ within the instantaneous auroral oval; A/C in the polar cap poleward of the instantaneous auroral oval as defined by Q.
$r_2 = 10$	GB equatorward of the instantaneous auroral oval; $RP_1$ within the instantaneous auroral oval; $RP_2$ , A/C within the polar cap poleward of the instantaneous auroral oval as defined by Q.
$r_2 = 11$	GB, $RP_1$ equatorward of the instantaneous auroral oval; $RP_2$ within the instantaneous auroral oval; A/C in the polar cap poleward of the instantaneous auroral oval as defined by Q.
$r_2 = 12$	GB, $RP_1$ , $RP_2$ equatorward of the instantaneous auroral oval; A/C within the polar cap poleward of the instantaneous auroral oval as defined by Q.
$r_2 = 13$	GB, $RP_1$ equatorward of the instantaneous auroral oval; $RP_2$ , A/C within the polar cap poleward of the instantaneous auroral oval as defined by Q.

GB = Goose Bay

$RP_1$  = First Reflection Point

A/C = Aircraft

$RP_2$  = Second Reflection Point

Table A2. Definitions of the Reilly Indices,  $R_2$ , in Terms of All the Possible  $r_2$ -Condition Transitions

$R_2$	$r_2$ -Condition Transition	$R_2$	$r_2$ -Condition Transition	$R_2$	$r_2$ -Condition Transition	$R_2$	$r_2$ -Condition Transition	$R_2$	$r_2$ -Condition Transition	$R_2$	$r_2$ -Condition Transition
1	1-2	27	3-4	53	5-6	79	7-8	105	9-10	131	11-12
2	1-3	28	3-5	54	5-7	80	7-9	106	9-11	132	11-13
3	1-4	29	3-6	55	5-8	81	7-10	107	9-12	133	12-1
4	1-5	30	3-7	56	5-9	82	7-11	108	9-13	134	12-2
5	1-6	31	3-8	57	5-10	83	7-12	109	10-1	135	12-3
6	1-7	32	3-9	58	5-11	84	7-13	110	10-2	136	12-4
7	1-8	33	3-10	59	5-12	85	8-1	111	10-3	137	12-5
8	1-9	34	3-11	60	5-13	86	8-2	112	10-4	138	12-6
9	1-10	35	3-12	61	6-1	87	8-3	113	10-5	139	12-7
10	1-11	36	3-13	62	6-2	88	8-4	114	10-6	140	12-8
11	1-12	37	4-1	63	6-3	89	8-5	115	10-7	141	12-9
12	1-13	38	4-2	64	6-4	90	8-6	116	10-8	142	12-10
13	2-1	39	4-3	65	6-5	91	8-7	117	10-9	143	12-11
14	2-3	40	4-5	66	6-7	92	8-9	118	10-11	144	12-13
15	2-4	41	4-6	67	6-8	93	8-10	119	10-12	145	13-1
16	2-5	42	4-7	68	6-9	94	8-11	120	10-13	146	13-2
17	2-6	43	4-8	69	6-10	95	8-12	121	11-1	147	13-3
18	2-7	44	4-9	70	6-11	96	8-13	122	11-2	148	13-4
19	2-8	45	4-10	71	6-12	97	9-1	123	11-3	149	13-5
20	2-9	46	4-11	72	6-13	98	9-2	124	11-4	150	13-6
21	2-10	47	4-12	73	7-1	99	9-3	125	11-5	151	13-7
22	2-11	48	4-13	74	7-2	100	9-4	126	11-6	152	13-8
23	2-12	49	5-1	75	7-3	101	9-5	127	11-7	153	13-9
24	2-13	50	5-2	76	7-4	102	9-6	128	11-8	154	13-10
25	3-1	51	5-3	77	7-5	103	9-7	129	11-9	155	13-11
26	3-2	52	5-4	78	7-6	104	9-8	130	11-10	156	13-12

The two-hop E mode was very sparse and occurred only during Experiments 141 and 142. Each mode lasted for only about one-half hour. However, both were generally at the maximum observable frequency window width of 10 MHz. Both had only an  $S_1$  and an  $E_1$ . The established set of propagation plots are shown in Figures A6, A7, and A8.

Figures A9 and A10 are the histograms of the temporal relationship of the significant propagation events which occurred during the two-hop E mode for the significant and relevant  $R_2$ 's and the Q's respectively. Again  $R_2$  is much more precisely related to the occurrence of significant propagation events than is Q.

The two-hop F mode occurred during Experiments 141, 142, 193, and 196. It was considerably more extensive than the two-hop E mode in all cases.



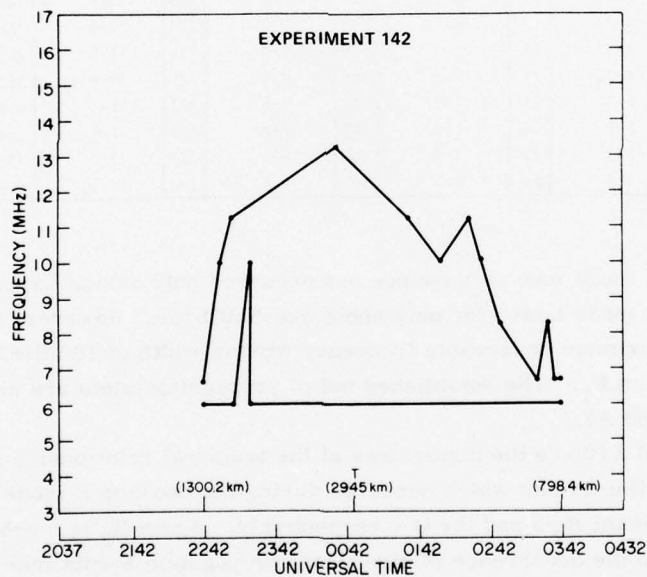
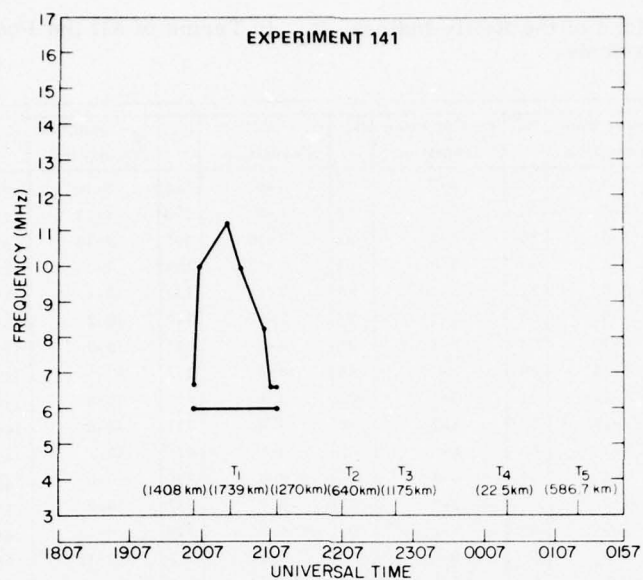


Figure A6. Elkins-Rush HF Polar Predictive Model, Service Probability = 0.70, 2-E Modes

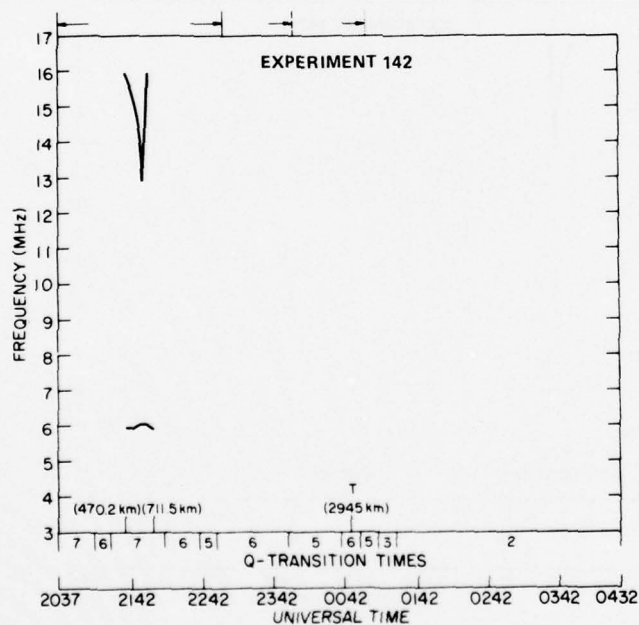
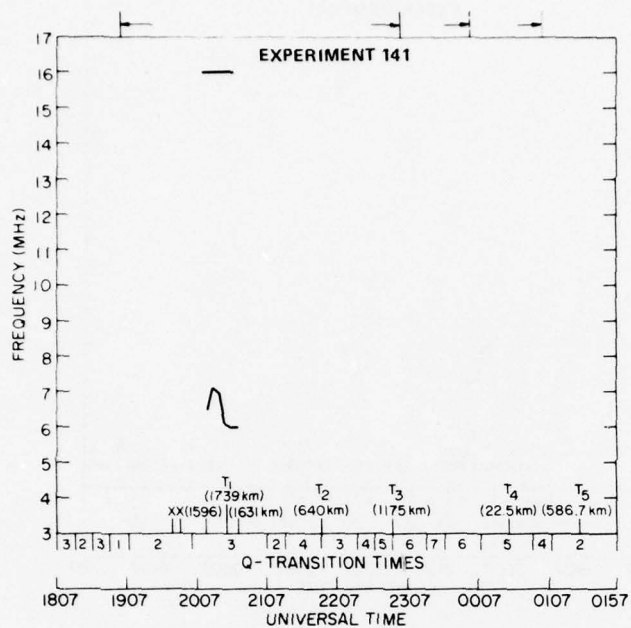


Figure A7. 2-E Modes Observed at Aircraft Showing Q-Transition Times

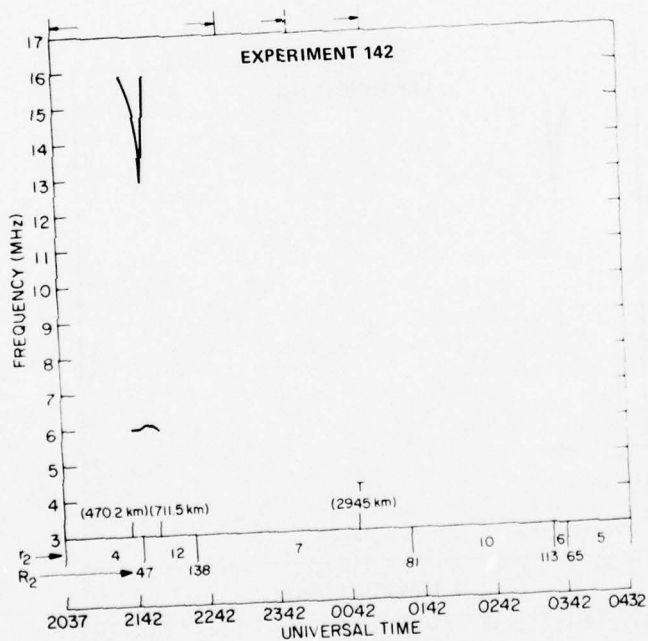
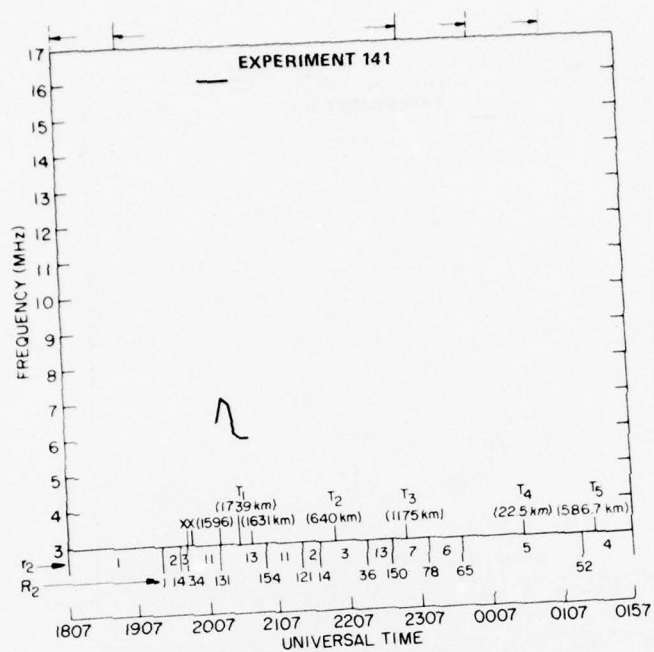


Figure A8. 2-E Modes Observed at Aircraft Showing  $r_2$ -Conditions and  $R_2$  Indices

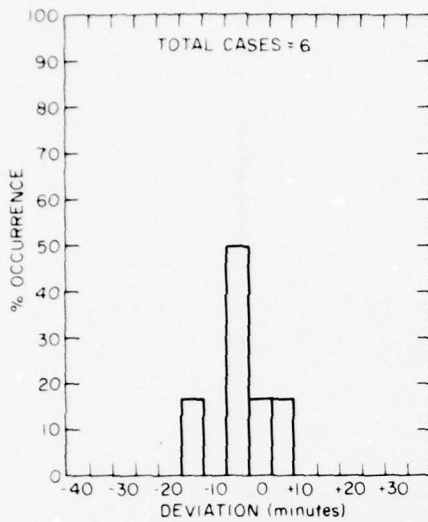


Figure A9. Histogram of Percentage of Occurrence of All Significant and Relevant Events for the Two-Hop E Mode for All Experiments Compared Temporally with  $R_2$  Occurrences

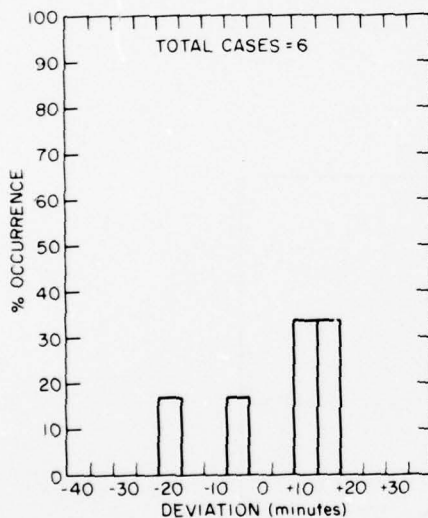


Figure A10. Histogram of Percentage of Occurrence of All Significant and Relevant Events for the Two-Hop E Mode for All Experiments Compared Temporally with Q-Transition Occurrences

The established set of propagation plots for the two-hop F mode are shown in Figures A11, A12, and A13. Figures A14 and A15 are the histograms of significant events relative to  $R_2$  and Q. Again,  $R_2$  is obviously more precisely related to the occurrence of significant propagation events than is Q.

Note that only 11 out of 24 relevant  $r_1$  and  $r_2$  transitions also involved Q-transitions. Again, it is the  $r_1$ -transition itself and not the Q-transition that is dominant.



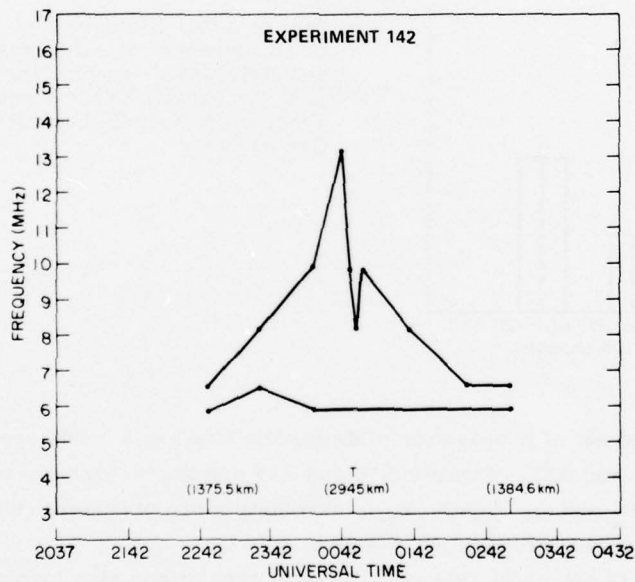
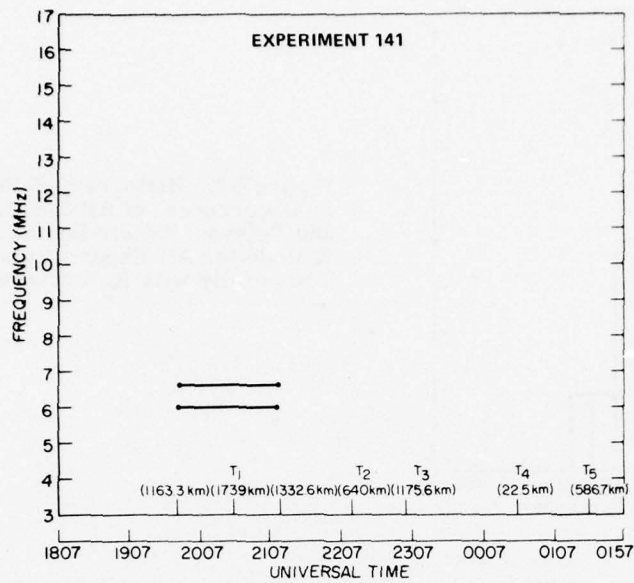


Figure A11. Elkins-Rush HF Polar Predictive Model, Service Probability = 0.70, 2-F Modes

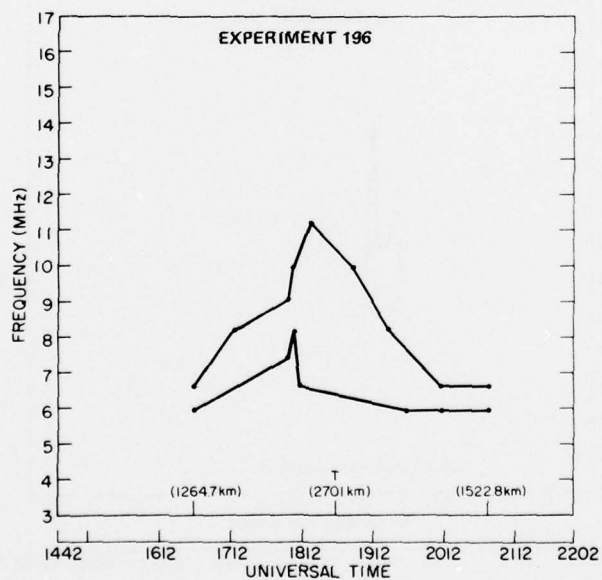
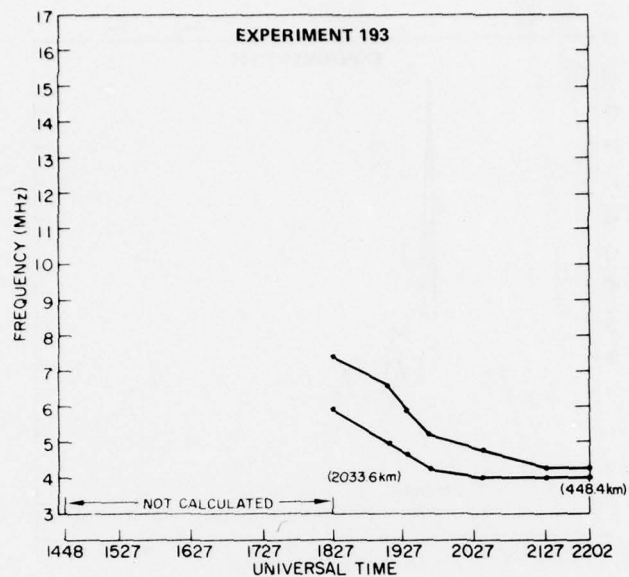


Figure A11. Elkins-Rush HF Polar Predictive Model, Service Probability = 0.70, 2-F Modes (Cont)

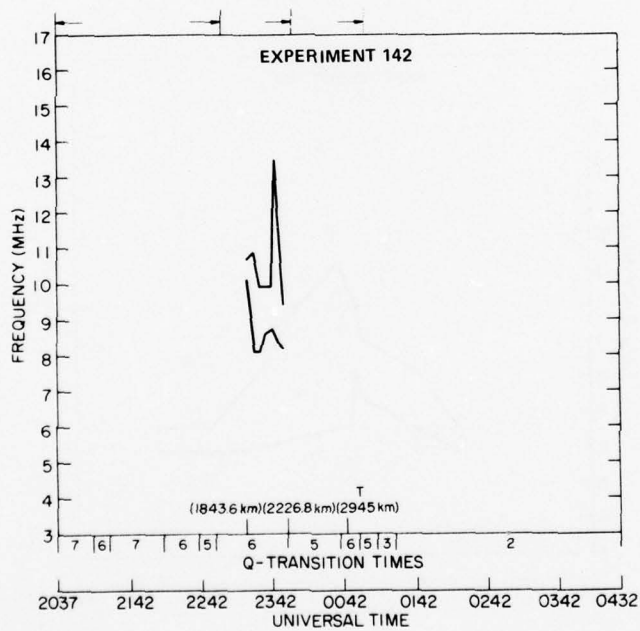
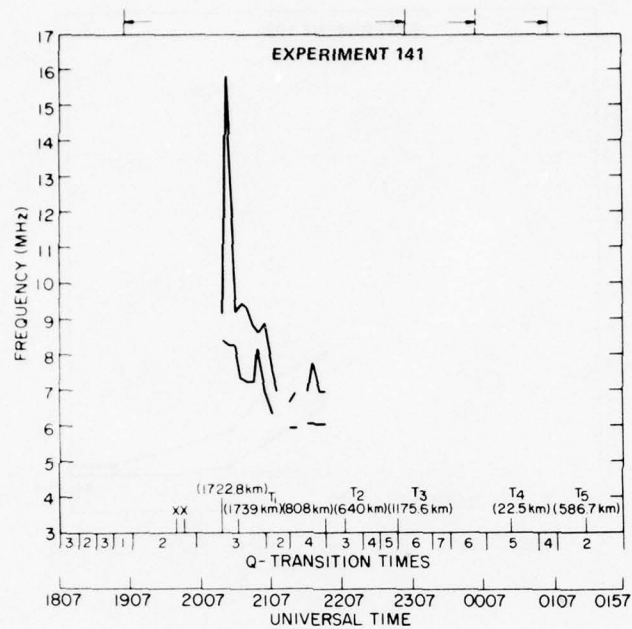


Figure A12. 2-F Modes Observed at Aircraft Showing Q-Transition Times

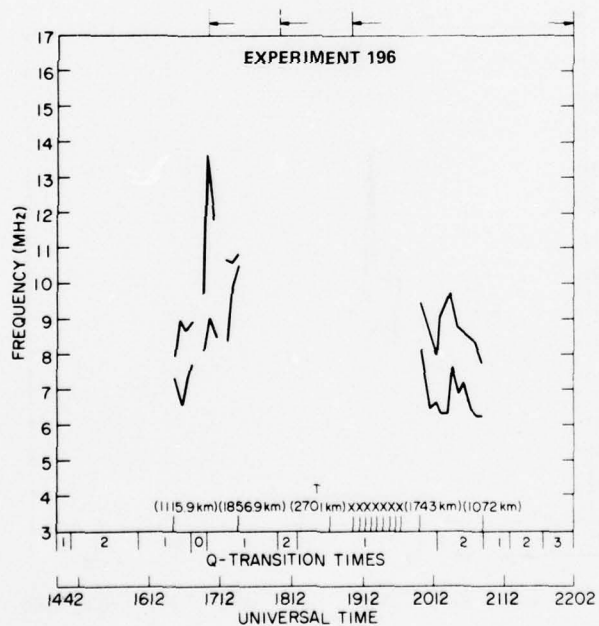
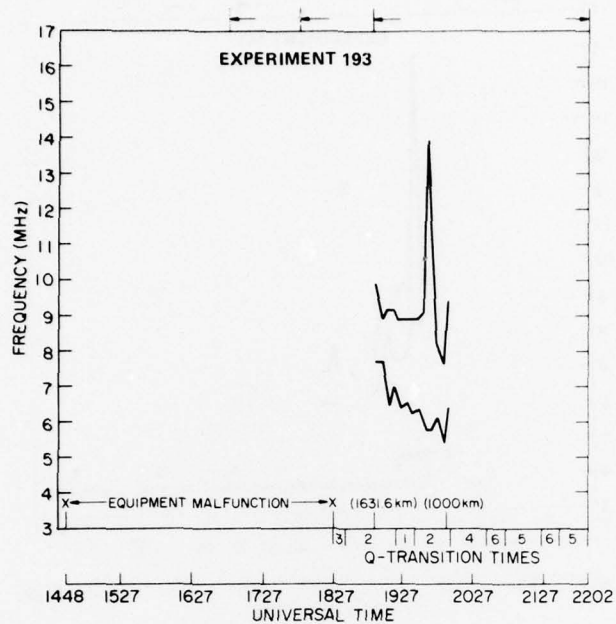


Figure A12. 2-F Modes Observed at Aircraft Showing Q-Transition Times (Cont)



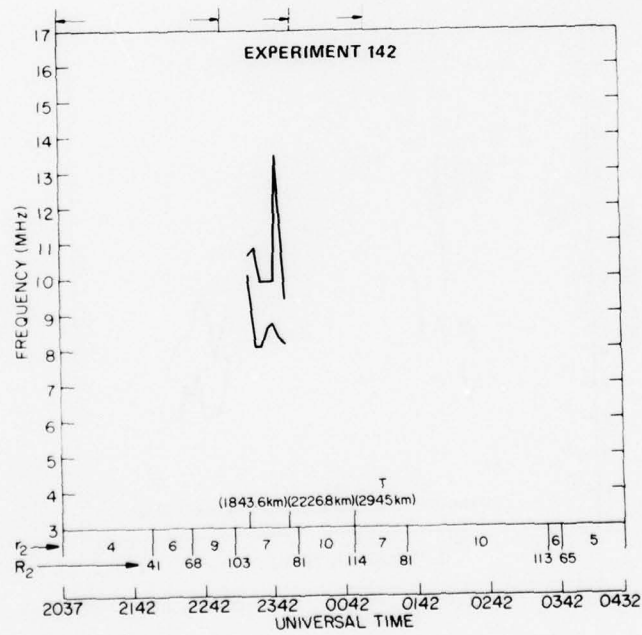
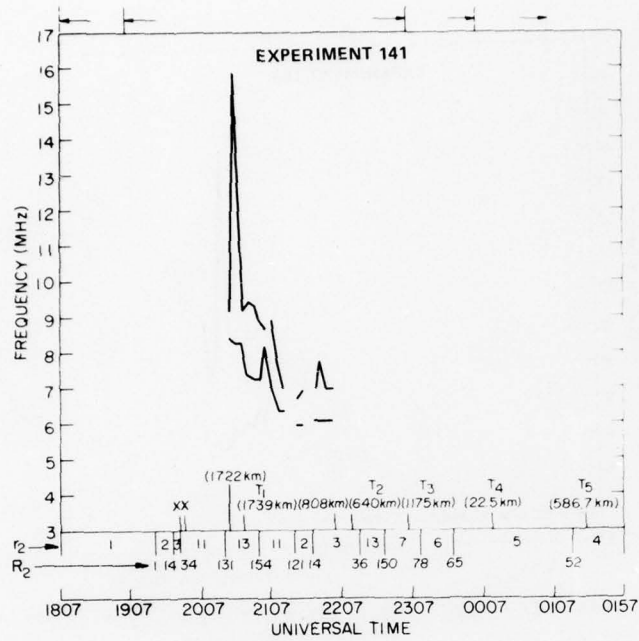


Figure A13. 2-F Modes Observed at Aircraft Showing  $r_2$ -Conditions and  $R_2$  Indices

AD-A043 027

AIR FORCE GEOPHYSICS LAB HANSCOM AFB MASS  
ANALYSIS OF SWEEP FREQUENCY OBLIQUE POLAR REGION HIGH FREQUENCY--ETC(U)  
APR 77 A E REILLY

F/G 20/14

UNCLASSIFIED

AFGL-TR-77-0102

NL

2 OF 2  
AD  
A043027



END  
DATE  
FILMED  
9-77  
DDC

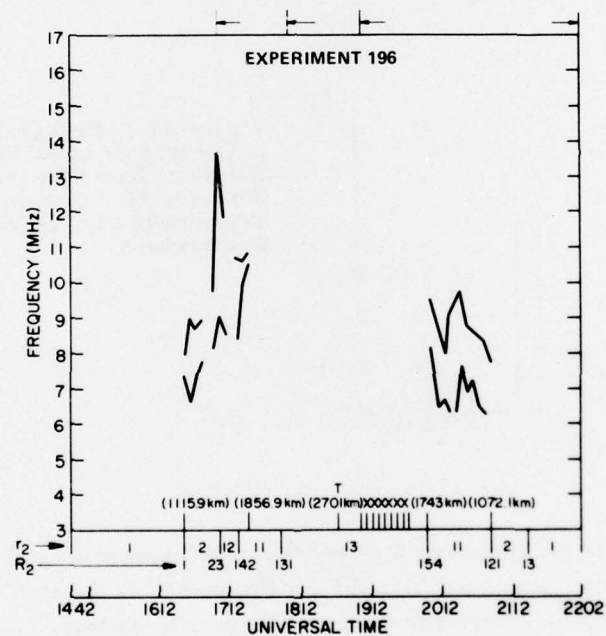
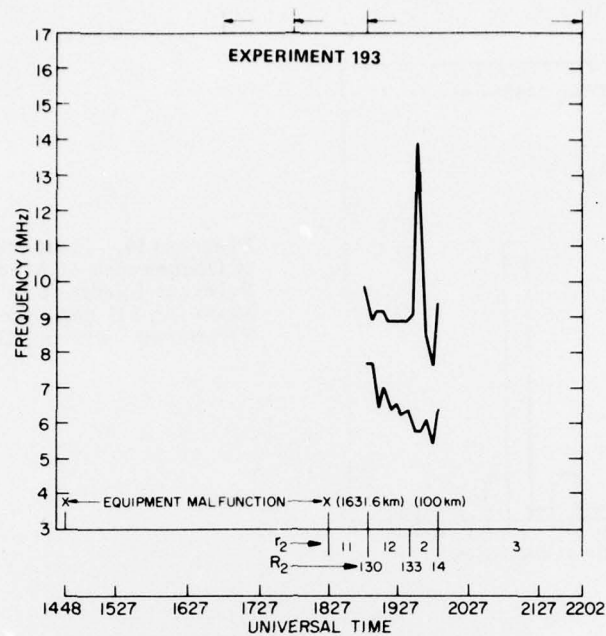


Figure A13. 2-F Modes Observed at Aircraft Showing  $r_2$ -Conditions and  $R_2$  Indices (Cont)

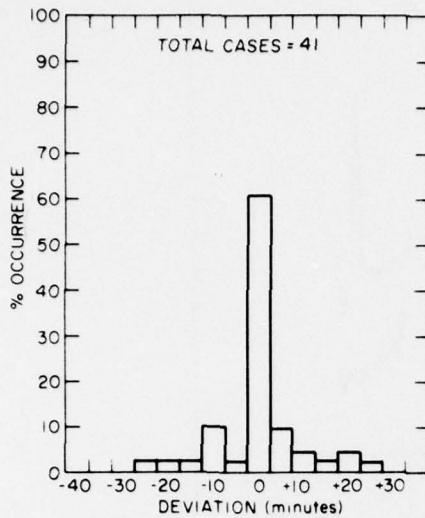


Figure A14. Histogram of Percentage of Occurrence of All Significant and Relevant Events for the Two-Hop F Mode for All Experiments Compared Temporally with  $R_2$  Occurrences

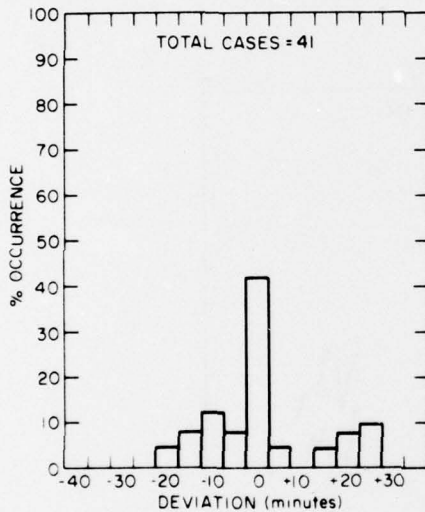


Figure A15. Histogram of Percentage of Occurrence of All Significant and Relevant Events for the Two-Hop F Mode for All Experiments Compared Temporally with Q-Transition Occurrences

Figure A16 is the histogram for all of the significant propagation events for all modes and all experiments for  $R_1$  and  $R_2$ . Figure A17 is the similar plot with Q as a parameter. The superiority of  $R_1$  and  $R_2$  over Q is clear.



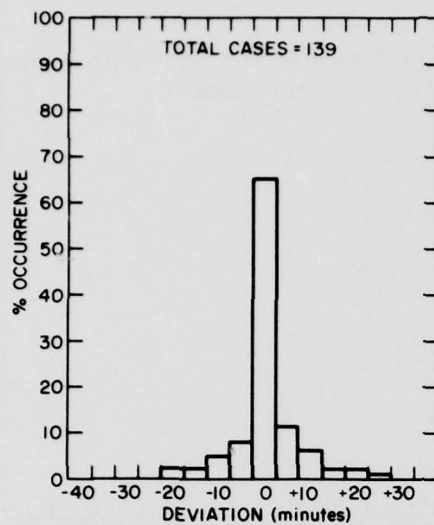


Figure A16. Histogram of Percentage of Occurrence of All Significant and Relevant Events for All Modes and All Experiments Compared Temporally with  $R_1$  and  $R_2$  Occurrences as Appropriate

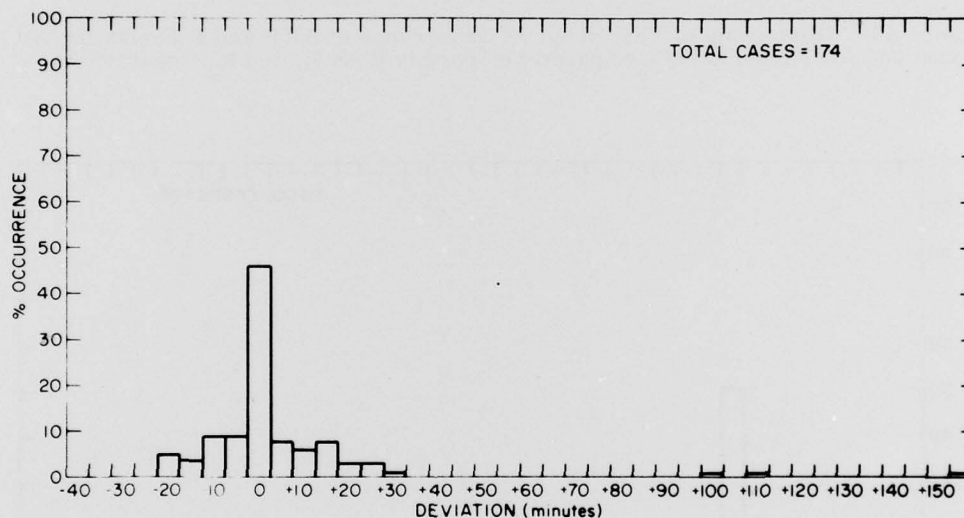


Figure A17. Histogram of Percentage of Occurrence of All Significant and Relevant Events for All Modes and All Experiments Compared Temporally With Q-Transition Occurrences

Figure A18 is the histogram of all the significant and relevant S and E events which occurred in all of the six experiments with  $R_1$  and  $R_2$  as parameters while Figure A19 is the same histogram with Q as a parameter. Again the superior precision of the R Indices over Q for this purpose is obvious.

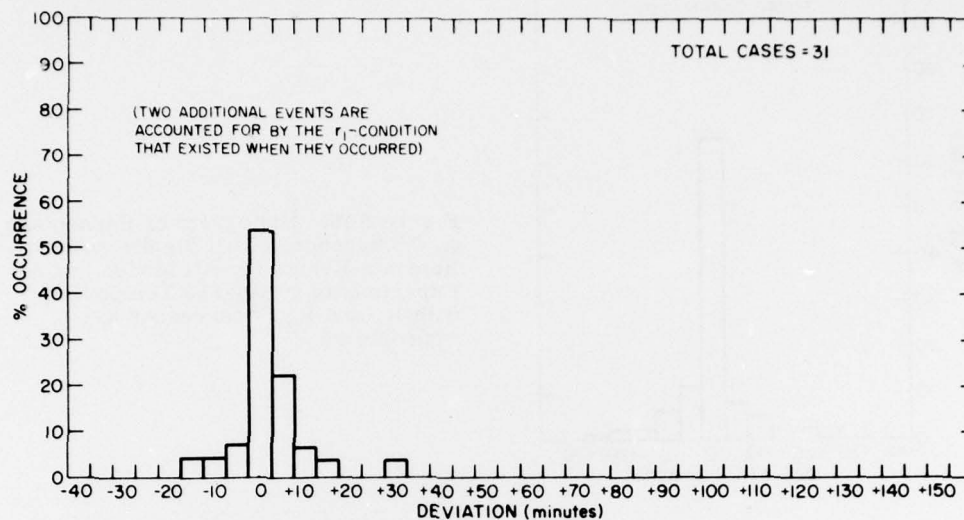


Figure A18. Histogram of Percentage of Occurrence of All S and E Events for All Modes and All Experiments Compared Temporally With  $R_1$  and  $R_2$  Occurrences

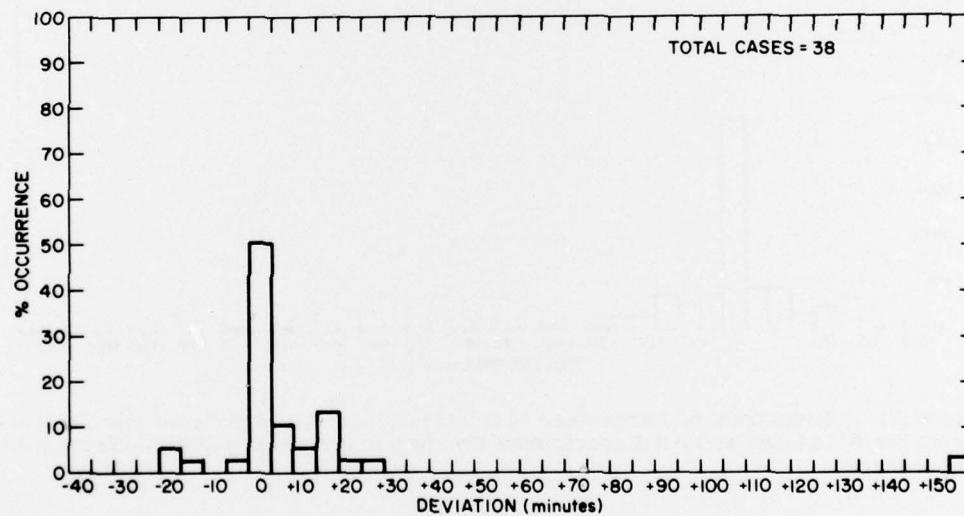


Figure A19. Histogram of Percentage of Occurrence of All S and E Events for All Modes and All Experiments Compared Temporally With Q-Transition Occurrences

## A2. INSTRUMENTATION

The analysis of these data has produced results that should be very useful both for practical and scientific purposes. The design and development of some equipment used in these experiments as well as its technical characteristics will be discussed in a separate report. There was no special advantage, per se, to the step-frequency ionosonde that will be described in that report as far as this study is concerned, but it has advantages in other applications.

## A2. INSTRUMENTATION

The analysis of these data has produced results that should be very useful both for practical and scientific purposes. The design and development of some equipment used in these experiments as well as its technical characteristics will be discussed in a separate report. There was no special advantage, per se, to the step-frequency ionosonde that will be described in that report as far as this study is concerned, but it has advantages in other applications.